Decentralized Control Techniques Applied to Electric Power Distributed Generation in Microgrids

Juan Carlos Vásquez Quintero

Advisor

Dr. JOSEP MARIA GUERRERO ZAPATA

Programa de Doctorat en Automàtica, Robótica y Visió

Departament d'Enginyerìa de Sistemes,
Automàtica i Informàtica Industrial (ESAII)

A dissertation submitted for
the degree of European Doctor of Philosophy

June 10, 2009

To my mom and the
memories of my father and grandmother.

ACKNOWLEDGEMENT

This work was supported by the Spanish Ministry of Science and Technology under grants CICYT ENE 2006-15521-C03-01/CON and ENE2007-67878-C02-01/ALT.

First, I would like to thank deeply my father who was my role model, and to whom I dedicate this thesis. I want to express sincere gratitude to all people who have helped and inspired me and all my colleagues at Escola Industrial in Barcelona who made it a comfortable place to work.

I would like to thank my advisor, Professor Josep M. Guerrero, for his guidance and support throughout the course of this work. Equally, I am thankful to the *SEPIC* research team for creating and maintaining an excellent academic environment, a factor which had a positive impact on this work.

Also, I would like to thank Professor R. Teodorescu from *IET* department and his team for allowing me to work at the Green Power Laboratory in Aalborg University, first as student of the *PERES* course, second, because of his hospitality and support while I was a guest and finally because thanks to that, several experimental results exposed in this work based on line-interactive PV systems were obtained. Equally, thanks to the Professor M. Liserre from the Department of Electrical and Electronic Engineering in the Politecnico di Bari, Italy, where some experimental results based on novel power quality conditioning functionalities were realized. Finally, I would also like to thank Professor P. Rodriguez from *UPC*, for his scientific contributions and support.

ABBREVIATIONS AND SYMBOLS

f	Grid frequency [Hz]
T	Grid frequency period [s]
Z_g	Magnitude of the grid impedance [Ω]
R_g	Resistive part of the grid impedance [Ω]
L_g	Inductive part of the grid impedance [H]
V_g	Magnitude of the grid voltage [V]
I_g, I_c, I_L	Grid, converter and load current [A]
X	Inductor reactance [Ω]
i_{pcc}	PCC Measured current [A]
v_{pcc}	PCC Measured voltage [V]
$\overrightarrow{I}$	Current phasor at pcc [A]
$\overrightarrow{V_g}, \overrightarrow{I_g}$	Grid Voltage and current phasors [V]
θ_g	Grid angle impedance [deg]
v	Measured grid voltage [V]
v_{ref}	Output voltage reference of the inverter [V]
V_c, I_c	Converter output voltage and current [V,I]
θ'	Measured grid angle [deg]
P, Q	Active and reactive power injected into the grid [W,VAr]
P_{max}	Maximum active power delivered by the VSI [W]
E	Voltage magnitude of the VSI [Vrms]
ϕ	Phase of the VSI [deg]
P_c, Q_c	Active and reactive power independent from the grid impedance [W,VAr]
P^*, Q^*	Desired active and reactive power [W,VAr].

P_i^*, Q_i^*	Nominal active and reactive power of the inverter i [W,VAr]
E^*	Amplitude output voltage reference [V]
ω	Angular frequency of the output voltage [rad/s]
ω^*	Reference angular frequency [rad/s]
ω_c	Cut-off angular frequency [rad/s]
ω_o	Resonant frequency [rad/s]
$G_p(s)$	Compensator transfer function of P_c
$G_q(s)$	Compensator transfer function of Q_c
m_i	Integral phase droop coefficient [W^-1s]
m_p	Proportional phase droop coefficient [W^-1]
m_d	Derivative phase droop coefficient [W^-1s^-1]
n_i	Integral amplitude droop coefficient [Vs/VAr]
n_p	Derivative amplitude droop coefficient [V/VAr s]
n_d	Derivative droop coefficient
$\widehat{p_c}(s), \widehat{q_c}(s)$	Active and reactive power small signal values
$\widehat{e}$	Perturbed value of E
ζ	Damped coefficient
m, n	Proportional droop coefficients
k_p	Proportional coefficient
k_i	Integral coefficient

Acronyms

ac	Alternating current
CSI	Current source inverter
dc	Direct current
DER	Distributed energy resource
DG	Distributed generation
DPGS	Distributed power generation systems
DSP	Digital signal processor
FLL	Frequency locked loop
IBS	Intelligent bypass switch
MPPT	Maximum power tracking point
PCC	Point of common coupling
PLL	Phase locked loop
PV	Photovoltaic
PWM	Pulse width modulation
SOGI	Second order generalized integrator
THD	Total harmonic distortion
UPS	Uninterruptible power supply
VSI	Voltage source inverter

CONTENTS

LIST OF TABLES

LIST OF FIGURES

CHAPTER 1

INTRODUCTION

Renewable energy emerges as an alternative way of generating clean energy. As a result, increasing the use of 'green' energy benefits the global environment, making it a global concern. This topic relies on a variety of manufacturing and installation industries for its development. As a solution, continuously small and smart grid energy systems appear including renewable energy resources, microgenerators, small energy storage systems, critical and noncritical loads, forming among them a special type of distributed generation system called the Microgrid.

Microgrids concerns issues like energy management, system stability, voltage quality, active and reactive power flow control, islanding detection, grid synchronization, and system recovery. All this, making optimal use of small scale energy generation interacting together, increasing the use of renewable energy sources, and operating in grid connected or in autonomous mode. These small but smart grids present a new paradigm for low voltage distribution systems, in which a multilevel control system must be performed in order to ensure the proper operation of the Microgrid.

1.1 Smart-Grids using Distributed Energy Resources

The smart grid as part of a Microgrid increases the integration of technologies that allows to regard electric grid operations and design. Also, this small but smart grid will

Figure 1.1: A Microgrid based on renewable energy sources. (Courtesy of Mastervolt).

use advanced technology to transform the energy production and power distribution system into a more intelligent, reliable, self-balancing, and interactive network that enables enhanced environmental stewardship, operational efficiencies, and energy security. The debate over what constitutes a smart grid is still emerging. A smart power grid refers to a ”vision” of a power distribution network that will see upgrades made on long distance power transmission lines and grids to both optimize current operations, as well as open up new markets to alternative energy. This allows more power to travel with less resistance to further reaches of markets (cities, towns, rural areas, etc).

Recent advances using smart grids to maximize operations efficiency, monitoring and supervisory control, power management, and utility grid supplying, make this kind of systems a suitable solution for decentralizing the electricity production. Thus, the study of this small grids is imperative because they are helpful to fulfill the maximization of the following issues:

- ▷ Efficiency and demand trends involving technological changes.
- ▷ Advanced energy storage systems.

- ▷ Reduced system restoration time due to transitions between the utility grid and the smart grid, improving network reliability.

- ▷ Increased integration of distributed generation resources.

- ▷ Increased security and tolerance to faults.

- ▷ Power quality and system reliability.

- ▷ Decentralized Power Management: how to generate an amount of power in a lot of places, rather than a lot of power in one place.

A smart grid will use digital technology to allow two-way communication between electricity generators and customers. It will, allow appliances in homes to use electricity when it is abundant and inexpensive. It will allow electricity managers to peer into their systems to identify problems and avoid them. In addition, it will provide rapid information about blackouts and power quality. These facts leads to integrate technologies that can detect emerging problems through extensive measurements, fast communications, centralized advanced diagnostics, and feedback control that quickly return the system to a stable state behavior after interruptions or disturbances are presented.

Finally, because a smart grid is a complex system and contains many interdependent technologies and strategies, is imperative to know the difficulty of to control it in order to warranty both quality of supply and ensuring power management supervising critical and non-critical loads. Also, the basic issue on small grids is the control of the number of microsources. Microgrid concept allows larger distribution generation by placing many microsources behind singles interfaces to the utility grid. Some key power system concepts based on power vs. frequency droops methodology, voltage control and hierarchical control levels can be applied to improve system stability, enhance active and reactive support, ride through capability, among others.

1.2 Thesis Objectives

The main aim of this thesis is to solve problems related to the modeling, control, and power management of distributed generation (*DG*) systems based on the Microgrid operating modes. After an introductive description of the Microgrid paradigm, some of the control objectives related to *DG* systems starting from a single *DG* unit to a number of interconnected units forming a Microgrid, will be solved. The research methodology will be developed as follows:

- ▷ Develop the system modeling based on the variables useful for an optimal control of active and reactive power flows. The use of voltage source inverters (*VSI*) as electronic interface with the Microgrid, needs for new analysis tools. As a primary goal, an accurate model derived from the electrical scheme of a grid interactive *VSI* system is demanded. The control variables of such *VSIs* will be the amplitude, frequency and phase of the output voltage.

- ▷ Analyze how to perform an accurate power flow control during transients, using an active and reactive power decoupling control algorithm to make the system independent from grid parameters.

- ▷ Analyze and develop a virtual output impedance scheme solving the output impedance of the inverter and its impact on the power sharing. The virtual output impedance can be regarded as a new control variable. It can be helpful for special functionalities like: nonlinear voltage supply, seamlessly connection (hot swap operation), adaptive control laws, among others.

- ▷ Realize the corresponding control laws based on a decentralized control methodology (droop functions) to improve system stability and dynamic performance,being able to share power with the grid in function of its nominal power.

- ▷ Develop closed loop stability analysis, such as small-signal dynamics, frequency domain behavior, pole dominance, or root locus diagrams, in order to obtain the desired transient response that allows choosing the loop control parameters properly.

Finally, the performance validation of the proposal control through experimental results will be realized finding solutions to the following problems:

- ▷ In grid-connected mode: Power injection accuracy due to sensitivity to the grid parameters: line-impedance imbalance, amplitude and frequency.
- ▷ In islanded mode: Power sharing accuracy due to the power line mismatches. Further aspects will be studied about how to deal with utility failures, as well as the frequency and amplitude regulation based on different levels of modeling, control, and analysis.
- ▷ Transition between grid connected and islanded operation: Synchronization and system restoration process when a grid fault is cleared.
- ▷ Voltage and frequency deviations inherent to the conventional droop methodology. Since it is not desirable to operate the system in a much lower frequency, a complementary frequency restoration strategy must be imposed.
- ▷ Reduction of grid voltage sag and harmonic distortion of the output voltage when supplying linear and non-linear loads.

1.3 Outline of the Thesis

This thesis is organized in 6 chapters, as follows:

Chapter 2 introduces a survey of past work focusing on distributed generation of electrical power, power management, control, and modes of operation in flexible Microgrids. The development of this chapter is developed based on the following reference,

- ▷ Josep M. Guerrero and Juan. C. Vasquez, *Uninterruptible Power Supplies*, The Industrial Electronics Handbook, Second edition, Irwin, J. David (ed.).

Chapter 3 considers the modeling principles, power flow analysis, small signal analysis based on a estimation of the grid parameters algorithm and finally a control structure using novel adaptive droop strategy which is explained and discussed. Equally, the

case-study corresponds to a voltage source inverter (*VSI*) capable of operating in both connected and islanded modes, as well as to transfer between these modes, seamlessly. The development of this chapter is developed based on the following references,

- J. C. Vasquez, J. M. Guerrero, A. Luna, P. Rodriguez, R. Teodorescu, *Adaptive Droop Control Applied to Voltage Source Inverters Operating in Grid-Connected and Islanded modes*, (Forthcoming to be included in *IEEE Transactions on Industrial Electronics (T-IE)*).
- J. C. Vasquez, J. M. Guerrero, E. Gregorio, P. Rodriguez, R. Teodorescu and F. Blaabjerg, *Adaptive Droop Control Applied to Distributed Generation Inverters Connected to the Grid*, *IEEE International Symposium on Industrial Electronics (ISIE'08)*. Pages 2420-2425. Dec. 18, 2008.

Based on the control strategy proposed in chapter 3, *chapter 4* is focused on a single phase multifunctional inverter allowing the obtainment of voltage dip compensation to the system and providing voltage ride-through capability applied to local loads. A model and system stability analysis is given to properly choose the control parameters. The development of this chapter is developed based on the following references,

- Juan C. Vasquez, Rosa A. Mastromauro, Josep M. Guerrero, and Marco Liserre, *Voltage Support Provided by a Droop-Controlled Multifunctional Inverter*, (Forthcoming to be included in IEEE Transactions on Industrial Electronics (T-IE)).
- R. A. Mastromauro, M. Liserre, A. dell'Aquila, J. M. Guerrero and J. C. Vasquez, *Droop Control of a Multifunctional PV Inverter*. *IEEE International Symposium on Industrial Electronics (ISIE'08)*, pages 2396-2400. Dec. 18, 2008.
- J. Matas, P. Rodriguez, J. M. Guerrero, J. C. Vasquez, *Ride-Through Improvement of Wind-Turbines Via Feedback Linearization*, *In IEEE International Symposium on Industrial Electronics (ISIE'08)*, Pages 2377-2382, Dec. 18, 2008.

In *chapter 5*, a control strategy for a flexible Microgrid is presented. The Microgrid presented consists of several line-interactive uninterruptible power supply (*UPS*)

systems. The control technique is based on the droop method to avoid critical communications among UPS units. Also, a control technique applied to a flexible Microgrid capable of operating in either grid-connected or islanded mode importing/exporting energy from/to the grid, is obtained. A small-signal analysis is presented in order to analyze the system stability, which gives the rules to design the main control parameters. The hierarchical control concept is extended and explained for an AC Microgrid based on a voltage and current regulation loops, an intermediate virtual impedance loop and an outer power sharing loop. Microgrid operation and transitions, harmonic current sharing and hot-swap operation topics are detailed as well. The development of this chapter is developed based on the following references,

- J. M. Guerrero, J. C. Vasquez, J. Matas, J. L. Sosa and L. Garcia de Vicuña. *Control Strategy for Flexible Microgrid Based on Parallel Line-Interactive UPS Systems, IEEE Transactions on Industrial Electronics*, Vol. 56, pages 726-736. March 2009.

- J. M. Guerrero, J. C. Vasquez, J. Matas, J. L. Sosa and L. Garcia de Vicuña, *Parallel Operation of Uninterruptible Power Supply Systems in Microgrids*, 12^{th} *European Conference on Power Electronics and Applications (EPE'07)*, sept.2007.

- Josep M. Guerrero and Juan. C. Vasquez, *Uninterruptible Power Supplies*, The Industrial Electronics Handbook, Second edition, Irwin, J. David (ed.).

Chapter 6 serves as a conclusion for this thesis point out all the contributions made and the ways for future trends in Microgrids researching are discussed.

CHAPTER 2

STATE OF THE ART AND CASE STUDY DESCRIPTION

2.1 Microgrids as a new energetic paradigm

In recent years, distributed generation of electrical power integrating renewable and non-conventional energy resources has become a reality. Relevant issues such as energy management, new control strategies for power electronic converters in the system, and the detection and management of the Microgrid operation modes are considered in this topic. To achieve efficient and safe operation of these systems in this new scenario, it is necessary to carry out research at different levels in order to get a better use of the energy sources.

First, most recent research works show the technical difficulty of efficiently controlling the Microgrid as a complete system. Second, energy management includes topics like power electrical quality, protections, energy delivery to the loads, and flexible operation that allows the Microgrid to work in grid connected or islanded modes. This line of research addresses all these questions, aiming at a rigorous study of this complex problem by using appropriate models of the parts that constitute the system, and by introducing a methodology for the design of the control algorithms based on linear adaptive control and nonlinear control techniques.

Another new concept is becoming one of the solutions to the power crisis: *DG* also

called micro generation in the origin. *DG* of electric energy has become part of the current electric power system; it consists of generating electrical power near the consumption area [47, 49–51], breaking with the traditional concept, in which generation and consumption areas are far away from each other. The future of power supply system will be composed by a great quantity of low voltage Microgrids interconnected through the distribution and transportation systems. Moreover, energy and ecological issues such as the oil crisis, climate change and the high power supply demand around the world have increased the need of new energy alternatives. In this context a new scenario is arising in small energy sources make up a new supply system: the Microgrid. The use of this kind of power supply sources would not only assure its quality and its opportune supply, but also a more efficient use of the natural resources. Likewise, the amount of *DG* sources directly connected to the distribution network will be increased actively [83]. The profits associated to the Microgrid concept are clear. On one hand, an improvement of the efficiency in energy transportation (reduction of energy losses) is achieved, when it is brought near the generation and consumption points. On the other hand, the electricity generation with low or null emissions of CO_2 and SO_2 to the atmosphere is possible, achieving a more responsible use of the available natural resources. A last but not least important merit of Microgrids comes from the inherent redundancy of generation systems, a fact that predicts that future power systems will be more robust and safer from eventual faults in the electrical supply system.

In recent last years, different Microgrids management structures have been proposed. In these proposed structures, various aspects of that question have been outlined, but few works address the problem in all its extension [48]. Most recent research projects show the technical difficulty of controlling the operation of Microgrid, because they are complex systems in which several subsystems interact: energy sources, power electronic converters, energy storage systems, loads and the grid. Among the goals of this line of research, all the above subjects will be studied in the case of a Microgrid that is capable of operating both isolated (autonomous) and seamlessly connected to the utility main (grid-connected mode) [42, 43]. The implications for the control of the Microgrid derived from the transition between both operation modes will be considered. Important contributions are expected about the control of power electronic converters operating in Microgrids, as well as about the power system management.

Further questions of special interest in the environment of distributed generation and of Microgrids to which a strong research effort has been dedicated, are:

- ▷ Synchronization techniques with the grid, such as phase locked loops, and network estimators that allow the calculation of the grid phase from the measurement of the supply voltages. The correct synchronization under imperfect conditions (imbalances, notches, distortion, etc.) is one of the key problems described in the related literature. In the case of systems working in parallel, particularly in grid isolated systems, the use of synchronization techniques among parallel modules is also required, achieving an equal distribution of the power delivered by each module.
- ▷ The reduction of circulating currents among parallel connected modules [30]. The parallel connection of converters is a highly complex problem both in the case of network connected systems and in isolated systems. With inadequate control algorithms, important currents can appear circulating among the power converters without arriving to the loads, overloading the generation capacity in a useless way. Moreover, because is necessary to warrant some reliability and stability among these modules, an extended control strategy analysis within literature has been proposed [17, 44, 78, 81]. With some inadequate control algorithms, some relevant currents among the converters (without reaching the loads) could arise overcharging the generation capability, pointlessly.

2.2 Microgrid Control

An experimental Microgrid is based on small wind generator, photovoltaic sources, energy storage systems and among others, and the overall system and the model approximation consist of several modules: the utility grid power, inverters and loads. A simple inverter is essentially integrated with a dc power source and a full bridge and an L−C output filter [56] as shown in Figure 2.1. In this stage, inverter management and control will be addressed. Moreover, inverters can be individually modelated, and its operation frequency can be configured by means of its local controller, which includes the dynamic of the controller, the output filter, and the voltage and current

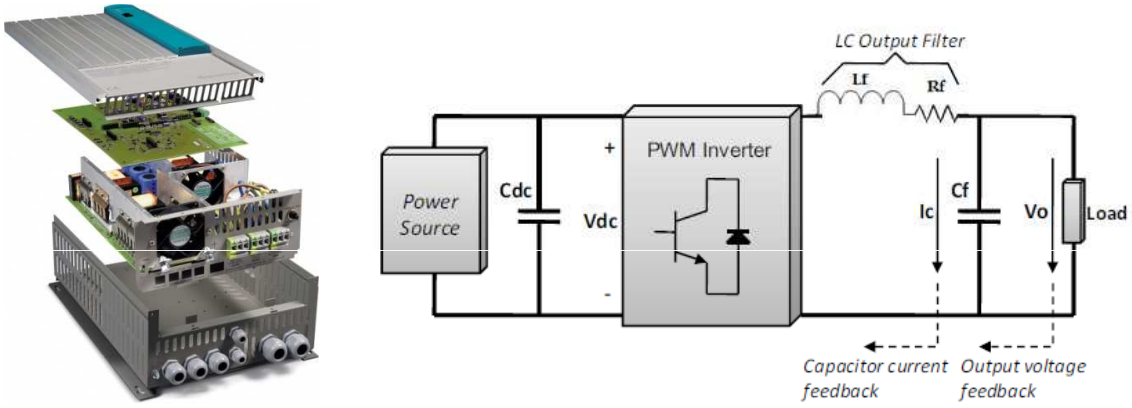

Figure 2.1: a) Multiple layers of an inverter (Courtesy of Mastervolt). b) Basic schematic diagram of a power stage of a single phase inverter.

control loops [38, 46, 69]. In the same way, parallel inverter operation has a lot of advantages, both economic and in terms of equipment maintenance in comparison to a simple inverter. However, the circulating current through them could produce damage in some semiconductors. That is why, a well-designed parallel inverter system not only provides the means for an excellent current distribution, but also, a high viability, modularity, easy-maintenance and flexibility [89]. Two or more parallel inverters are subject to the following restrictions:

- ▷ All the parallel inverters must operate synchronously.
- ▷ All the inverter output voltages must have the same amplitude, frequency and phase.
- ▷ The inverters output current needs to be distributed according to their nominal power.

Each inverter will have a external power loop based on droop control [21–23, 36, 63, 81, 84], called also as autonomous or decentralized control, whose purpose is to share active and reactive power among *DG* units and to improve the system performance and

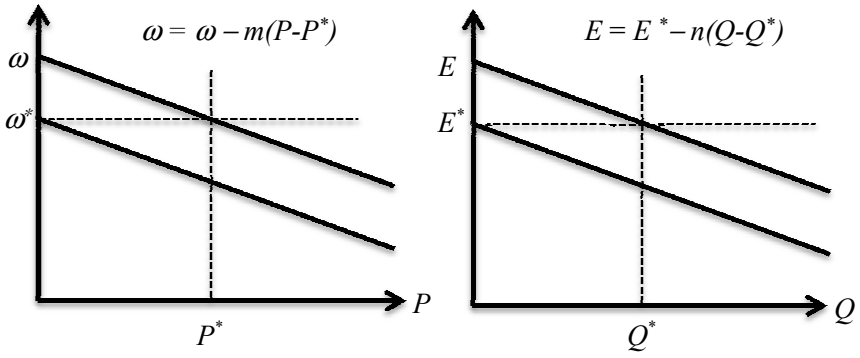

Figure 2.2: $P - \omega$ and $Q - E$ grid scheme using P^* and Q^* as setpoints.

stability, adjusting at the same time both the frequency and the magnitude of the output voltage. The droop control scheme, can be expressed as follows

$$\omega = \omega^* - m \cdot (P - P^*), \tag{2.1}$$

$$E = E^* - n \cdot (Q - Q^*), \tag{2.2}$$

where ω and E^* are the frequency and the amplitude of the output voltage. m and n coefficients define the corresponding slopes. P^* and Q^* are the active and reactive power references, which are commonly set to zero when we connect UPS units in parallel autonomously, forming energetic island. However, if we want to share power with a constant power source, $e.g.$ the utility grid, is necessary to fix both active and reactive power source to be drawn from the unit. This droop method increases the system performance due to the autonomous operation among the modules. This way, the amplitude and frequency output voltage can be influenced by the current sharing through a self-regulation mechanism that uses both the active and reactive local power from each unit [59], [82].

In order to obtain good power sharing, the frequency and amplitude output voltage must be fine-tuned in the control loop, with the aim of compensating active and reactive power imbalance [66], [54]. This concept is derived from the classic high power system theory, in which generator frequency decreases when the grid utility power is increased [26], [9]. To implement the droop method, equations 2.1 and 2.2, can be used, keeping

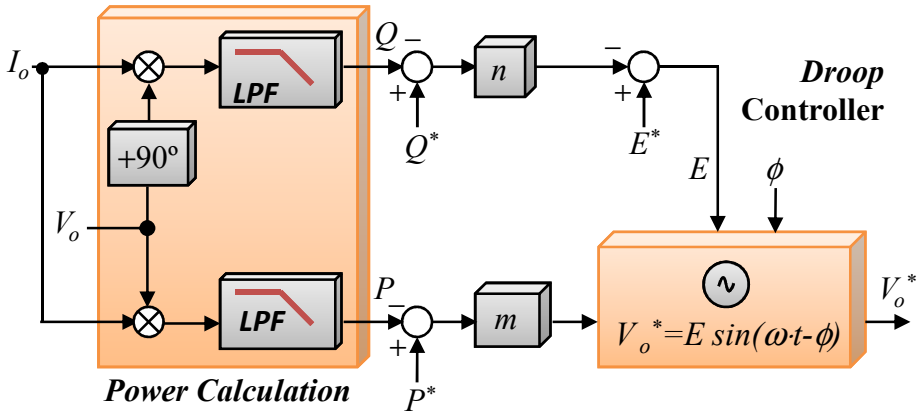

Figure 2.3: Block diagram of a P/Q droop controller.

in mind that active and reactive power must be measured and averaged with a running average window over one cycle of the fundamental frequency, so that the powers are evaluated at fundamental frequency. This operation can be implemented by means of low-pass filters with a reduced bandwidth. Furthermore, the filters that calculate the mean values both the active and reactive power and the coefficients of the slopes, are strong determinants of the system dynamic and performance, especially in paralleled power supplies. The oscillating phenomena due to the phase difference among modules could produce some instability, and a high circulating transient current could overcharge the system and equipment as well.

In transmission systems, the grid impedance is mainly inductive; This is the reason why it is used to adopt $P-\omega$ and $Q-E$ slopes. Hence, the inverter can inject desired active and reactive power to the main grid, regulating the output voltage and responding to some linear load changes. The inverter inner control will include voltage and current controllers, which will be designed in order to reject high frequency disturbances and absorbing the output $L-C$ filter to avoid any resonant signal with the main grid. Considering droop method, a compromise between both frequency and voltage regulation as active and reactive power equalization can exist. In other words, if the droop slope coefficients are increased is possible to obtain good power equalization, even though regulation could be compromised. In practice, these deviations are acceptable if for instance, they are less of 2% in frequency and 5% in amplitude.

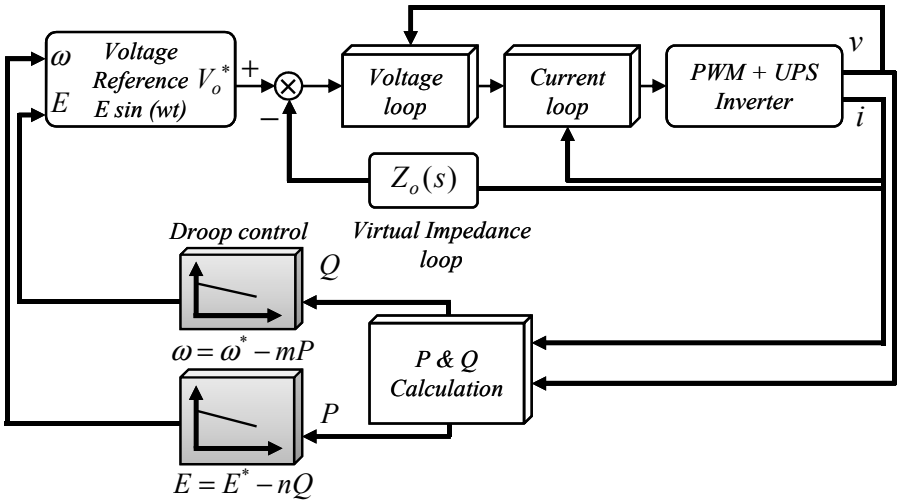

Figure 2.4: Multi-loop control droop strategy with the virtual output impedance approach.

One of the primary aspects in Microgrids control field in order to synchronize an inverter output is using a phase-locked loop (*PLL*). However, one inconvenience of this scheme is the poor dynamic response, and a small phase error among the inverters, causing high circulating current between them. Moreover, if the output voltage of each inverter had the same amplitude, frequency and phase, in theory the load current would be shared equally. In practice, due to the component tolerance and the wrong adjustment of the line impedance, the load current not be shared in an optimal form, resulting in circulating current among the inverters overloading the overall system. From these inconveniences, different methods in literature have been developed, such as the multi-loop control strategies, shown in Figure 2.4. This scheme is composed of an external loop whose function is to regulate the output voltage, whereas the inner loop supervises the inductor current [55,90,91] or the capacitor current [19,29,74] of the output filter in order to reach a fast dynamic response. This control diagram provides a high viability in parameters design and a Low Total Harmonic Distortion (*THD*), but it requires both complex analysis and a parameter synchronization algorithm. Similarly, another relevant aspect to provide proper output impedance is the virtual output impedance loop.

2.3 Microgrid operation modes

The Microgrid energy management must be performed by considering the energy storage systems and the control of the energy flows in both operation modes (with and without connection to the public grid). In this sense, the Microgrid must be capable of exporting/importing energy from/to the main grid, to control the active and reactive power flow, and to supervise the energy storage [68]. In grid-connected mode, some of the system dynamics are supplied by the utility grid due to the small size of the micro sources. In islanded mode, system dynamic is depicted by its own micro sources, its power regulation control and finally the main grid. Also, a small deviation from the nominal frequency could be noticed. As a result, the storage unit will support all power deviations by injecting or absorbing some active power proportionally to the frequency deviation.

Likewise, most of the Microgrids are not designed in order to have a direct link with the low voltage grid due to the characteristics of the power produced; hence, some electronic interfaces are required such as *dc/ac* or *ac/dc/ac* converters. Another problem is the slow response at the control signals when a change of the output power occurs. The absence of synchronous machines connected to the low-voltage power grid requires that power balancing during the transient must be provided for power storage devices such as batteries or flywheels. After some equipment faults and a power supply shutdown in a conventional power system, some restoration difficulties could be produced, therefore, as a Microgrid starting point; it must always be supplied by a local generation power grid. In addition, the Microgrid should start correctly even though a power supply is not present (blackstart).

When a power supply shutdown occurs, restoration process must be reduced as much as possible in order to ensure a high reliability level. The restoration stages are aimed at the plant restart, power generation of the main grid, and system frequency synchronization. During this stage, some details must be considered such as the reactive power balance, commutation of the transient voltages, balancing power generation, starting sequence, and coordination of the generation units. Thanks to its flexibility, Microgrids restoration process is simpler due to the number of controller variables to

be manipulated (switch, micro sources, and loads). When the Microgrid is again in grid-connected operation mode, the main utility grid will provide both active and reactive power requirements as to ensure its operation frequency [8]. In this operation mode, all the distributed generation units must supply the specified power, e.g. to minimize the power importing from the grid (peak shaving), whose requirements depend on the global system, which vary from one system to the other. In addition, each distributed generation unit can be controlled through voltage regulation for active and reactive power generation using a communication bus. Typically, depending of the custom desire, when the Microgrid is in grid-connected mode, both main grid and the local micro sources send all the power to the loads. Hence, if any events in main grid are presented, such as voltage dips or general faults, among others, islanded operation must be started.

2.3.1 Islanded operation mode of a Microgrid

Microgrid autonomous mode is realized taking into account the static bypass switch (*IBS*) opening [36] itself as a controllable load or source. Therefore, when the Microgrid is in islanded operation mode, the micro sources that feed the system are responsible for nominal voltage and frequency stability when power is shared by the generation units. It is important to avoid overload the inverters and to ensure that load changes are controlled in a proper form. Some control techniques which are based on communication links as master-slave scheme by can be adopted in systems where micro sources are connected through a common bus or being close enough. However, a communication link through a low-bandwidth system can be more economic, more reliable and finally, attractive. Equally, in autonomous mode the Microgrid must satisfy the following issues:

- ▷ Voltage and frequency management: The primary purpose is to balance the system against losses and system disturbances so that the desired frequency and power interchange is maintained. that is why, voltage and frequency inner loops must be adjusted and regulated as reference within acceptable limits.

- ▷ Supply and demand balancing: when the system is importing from the grid before islanding, the resulting frequency is smaller than the main frequency, been possible that one of the units reaches maximum power in autonomous operation. Besides, the droop characteristic slope tries to switch in vertical as soon as the maximum power limit has been reached and the operating point moves downward vertically as load increases. In the opposite case, when the unit is exporting and the new frequency is larger than nominal.

- ▷ Power quality: power quality must synthesize quality of supply and quality of consumption using sustainable development as transporting of renewable energy, embedded generation, using high requirements on quality and reliability by industrial, commercial and domestic loads/costumers avoiding variations as harmonic distortion or sudden events as interruptions or even voltage dips.

Also, when the Microgrid is operating in islanded mode all the micro sources are constant power sources, injecting the desired power towards the utility grid. At the same time, the micro sources are controlled in order to provide all the load voltage while frequency is kept within the allowed limits. Islanded operation mode of a Microgrid can be started because of two main reasons: first, a non-intentioned form in order to do maintenance or economical criterion. Second, due to main utility grid faults for non-intentionally causes. The interrupting time of the power supply can be reduced using this method until the grid utility service is disposed again.

2.3.2 Transition between grid-connected and islanded mode

As commented above, the *IBS* is continuously supervising both the utility grid and the Microgrid status is depicted in the figure 2.5. When a fault in the main grid has been detected by the *IBS*, it must disconnect the Microgrid. In such a case, this switch can readjust the power reference at nominal values, although it is not strictly necessary. In addition to this, if maximum permissible deviation is not exceeded, (typically, 2% for frequency and 5% amplitude) the voltage amplitude and frequency can be measured inside the Microgrid, and operation points (P^* and Q^*) avoids the frequency deviation and amplitude of the droop method. When the Microgrid is in islanded mode operation,

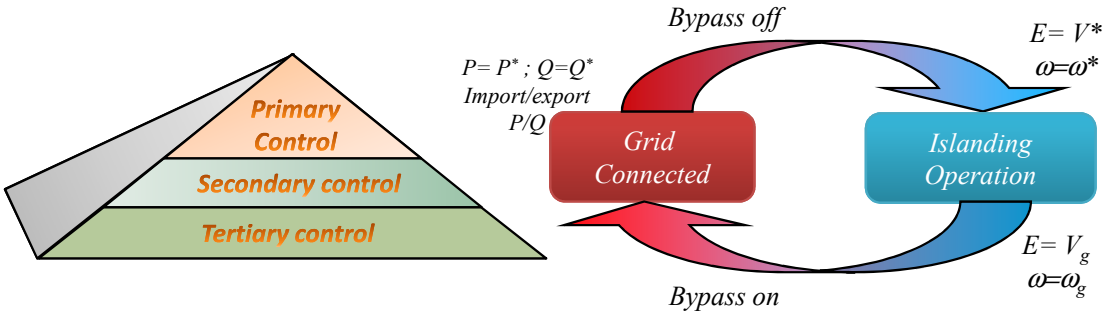

Figure 2.5: Hierarchical levels of a flexible Microgrid operations modes and transfer between modes.

and *IBS* detects main grid fault-free stability, synchronization among voltage, amplitude, phase and frequency must be realized for connecting operation. Hence, amplitude is adjusted through small steps in Q^*, and both frequency and phase are adjusted by means of small steps P^* proportionally to phase error between the Microgrid and the utility grid.

2.4 Hierarchical control and management of Microgrids

Functionally, the Microgrid (as a grid) must operate within three control hierarchical levels:

Primary Control : P/Q Droop Control.

As a control main loop, inverters are programmed to act as generators by including virtual inertias by means of the droop method. It specifically adjusts the frequency or amplitude output voltage as a function of the desired active and reactive power. Thus, active and reactive power can be shared equally among the inverters. For reliability and to ensure local stability, voltage regulation is needed. Without this supervision control, most of the micro sources can present reactive power and operation voltage oscillations. To avoid this fact, high circulating currents among the sources must be eliminated through the voltage control, in such a way that reactive power generation

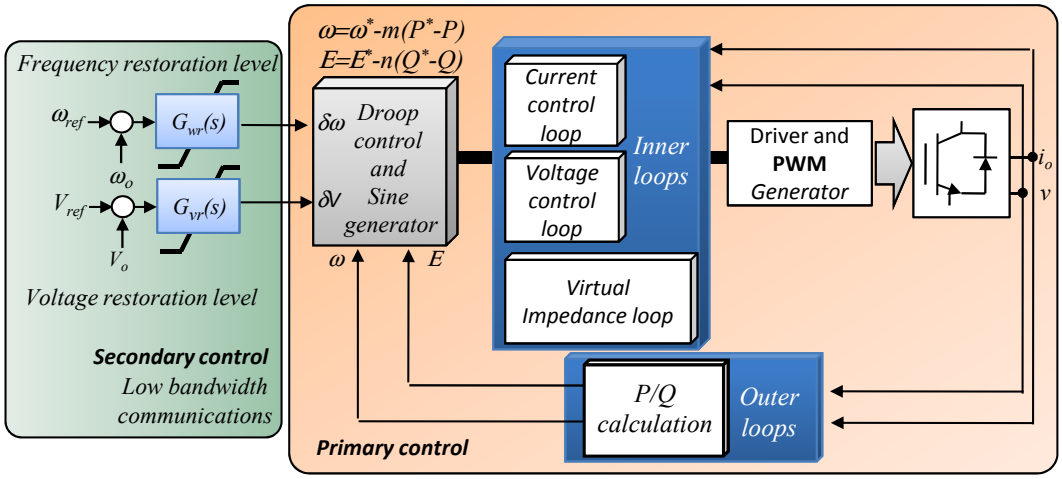

Figure 2.6: Primary and secondary control based on hierarchical management strategy.

of the micro source be more capacitive, reducing the voltage set point value. In other words, while Q is a high inductive value, the voltage reference value will be increased as Figure 2.7 shows.

Secondary control: Frequency-Voltage Restoration and Synchronization.

In order to restore the Microgrid voltage to nominal values, supervisor system must send the corresponding signals using low-bandwidth communication. Also, this control can be used for Microgrid synchronization to the main grid before performing the interconnection, transiting from islanded to grid-connected mode. The power distribution through the control stage is based on a static relationship between f and P, and it is implemented as a droop scheme. Likewise, frequency and voltage restoration to their nominal values must be adjusted when a load change is realized. Originally, frequency deviation from the nominal measured frequency grid brings to a integrator implementation [16]. For some parallel sources, this displacement can not be produced equally due to measured errors. In addition, if the power sources are connected in islanded mode through the main grid at different times, the load behavior can not be completely ensured because all the initial conditions (Historical) from the integrators, are different.

Tertiary control: P/Q Import and Export.

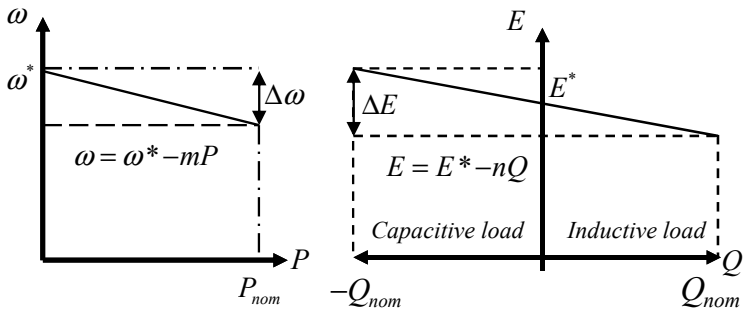

Figure 2.7: Droop characteristic when supplying capacitive or inductive loads.

In the third control hierarchy, the adjustment of the inverters references connected to the Microgrid and even of the generators maximum power point trackers is performed, so that the energy flows are optimized. The set points of the Microgrid inverters can be adjusted, in order to control the power flow, in global (the Microgrid imports/exports energy) or local terms (hierarchy of spending energy). Normally, power flow depends on economic issues. Economic data must be processed and used to make decisions in the Microgrid. Each controller must respond autonomously to the system changes without requiring load data, the *IBS* or other sources. Thus, the controller uses a power and voltage feedback control based on the real-time measured values of both P, Q, frequency and ac voltage to generate the desired voltage amplitude and phase angle by means of the droop control.

2.5 Conclusions

This chapter exposes Microgrids field as a multidisciplinary area, which encompasses power stage topologies, control techniques, technological storage solutions, and complex power systems, among others. Hence, Microgrids are becoming a reality in a scenario in which renewable energy and distributed storage systems can be conjugated and also integrated into the grid. These concepts are becoming more important due to not only environmental aspects, but also social, economic, and political interests. Equally,

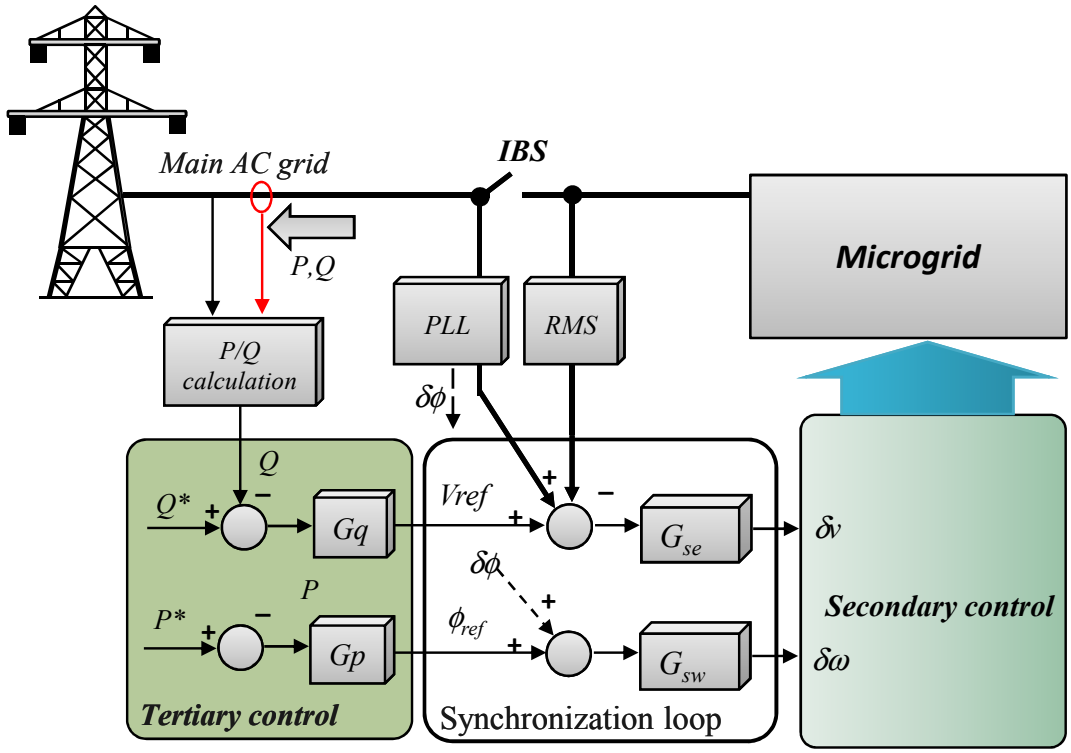

Figure 2.8: Block diagram of the tertiary control and the synchronization control loop.

DG concept is pointing out that the future utility line will be formed by distributed energy resources and small grids (minigrids or Microgrids) interconnected between them. In fact, the responsibility of the final user is the production and storage part of the electrical power of the whole system.

CHAPTER 3

ADAPTIVE DROOP METHOD

3.1 Introduction

DG systems and Microgrids are becoming more and more important when trying to increase the renewable energy penetration. In this sense, the use of intelligent power interfaces between the electrical generation sources and the grid is mandatory. These interfaces have a final stage consisting of dc/ac inverters, which can be classified in current-source inverters (*CSI*) and voltage-source inverters (*VSI*). In order to inject current to the grid, *CSI* are commonly used, while in island or autonomous operation, *VSI* are needed to maintain the voltage stable [86]. *VSIs* are relevant for *DG* applications since they do not need any external reference to stay synchronized [45], [14]. In fact, they can operate in parallel with other inverters by using frequency and voltage droops, forming autonomous or isolated Microgrids [8]. Also, *VSIs* are convenient since they can provide to distributed power generation system performances like ride-through capability and power quality enhancement [85], [76], [93], [87], [24], [88], [53], [79], [35]. When these inverters are required to operate in grid-connected mode, they often change their behavior from voltage to current sources [80].

Nevertheless, to achieve flexible Microgrids, $i.e.$ to be able to operate in both grid-connected and islanded modes, *VSIs* are required to control the exported or imported power to the main grid and to stabilize the Microgrid [36], [70]. In this sense, the droop method can be used to inject active and reactive power from the *VSI* to the grid

by adjusting the frequency and amplitude of the output voltage [8, 14, 45]. However, in order to independently control the active and reactive power flows, the conventional droop method needs some knowledge of some parameters of the grid. In this sense, the estimation of the grid impedance can be useful not only for injecting P and Q into the grid with high precision, but also for islanding detection.

In this chapter, we propose a control scheme based on the droop method which automatically adjusts their parameters by using a grid impedance estimation method based on analyzing the voltage and current variations at the point of common coupling (*PCC*) resulting from small deviations in the power generated by the *VSI* [84]. The *VSI* is able to operate in both grid-connected and islanded modes, as well as to seamlessly transfer between these modes.

3.2 Estimation of the Grid parameters

The grid characterization technique used is based on processing the voltage and current phasors at the *PCC* between the power converter and the grid. A frequency locked loop based on the second order generalized integrator (*SOGI-FLL*) is used to monitor such voltage and current phasors. As Figure 3.1 shows, two cascaded integrators working in closed loop are used to implement the *SOGI* [92], [84]. This grid monitoring technique provides high precision, low computational cost and frequency adaptation capability [73], [72]. The aforementioned *SOGI-FLL* is also applied to monitoring the current injected into the *PCC* in order to obtain the current phasor $\overrightarrow{I} = i_d + ji_a$. The *SOGI-FLL* acts as a selective filter for detecting two in-quadrature output signals, being a very useful feature to attenuate harmonics on the monitored voltage and current and to accurately detect the phasors of the grid voltage and current ($\overrightarrow{V_g}$ and $\overrightarrow{I_g}$) at the fundamental grid frequency. The detected voltage and current in-quadrature signals are projected on a $d-q$ rotating reference frame to obtain coherent voltage and current phasors. The technique used for estimating the grid-parameters stems from a linear interpretation of the grid in which distributed power generators are connected to. Therefore, the grid can be seen from the *PCC* of a power generator as a simple Thevenin circuit

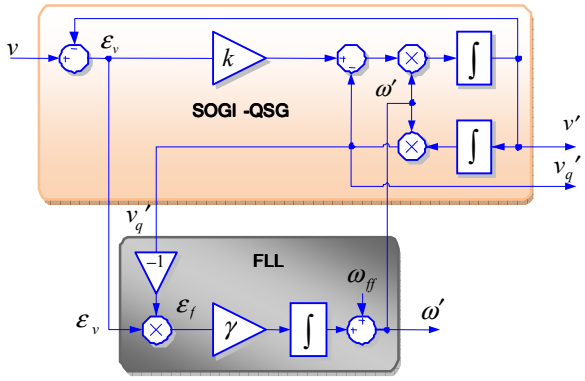

Figure 3.1: Block diagram of the SOGI-FLL.

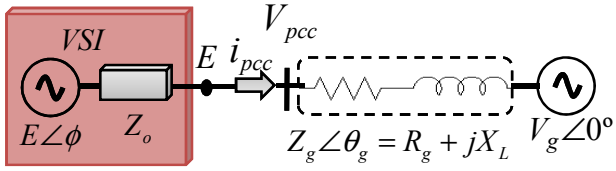

Figure 3.2: Equivalent circuit of the VSI connected to the grid.

constituted by a grid impedance $\overrightarrow{Z_g}$ and a header voltage $\overrightarrow{V_g}$. Even though the $v-i$ characteristic of the ac grid can not be represented by a simple two-dimensional Cartesian plane, Figures 3.2 and 3.3 help to illustrate further explanations about the impedance detection method used in this section since it depicts the relationship between voltage and current phasors at the *PCC* for a particular frequency. From the measurement of the voltage and current phasors at the *PCC* at two different operating points, linearity in the $v-i$ characteristic of Figure 3.3 allows writing (3.1) and (3.2) for estimating the grid impedance $\overrightarrow{Z_g}$ and the open circuit voltage $\overrightarrow{V_g}$, respectively

$$\overrightarrow{Z_g} = Z_g\angle\theta_g = \frac{\triangle\overrightarrow{V_{pcc}}}{\triangle\overrightarrow{I_{pcc}}} = \frac{\overrightarrow{V_1}-\overrightarrow{V_2}}{\overrightarrow{I_1}-\overrightarrow{I_2}}, \tag{3.1}$$

$$\overrightarrow{V_g} = V_g\angle\phi = \overrightarrow{V_{pcc(i)}} - \overrightarrow{Z_g}\overrightarrow{I_{pcc(i)}} = \frac{\overrightarrow{I_1}\overrightarrow{V_2}-\overrightarrow{I_2}\overrightarrow{V_1}}{\overrightarrow{I_1}-\overrightarrow{I_2}}, \tag{3.2}$$

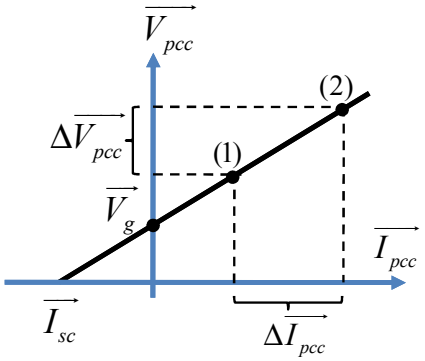

Figure 3.3: V-I characteristic of the grid for a particular frequency.

---

where Z_g and θ_g are the magnitude and the angle grid impedance, respectively. Several techniques for detecting the grid impedance are either directly or indirectly based on this basic principle [7,10,40,71,77]. In this work, the grid parameters are estimated from the active and reactive power variations generated by a grid-connected converter in which a droop-controller is implemented. The cornerstone of this estimation technique is the accuracy in the on-line measurement of voltage and current phasors at the *PCC*, which is performed based on the *SOGI-FLL*. Figure 3.4 shows the diagram of the algorithm used in this work to identify the grid parameters. It is worth saying that the estimated values of the angle and magnitude of the grid voltage impedance, and their voltage and the frequency are transiently wrong after each change in the grid parameters. Therefore, as shown in Figure 3.4, the *FLL* block is only implemented on the monitored voltage v and the angle θ' is calculated from the integration of the voltage frequency. As transient values cannot be sent to the droop-controller of the *VSI*, a small buffer of three rows is added at the output of the grid parameters identification block of Figure 3.4.

3.3 Droop method concept

With the aim of connecting several parallel inverters without control intercommunications, the droop method is often proposed [70]. The applications of such a kind of control are typically industrial *UPS* systems [30] or islanding Microgrids [29], [33].

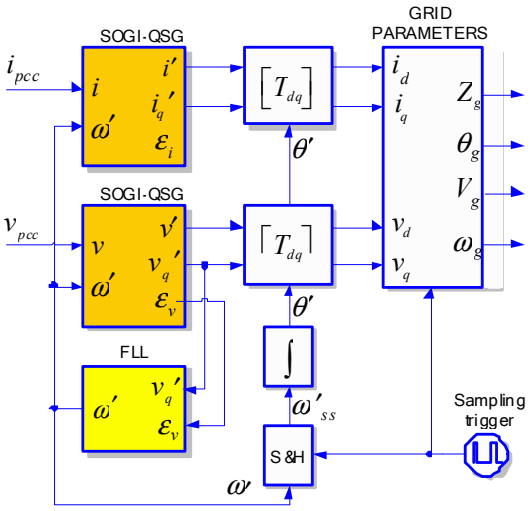

Figure 3.4: Block diagram of the grid parameters identification algorithm.

The conventional droop method is based on the principle that the phase and the amplitude of the inverter can be used to control active and reactive-power flows [82]. Hence, the conventional droop method can be expressed as follows:

$$\omega = \omega^* - m \cdot P, \tag{3.3}$$

$$E = E^* - n \cdot Q, \tag{3.4}$$

where E is the amplitude of the inverter output voltage; ϕ is the frequency of the inverter; ω^* and E^* are the frequency and amplitude at no-load, respectively; and m and n are the proportional droop coefficients. The active and reactive powers flowing from an inverter to a grid through an inductor can be expressed as follows [9]:

$$P = \left[\left(\frac{EV_g cos\phi}{Z_g} - \frac{V_g^2}{Z_g}\right)\cos\theta_g + \frac{EV_g}{Z_g}\sin\phi\sin\theta_g\right], \tag{3.5}$$

$$Q = \left[\left(\frac{EV_g cos\phi}{Z_g} - \frac{V_g^2}{Z_g}\right)\sin\theta_g - \frac{EV_g}{Z_g}\sin\phi\sin\theta_g\right], \tag{3.6}$$

where Z and θ are the magnitude and the phase of the output impedance, respectively; V is the common bus voltage; and ϕ is the phase angle between the inverter output and the Microgrid voltages. Notice that there is no decoupling between $P - \omega$ and $Q - E$.

However, it is very important to keep in mind that the droop method is based on two main assumptions.

*Assumption 1:*The output impedance is purely inductive, and $Z_g = X$ and $\omega = 90^o$ with 3.5 and 3.6 become

$$P = \frac{EV_g}{X} \sin \phi, \tag{3.7}$$

$$Q = \frac{EV_g}{X} \cos \phi - \frac{V_g^2}{X}. \tag{3.8}$$

This is often justified due to the large inductor of the filter inverter and to the impedance of the power lines. However, the inverter output impedance depends on the control loops, and the impedance of the power lines is mainly resistive in low voltage applications. This problem can be overcome by adding an output inductor, resulting in an *LCL* output filter, or by programming a virtual output impedance through a control loop.

Assumption 2: The angle ϕ is small; we can derive that $\sin \phi \approx \phi$ and $\cos \phi \approx 1$, and consequently,

$$P \approx \frac{EV_g}{X} \phi, \tag{3.9}$$

$$Q \approx \frac{V_g}{X}(E - V_g). \tag{3.10}$$

Note that, taking these considerations into account, P and Q are linearly dependent on ω and E. This approximation is true if the output impedance is not too large, as in most practical cases. In the droop method, each unit uses frequency instead of phase to control the active-power flows, considering that they do not know the initial phase value of the other units. However, the initial frequency at no load can be easily fixed as ϕ . As a consequence, the droop method has an inherent tradeoff between the active-power sharing and the frequency accuracy, thus resulting in frequency deviations. In [15], frequency restoration loops were proposed to eliminate these frequency deviations. However, in general, it is not practical, since the system becomes unstable due to inaccuracies in inverters output frequency, which leads to increasing circulating currents.

3.4 Adaptive Droop Control

In this section, based on the estimation of the grid parameters provided by the identification algorithm, an adaptive droop controller able to inject active and reactive power into the grid with high accuracy is proposed.

3.4.1 Power flow analysis

Using (3.5) and (3.6), as they depend highly on the grid impedance $(Z_g \angle \theta_g)$ is possible to transform P and Q into novel variables (P_c and Q_c) which are independent from the magnitude and phase of the grid impedance

$$P_c = (P \sin\theta_g - Q \cos\theta_g)\,, \tag{3.11}$$

$$Q_c = (P \cos\theta_g - Q \sin\theta_g)\,. \tag{3.12}$$

By substituting 3.5 and 3.6 into 3.11 and 3.12, it yields the following expressions

$$P_c = (EV_g \sin\phi)\,, \tag{3.13}$$

$$Q_c = \left(EV_g \cos\phi - V_g^2\right). \tag{3.14}$$

Note that P_c is mainly dependent on the phase, while Q_c depends on the voltage difference between the *VSI* and the grid ($E - V_g$). Once these control variables (P_c and Q_c) are obtained, we can use them into the droop control method to inject active and reactive power.

Similarly, with the aim to inject the desired active and reactive powers (defined as P^* and Q^*), the following droop control method which uses the transformation (3.11) and (3.12), is proposed

$$\phi = -G_q(s) Z_g \left[(P - P^*)\sin\theta_g - (Q - Q^*)\cos\theta_g\right], \tag{3.15}$$

$$E = E^* - G_q(s) Z_g \left[(P - P^*)\cos\theta_g + (Q - Q^*)\sin\theta_g\right], \tag{3.16}$$

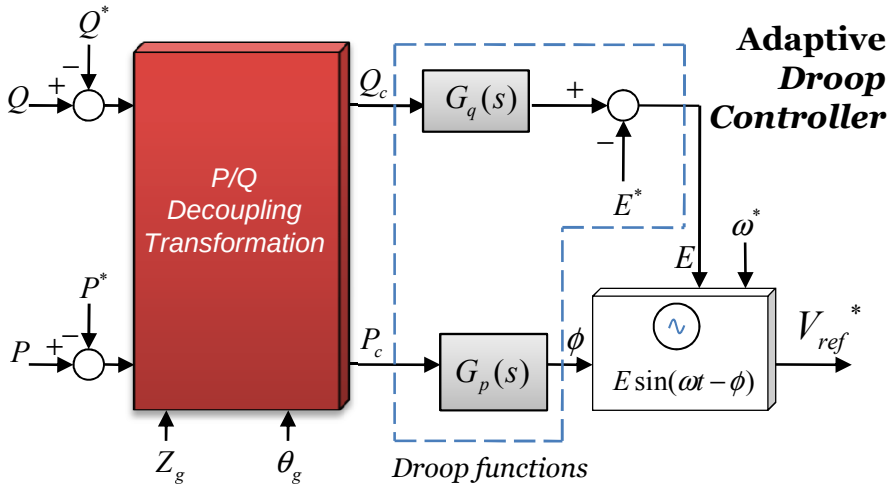

Figure 3.5: Block diagram of the adaptive droop control.

where E^* is the amplitude voltage reference, which takes the values of the estimated grid voltage (V_g). By using these equations we can obtain the voltage reference of the *VSI*: $V^*_{ref} = E \cdot \sin(\omega * t + \phi)$, being ω the angular frequency of the output voltage. The compensator transfer functions of P_c and Q_c can be expressed as

$$G_p(s) = \frac{m_i + m_p s + m_d s^2}{s}, \tag{3.17}$$

$$G_q(s) = \frac{n_i + n_p s}{s}. \tag{3.18}$$

In practice, the derivative term in $G_q(s)$ is avoided since it barely affects the system dynamics. Figure 3.4 shows the block diagram of the droop controller proposed to inject the desired active P^* and reactive power Q^*.

3.4.2 Small signal modeling

In order to show the system stability and the transient response, a small signal analysis is provided allowing the designer to adjust the control parameters [21, 36]. Taking into account that P and Q are the average values of the instantaneous active and reactive

power $p(t)$ and $q(t)$, it can be expressed as

$$P = \overline{v_d i_d} = \frac{1}{T}\int_t^{t-T} p(t)dt, \tag{3.19}$$

$$Q = \overline{v_q i_d} - \overline{v_d i_q} = \frac{1}{T}\int_t^{t-T} q(t)dt, \tag{3.20}$$

being T the period of the grid frequency. By using the first order Padé approximation, the average value P and Q can be stated

$$e^{-Ts} \approx \frac{2-Ts}{2+Ts}. \tag{3.21}$$

By substituting (3.13), (3.14) and (3.15), (3.16) into (3.19) and (3.20), and using a small signal approximation to linearize the equations, it yields

$$\hat{P}_c = \frac{1}{1+(T/2)s} \cdot (V_g \sin\Phi\hat{e}(s) + V_g E\cos\Phi\hat{\phi}(s)), \tag{3.22}$$

$$\hat{Q}_c = \frac{1}{1+(T/2)s} \cdot (V_g \cos\Phi\hat{e}(s) - V_g E\sin\Phi\hat{\phi}(s)), \tag{3.23}$$

where the lower-case variables with the symbol ˆ indicate small signal values, and uppercase variables are the steady-state values. By using (3.15), (3.16), (3.17), (3.18) and (3.22), (3.23) it can be obtained

$$\hat{\phi}(s) = \left(\frac{m_i + m_p s + m_d s^2}{s}\right)\hat{p}_c(s), \tag{3.24}$$

$$\hat{e}(s) = -\left(\frac{n_i + n_p s}{s}\right)\hat{q}_c(s). \tag{3.25}$$

From (3.24), (3.25) it can be derived the following expressions

$$\hat{\phi}(s) = -\left(\frac{m_i + m_p s + m_d s^2}{s}\right) \cdot \frac{V_g \sin\Phi\hat{e}(s) + V_g E\cos\Phi\hat{\phi}(s)}{1+(T/2)s}, \tag{3.26}$$

$$\hat{e}(s) = -\left(\frac{n_i + n_p s}{s}\right) \cdot \frac{V_g \cos\Phi\hat{e}(s) - V_g E\sin\Phi\hat{\phi}(s)}{1+(T/2)s}. \tag{3.27}$$

By combining (3.26) and (3.27), a fourth order characteristic equation can be obtained

$$a_4 s^4 + a_3 s^3 + a_2 s^2 + a_1 s + a_0 = 0. \tag{3.28}$$

being,

$$
\begin{aligned}
a_4 &= T^2 + 2Tm_dV_gE\cos\Phi,\\
a_3 &= 4T + 4m_dn_pV_g^2E + 2V_g\cos\Phi(2m_dE + Tn_p + Tm_pE),\\
a_2 &= 2V_g\cos\Phi(Tm_iE + Tn_i + 2n_p + 2m_p) + 4V_g^2E(m_pn_p + m_dn_i) + 4,\\
a_1 &= 4V_g\cos\Phi(n_i + m_iE) + 4V_g^2E(m_in_p + m_pn_i),\\
a_0 &= 4n_im_iEV_g^2,
\end{aligned}
$$

where the steady-state values of the active and reactive power are $P = P^*$ and $Q = Q^*$, and, from (3.5) and (3.6), the steady-state phase and amplitudes can be calculated as follows

$$\Phi = \arctan\left(\frac{P^*\sin\theta_g - Q^*\cos\theta_g}{P^*\cos\theta_g + Q^*\sin\theta_g + (V_g^2/Z_g)}\right), \tag{3.29}$$

$$E = \frac{V_g^2\cos\theta_g + P^*Z_g}{V_g(\cos\theta_g\cos\Phi + \sin\theta_g\sin\Phi)}. \tag{3.30}$$

By using this model, it is possible to determinate the system stability by extracting the root locus family that can be seen in Figures 3.6, 3.7, and 3.8, by changing m_p, m_d, and n_d. In order to guarantee the stability condition (input/output behavior) of the closed-loop system dynamics, a poles study of the fourth order identified model is employed. The performance of this ind of system is often viewed in terms of pole dominance. The a_0 coefficient of the characteristic equation depends basically of m_i and n_i parameters that influence directly over the system fast response making it more damped. In some practical cases it is possible to adjust these parameters for fine-tuning purposes. Moreover, system stability can be determined by using (3.29) when islanding mode is taking place. In an autonomous operation mode, system stability can be compromised if any reactive power contributions from the main grid are considered. It is possible to solve if the parameter n_i in (3.29) equals to 0, reducing the system dynamics to a third order equation. That is why the fourth order system can be simplified to a third, second, or even first-order system.

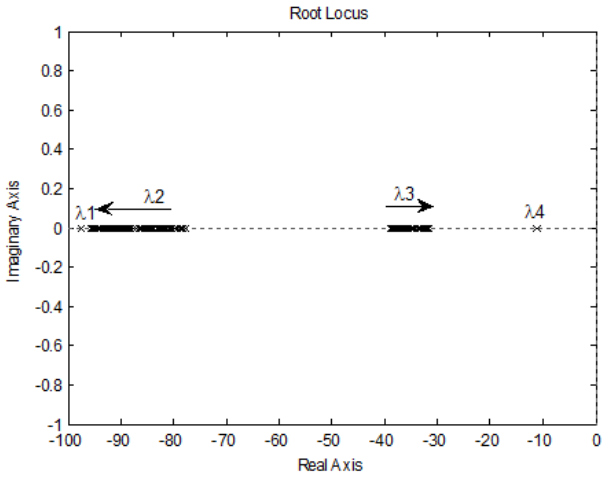

Figure 3.6: Trace of root locus for $0.00005 < m_p < 0.0001$.

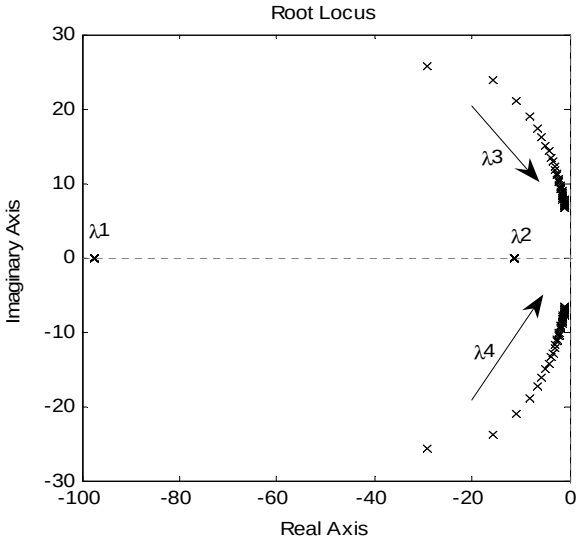

Figure 3.7: Trace of root locus for $1\text{x}10^{-6} < m_i < 4\text{x}10^{-5}$.

3.5 Control Structure

Figure 3.9 shows the proposed block diagram of the whole control structure of the *VSI* unit with grid-connected to autonomous mode transition capability. It consists

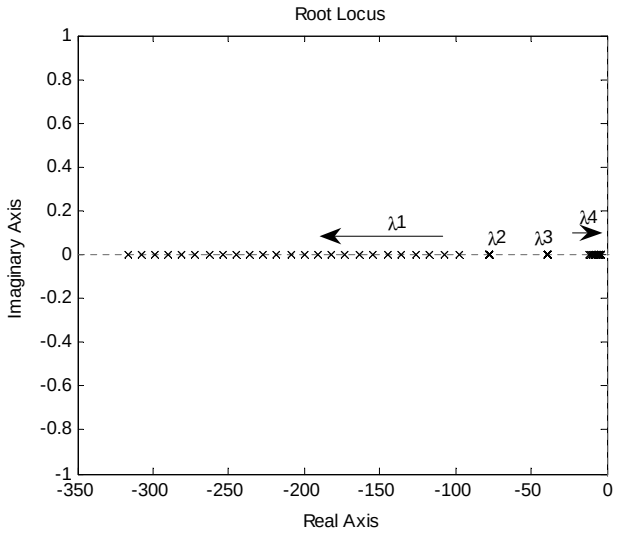

Figure 3.8: Trace of root locus for $0.0004 < n_p < 0.01$.

of several control loops, described as follows. The inner control loops regulate the inverter output-voltage and limit the output current. The loop of the *SOGI-FLL* and the associated algorithm is able to estimate the grid parameters: frequency, voltage, and module and angle of the grid impedance (ω_g, V_g, Z_g, and θ_g). These parameters are used by the adaptive droop controller to inject the required active and reactive power by the *VSI* into the grid. In addition, the estimation of the grid impedance can be useful for islanding detection. If $Z_g < 1.75$ or Z_g changes more than 0.5 in $5s$, the *VSI* will be in island mode. Islanding detection is necessary in order to achieve soft transition between grid-connected and islanding mode for a non-planned islanding scenario. In that case, the integral term of the reactive power control must be disconnected ($n_i = 0$) [23]. Starting from islanding mode the *VSI* is supplying the local load. When the grid is available, the *VSI* must start the synchronization process with the phase, frequency and amplitude of the grid, without connecting the bypass switch (indicated by the grid status variable /GS in Figure 3.10. Phase and frequency synchronization can be done by multiplying the quadrature component of the voltage grid by the *VSI* voltage, and processing this signal through a low pass filter and a *PI* controller to be sent to the phase control loop. In order to adjust the voltage amplitude, the *rms* voltage error between the grid and the *VSI* must be calculated, and process it through a *PI* to be sent to the

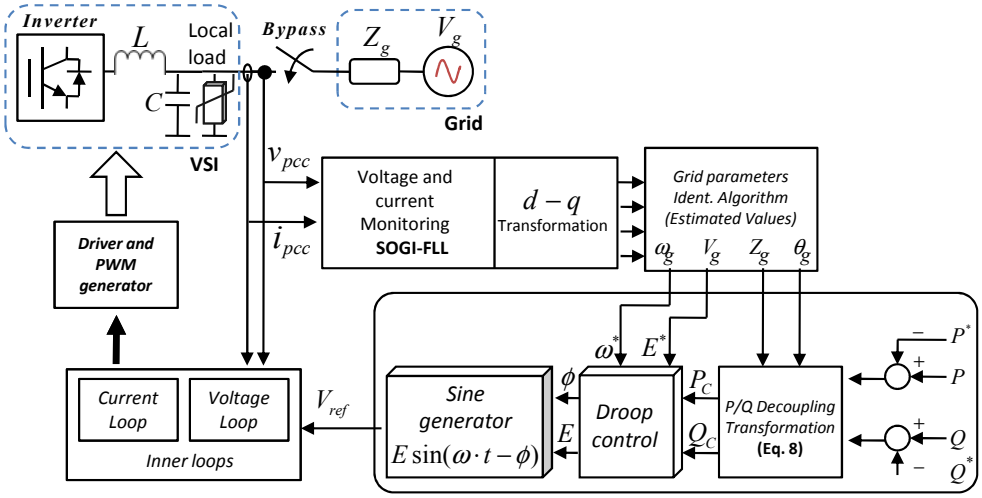

Figure 3.9: Block diagram of the *SOGI* and the proposed adaptive droop control strategy.

amplitude control loop. Hence, after several line-cycles the *VSI* will be synchronized to the grid and the bypass can interconnect the *VSI* and the grid. At this moment, the desired active and reactive powers can be injected to the grid.

3.6 Simulation Results

The proposed control is tested through proper simulations in order to validate its feasibility. A single-phase *VSI* with the controller proposed was simulated by using the control and system parameters shown in Table 3.1.

Figure 3.11 illustrates the grid impedance estimator performance. The inductive part of the grid impedance changes from $1.50mH$ to $1.65mH$ at $t = 10s$, while the resistive part changes from 1.1 to 1 at $t = 14s$. As can be observed, the transient values cannot be sent directly to the droop-controller of the *VSI*. For that reason, a small mismatch is appreciated due to the buffer of the grid parameters estimation algorithm (see Section 3.1).

Figure 3.12 demonstrates the validity of the model, showing a good resemblance

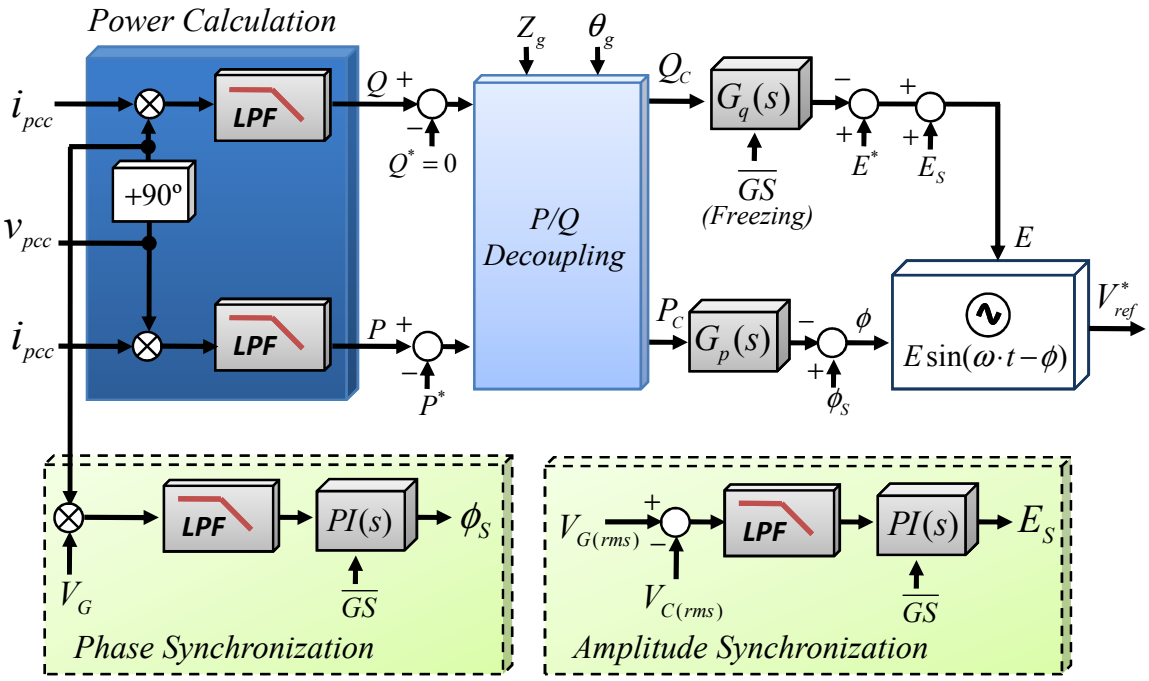

Figure 3.10: Block diagram of the whole proposed controller using the synchronization control loops.

Table 3.1: System Parameters

Parameter	*Symbol*	*Value*	*Units*
Voltage Grid	V_g	311	V
Frequency Grid	ω	50	Rad/s
Resistive Part of Z_g	R_g	2	Ω
Inductive Part of Z_g	Z_g	3	mH
Grid Z module	L_g	2.3	Ω
Grid Z angle	θ_g	28.8	Ws/rd
Integral phase droop	m_i	0.0018	W/rd
Proportional phase droop	m_p	0.00004	W/rd·s
Derivative phase droop	m_d	7e-7	VAr·s/V
Proportional amplitude droop	n_p	0.15	VAr/V
Integral amplitude droop	n_i	0.0004	VAr/V

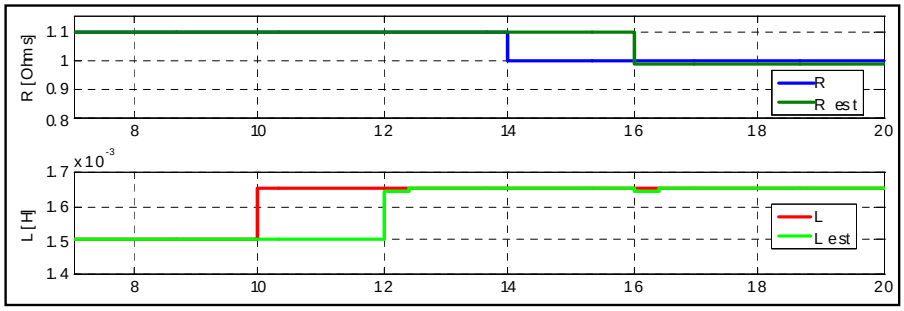

Figure 3.11: Variations of the grid impedance, R and L estimation.

between the system phase dynamics and the obtained model (3.29). The model has been proven for a wide range of grid impedance values, showing its validity. In addition, to illustrate the robustness in front of large grid impedance variations, some simulations have been performed with and without the estimator algorithm. Figure 3.13 shows the transient response of the active power by using the control with and without the grid impedance estimation loop, for grid impedance variations (R_g = 1, 2, and 3). Notice that this loop decouples to a large extent the system dynamics from the grid impedance value.

Figure 3.14(a) shows the synchronization process of the output voltage inverter respect to the grid voltage, during islanding operation. Figure 3.14(b) depicts the voltage difference between the voltage grid and *VSI* voltages. Once the synchronization is done, Figure 3.14(c) shows the transition from islanded mode to grid-connected mode. When the connection is realized and the system is under a steady-state condition, the active and reactive power injected to the grid can be independently controlled. Finally, the system is intentionally disconnected ($t = 20s$) in order to validate the transition operation from grid-connected to island mode. The seamless transfer can be seen between both modes, pointing out the flexible operation of the *VSI*.

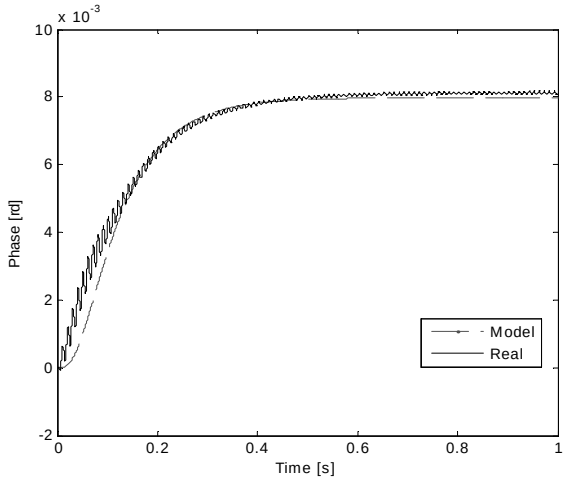

Figure 3.12: Transient response of the system dynamics and the obtained model (18).

3.7 Experimental Results

Experimental results have been obtained in order to show the feasibility of the controller proposed. The hardware setup shown in Figure 3.15 consists of the following equipment: a Danfoss VLT 5006 7.6*k*VA inverter with and *LC* filter (L=2x712μH and C=2.2μF), and a local load. A dSPACE 1104 system is used to implement the controller. The system sampling and switching frequency were running at 8*kHz*.

The inverter is connected through a bypass switch to a 5*kVA* low-voltage grid transformer with an equivalent impedance of 10 *mH*. The waveforms presented here were obtained through the ControlDesk software provided by dSPACE, as shown in Figure 3.16. By using this platform we can adjust in real-time the main control parameters within the specified limits. It includes the coefficients and references of the inner voltage and current control loops, the synchronization loop, and the active and reactive power outer control loops. Figure 3.17 shows the synchronization process of the inverter with the grid. As it can be seen, in less than 1s the inverter is synchronized to the grid. Afterwards, the inverter can be connected to the grid and, at that moment, we can change the power references, as also shown in Figure 3.17. Figure 3.18 shows the dynamics of the active power when changing the reference from 0 to 1 *kW*, from 0 to

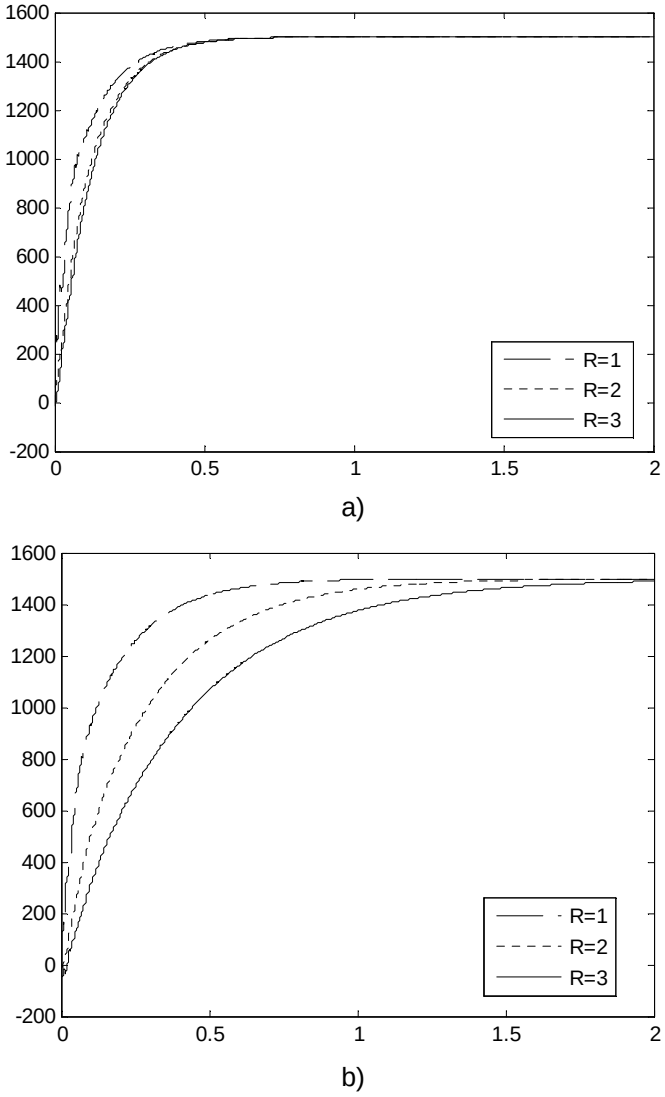

Figure 3.13: Start up of P for different line impedances, (a) without and (b) with the estimation algorithm of Z_g.

500 *W*, and Figure 3.19 a power step change from 500 W to 1000 W while keeping Q = 0 *VAr*. Figure 3.20 shows the capability of the *VSI* to absorb 1000*VAr* of reactive power. Notice the transient response and steady-state performances that endows the controller to the system. Figure 3.21 depicts the transition from islanded mode to grid-connected mode after the synchronization process (grid and VSI voltages), and P,Q step changes. Note how the active and reactive power injected to the grid can be independently controlled.

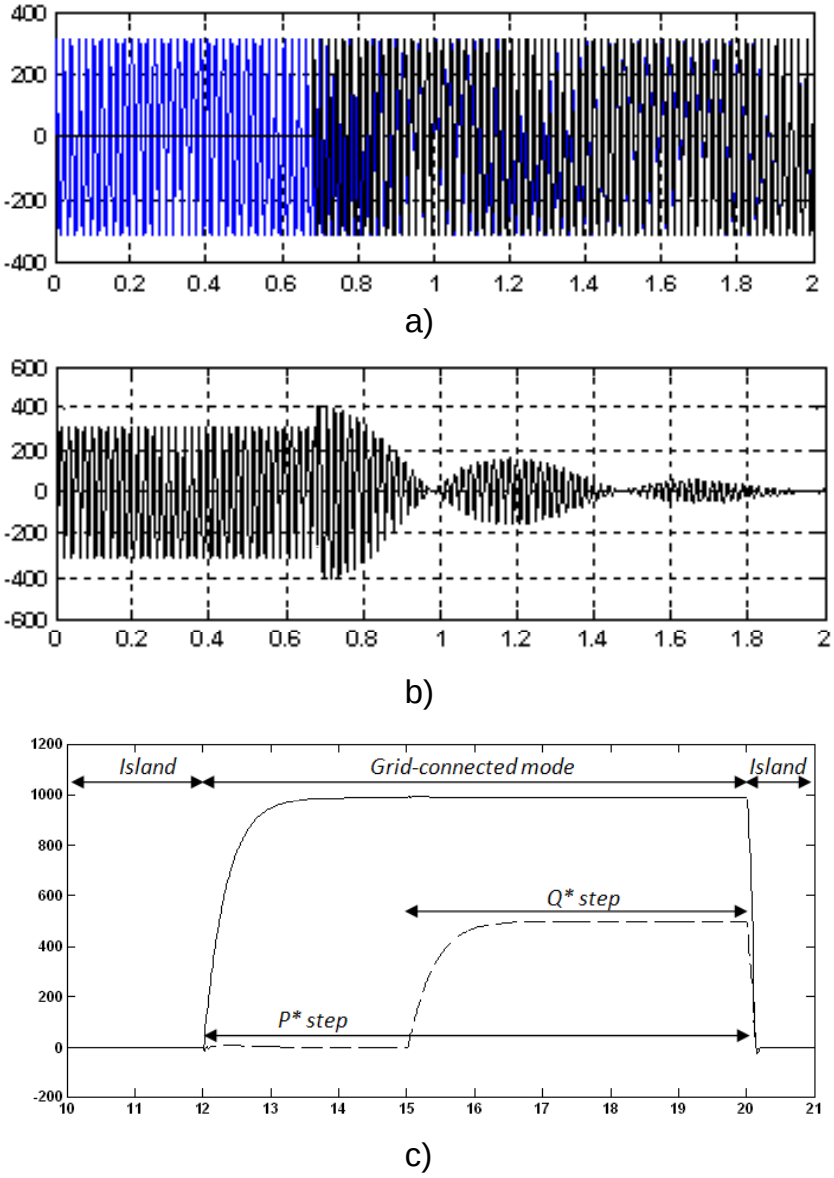

Figure 3.14: Transition from islanding to grid-connected mode:(a) synchronization process (grid and *VSI* voltages), (b) error between grid and inverter voltages, and (c) P and Q behavior in both operation modes.

Finally, the system is intentionally disconnected (t=11s). Notice the good resemblance between the experimental results and the corresponding simulation results shown in Figure 3.14(b)

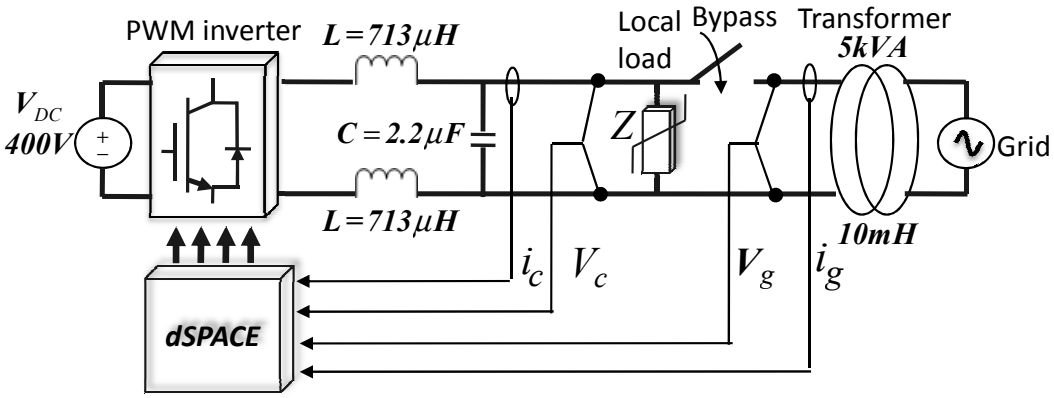

Figure 3.15: Scheme of the experimental setup.

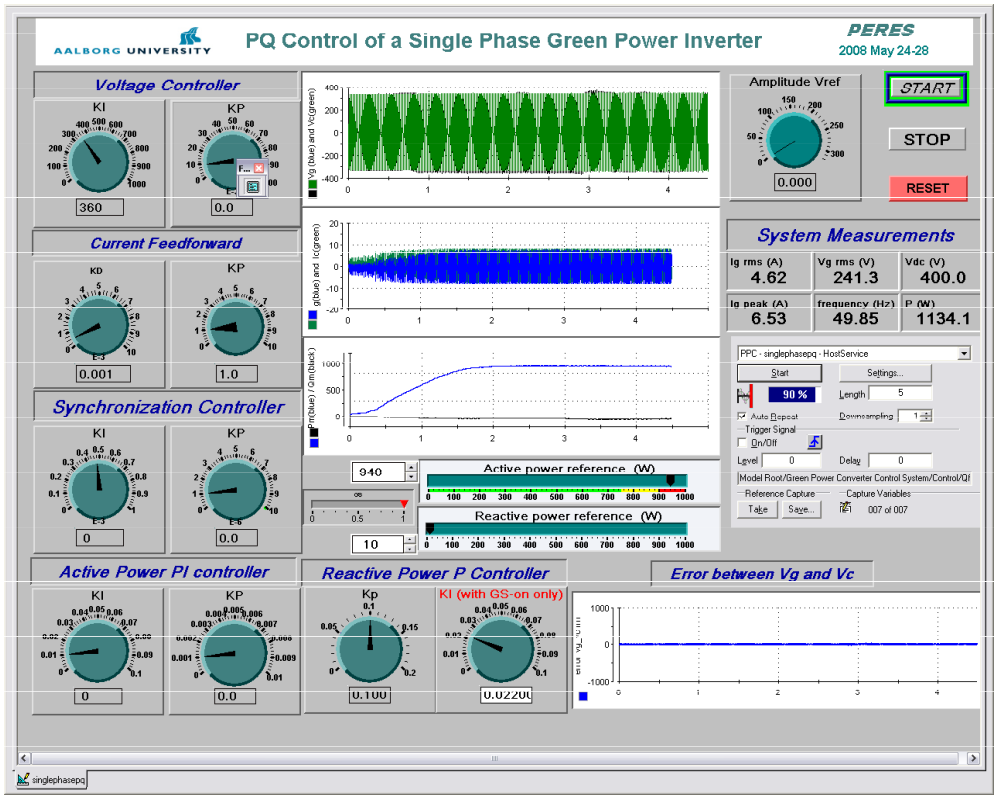

Figure 3.16: Panel supervisor of the ControlDesk from the dSPACE.

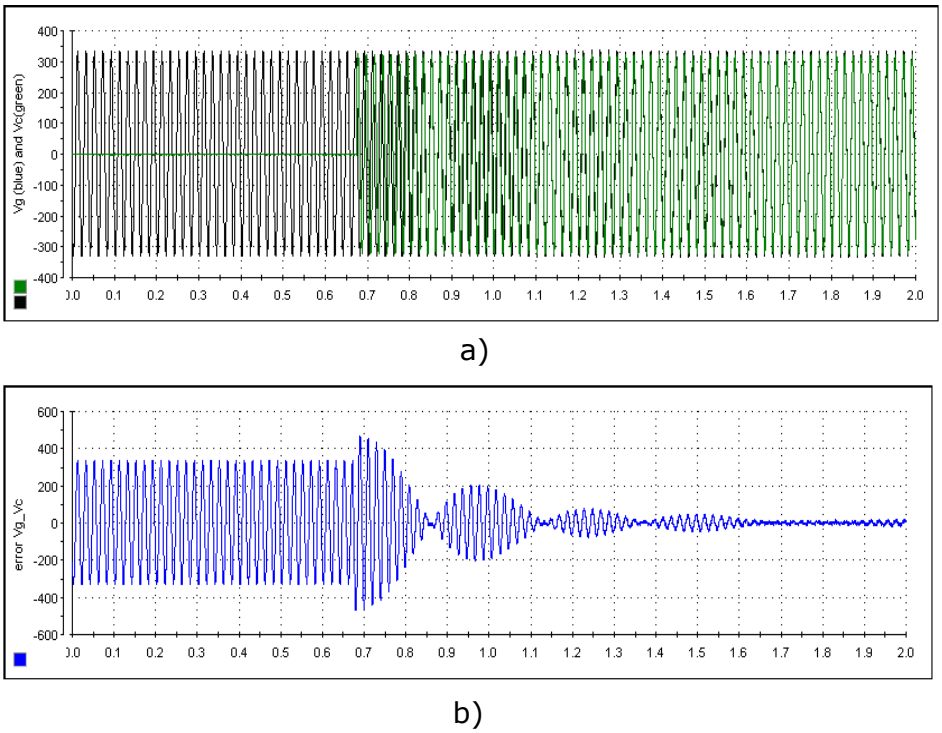

Figure 3.17: Synchronization of the inverter to the grid: (a) voltage waveforms (b) error between grid and inverter voltages.

3.8 Conclusions

In this Chapter, a novel control for a *VSI* able to operate both islanding and grid connected mode has been presented. In this last case, the inverter is able to inject the desired active and reactive power to the grid. The control has two main structures. The first one is the grid parameters estimation, which calculates the amplitude and frequency of the grid, as well as the magnitude and phase of the grid impedance. The second one is a droop control scheme, which uses these parameters to inject independently active and reactive power to the grid. The proposed droop control uses such parameters to close the loop, achieving a tight P and Q regulation. Thanks to the feedback variables of the estimator, the system dynamics are well decoupled from the grid parameters. The results point out the applicability of the proposed control scheme to *DG VSIs* for Microgrid applications.

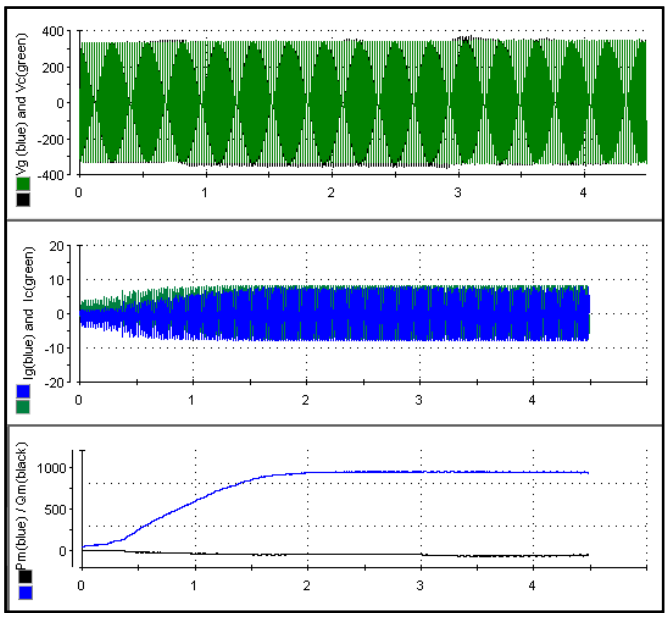

Figure 3.18: Active power transient response for Q = 0 VAr from 0 to 1000W (P: blue line, Q: black line).

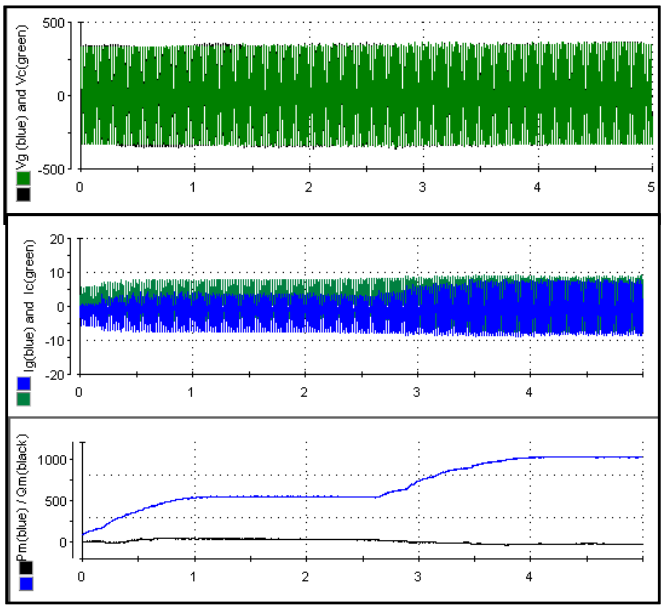

Figure 3.19: Active power step change for Q = 0 VAr (P: blue line, Q: black line).

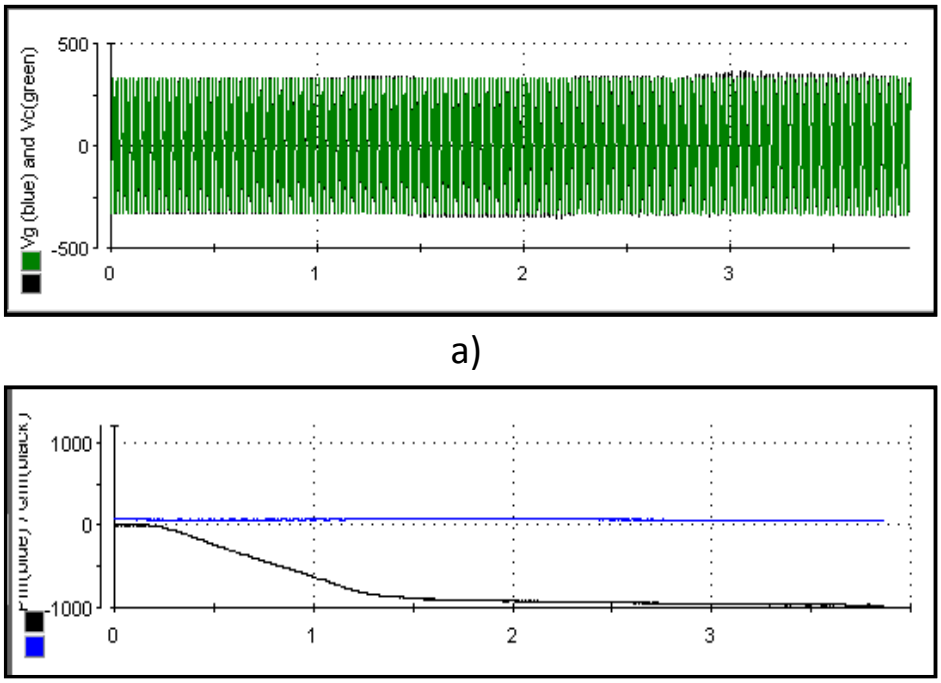

Figure 3.20: Reactive power transient response from 0 to -1000VAr for P= 0W. (P: blue line, Q: black line).

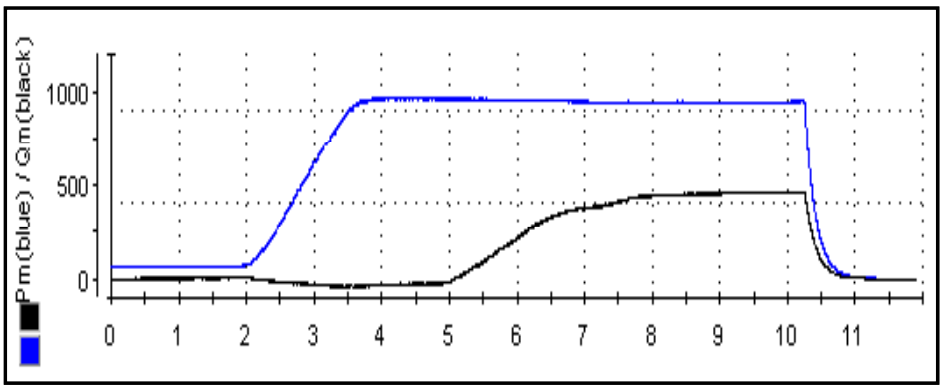

Figure 3.21: Power dynamic during transition from islanding to grid-connected mode.

CHAPTER 4

DROOP CONTROL METHOD APPLIED FOR VOLTAGE SAG MITIGATION

4.1 Introduction

The *IEEE* Standard 1547 [1, 2] defines the ancillary services in distributed power generation systems (*DPGS*) as: load regulation, energy losses, spinning and non-spinning reserve, voltage regulation, and reactive power supply. It recommends that low-power systems should be disconnected when the grid voltage is lower than $0.85p.u.$ or higher than 1.1 $p.u.$ as an anti-islanding requirement [1, 2]. Among low-power *DPGS*, the number of *PV* plants connected to low-voltage distribution lines has been increased in recernt years [11, 12]. Hence, the distributed *PV* systems should be designed to comply with anti-islanding requirements, but they can also sustain the voltage for local loads. Usually, grid-connected *PV* inverters work like current sources (*CSI*), in which the voltage reference is often taken from the grid voltage sensing using a phase-locked-loop (*PLL*) circuit, while an inner current loop ensures that the inverter acts as a current source. However, in order to maintain the voltage and frequency stability, voltage source inverters (*VSI*) are convenient since they can provide ride-through capability to the *DPGS*, island mode operation, power quality enhancement, and Microgrid functionalities [34]. Several control techniques based on the droop method have been proposed to connect *VSI* system in parallel to avoid communications between them. Droop method can be an useful way to control active and reactive power injected to the

grid. However, in this last case, the droop method has several problems to be solved, like line impedance dependence, bad regulation of active and reactive powers, and slow transient response.

This chapter is focused on a single-phase multifunctional inverter for *PV* systems application improved with additional power quality conditioning functionalities. The *PV* grid-connected converter is controlled on the basis of the droop control technique [27, 28, 34] which provides not only the voltage reference for the repetitive controller [61, 62], but it will also provide active power to local loads and injects reactive power into the grid voltage at fundamental frequency. Hence, it allows voltage sags compensation capability to be obtained, endowing voltage ride-through to the system. The proposed system can also support the voltage applied to local loads in the presence of voltage sags. A model and analysis of the whole system is given to properly choose the control parameters. Simulation and experimental results validate the proposed control using a 5*kVA PV* converter.

4.2 Voltage and frequency support

The power transfer between two sections of the line connecting a *DPGS* converter to the grid can be derived using the infinite bus model and complex phasors. From Figure 4.2, is possible to deduce that $Z_g = R + jX = Z_g \cdot e^{-j\theta_g} = Z_g(\cos\theta_g + j\sin\theta_g)$, being Z_g as the line impedance. The analysis below is valid for both single-phase and balanced three-phase systems. According to Figure 4.1, when the *DPGS* inverter is connected to the grid through a generic impedance, the active and reactive powers injected to the grid can be expressed as follows:

$$P = \frac{1}{Z_g}\left[\left(EV_g\cos\phi - V_g^2\right)\cos\theta_g + EV_g\sin\phi\cos\theta_g\right], \tag{4.1}$$

$$Q = \frac{1}{Z_g}\left[\left(EV_g\cos\phi - V_g^2\right)\sin\theta_g - EV_g\sin\phi\cos\theta_g\right], \tag{4.2}$$

where E is the *VSI* voltage, V_g is the grid voltage, ϕ is the phase between E and V_g. Considering that $\theta_g \approx 90^\circ$, $Z_g \approx X$ the line impedance is mainly inductive $X \gg R$, R may be neglected. Consequently, (4.1) and (4.2) can be rewritten as:

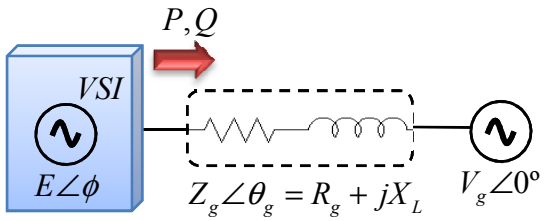

Figure 4.1: Scheme of the power flow transfer through the utility grid.

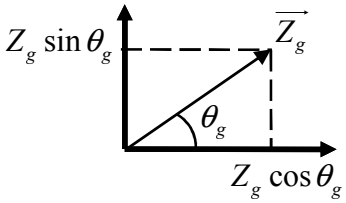

Figure 4.2: Graphical representation of the line impedance vectors.

$$P = \frac{EV_g}{X} \sin\phi, \tag{4.3}$$

$$Q = \frac{EV_g \cos\phi - V_g^2}{X}. \tag{4.4}$$

Arranging (4.3) and (4.4) and considering that the power angle ϕ is small,then $\sin\phi \cong \phi$ and $\cos\phi \cong 1$, the phase and the voltage difference between the grid and the *VSI* can be calculated as:

$$\phi \approx \frac{X}{EV_g} P, \tag{4.5}$$

$$E - V_g \approx \frac{X}{V_g} Q. \tag{4.6}$$

From these equations, it is possible to deduce that the power angle depends predominantly on the active power, whereas the voltage difference $E - V_g$ depends predominantly on the reactive power. In other words, the angle ϕ can be controlled by regulating the active power, whereas the inverter voltage E is controllable through the reactive power. The frequency control dynamically controls the power angle and, hence, the real power flow. Thus, by adjusting the active power P and the reactive power Q independently, frequency and amplitude of the grid voltage are determined. These conclusions form the basis of the frequency and voltage droop control through respectively active and reactive power.

4.3 Multifunctional converter for voltage sags mitigation

A. Shunt-converter for Voltage Sags mitigation

Often, series-converter topologies using instantaneous power theory are applied to multifunctional inverters with ride-through capability in presence of grid voltage sags [75], [52]. Alternatively, shunt devices are usually adopted to compensate small voltage variations which can be controlled by reactive power injection. Examples of applications can be found in line interactive uninterruptible power systems or active power filter topologies [4–6, 31, 44, 65, 79]. The ability to control the fundamental voltage at a certain point depends on the grid impedance and the power factor of the load. The compensation of voltage sags by current injection is difficult to achieve, because the grid impedance is usually low and the injected current has to be very high to increase the load voltage. The shunt converter can be current or voltage controlled for voltage sag compensation as shown in Figure 4.3. Following these figs, it is possible to observe that

$$\overrightarrow{I_c} = \overrightarrow{I_c} + \overrightarrow{I_L}, \tag{4.7}$$

where I_C, I_G and I_L are the currents delivered from the converter, to the grid, and to the load, respectively. Figure 4.4(a) shows the vector diagram of the voltage and currents.

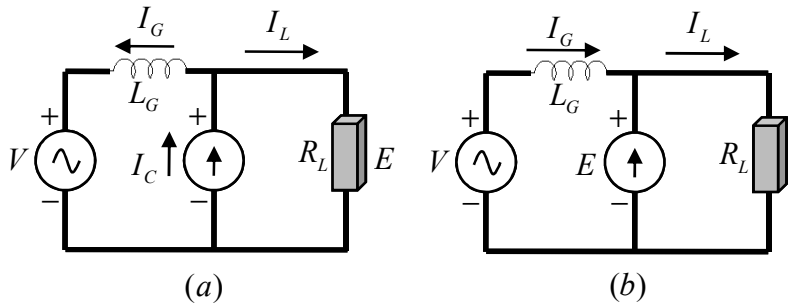

Figure 4.3: Equivalent circuit of the power stage of shunt converters: (a) Current controlled. and (b) Voltage controlled.

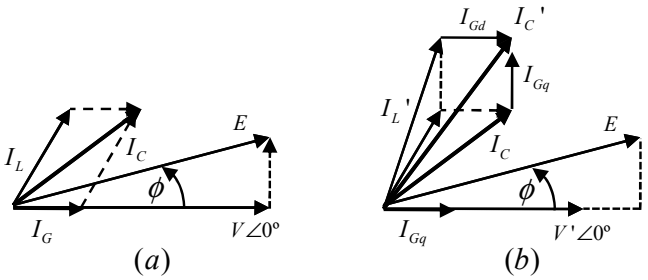

Figure 4.4: Vector diagram of the shunt converter providing both active and reactive power: (a) normal conditions; (b) voltage sag compensation of $0.15p.u.$

Note that when the amplitudes E and V_g are equal, only active power (direct I_G) flows into the inductor L_G. Therefore, if the controller is designed to provide only reactive power, when a voltage sag occurs $V_g' < E$, and

$$\overrightarrow{I_c'} = I_{Gd} + j\overrightarrow{I_{Gq}}, \tag{4.8}$$

with $I_{Gd} = I_G$, and $\overrightarrow{I_{Gq}}$ is the reactive current needed to compensate the voltage sag. The amplitude of the grid current depends on the value of the grid impedance since

$$\overrightarrow{I_c} = \frac{E\angle\phi - V_g\angle 0^{\mathrm{o}}}{jX}, \tag{4.9}$$

where X is the inductor reactance (ωL_G). If the shunt controller supplies the load with

both active and reactive power, in normal conditions it provides a compensating current $\overrightarrow{I_C} = \overrightarrow{I_L}$, hence, the system operates as in island mode and $\overrightarrow{I_G} = 0$. In the case of a voltage sag, the converter has to provide the active power required by the load and must still inject the reactive power needed to stabilize the load voltage as shown in Figure 4.4(b). The grid current in this case is mainly reactive.

It can be observed that during a voltage sag, the amount of reactive current needed to maintain the load voltage at the desired value is inversely proportional to the grid impedance. This means that a large inductance will help in mitigating voltage sags.

4.4 Power stage configuration

In case of PV systems, it can be advantageous to use the shunt-connected PV converter also for the compensation of small voltage sags. In this hypothesis, it is possible to control the voltage directly in order to stabilize the voltage profile while the current injection is controlled indirectly. Hence, the converter acts as a voltage source, supplying the load and maintaining the load voltage constant. Usually, the impedance of low-voltage distribution lines is mainly resistive, but, in the proposed topology, the PV converter is parallel connected to the grid through an extra inductance L_G (as shown in Figure 4.3).

From the exact expression of (4.3), we can conclude that the maximum active power transferred from or to the grid limits the maximum value of the inductance, as follows

$$X < \frac{EV_g}{P_{max}}, \tag{4.10}$$

whereas P_{max} is the maximum active power delivered by the *VSI* ($\theta_g = 90°$). By adding this inductance (L_G), the grid can be considered mainly inductive. In this hypothesis, it is possible to control the frequency and the voltage amplitude by adjusting active and reactive power independently. However, it is not convenient to choose a high value inductance L_G since the voltage regulation is directly affected by its voltage drop. The PV system shown in Figure 4.5 is controlled in order to provide the active and reactive power required. The converter is controlled with three control loops: in the outer one,

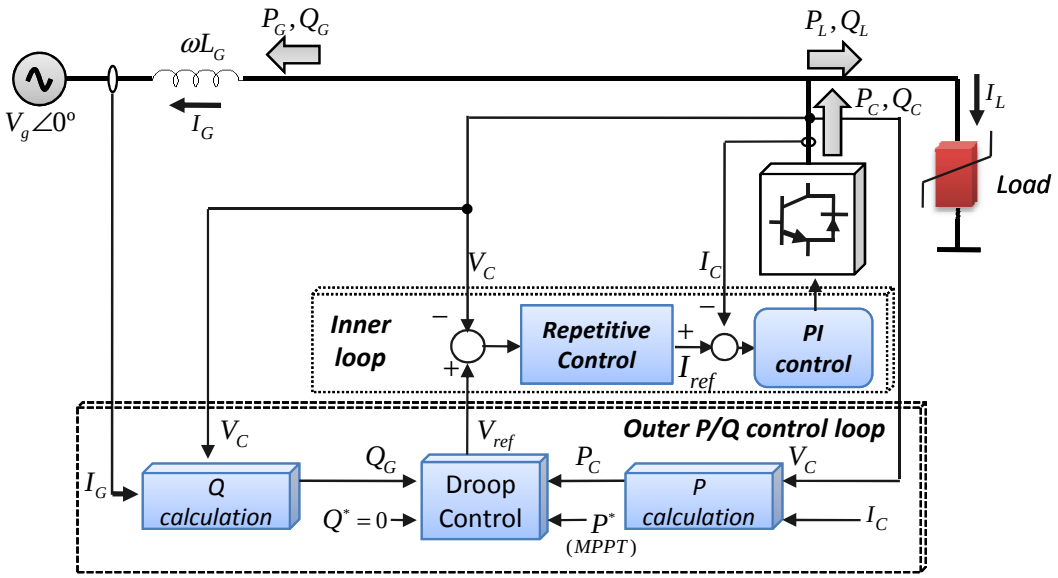

Figure 4.5: Block-diagram of the grid-connected *PV* system power stage and its control scheme.

the droop controller provides the voltage reference for the repetitive controller. It is possible to modify this voltage reference with the addition of another control loop designed to eliminate the average current present in the system due to a small offset in the inverter output voltage. This offset can be generated by errors in the voltage and current sensors, and by the physical differences between the upper and lower switches of the legs in the *PWM* inverter bridge [75], [52]. The new reference voltage is denoted in Figure 4.5 as V_{ref}. Hence, the voltage error is pre-processed by the repetitive controller, which is the periodic signal generator of the fundamental component of the selected harmonics. This kind of controller is suitable in cases where nonlinear loads are used, since it is able to supply current harmonics while maintaining low voltage distortion *THD*. In this case the third and the fifth ones are compensated [61], [62]. Finally the *PI* controller, in the inner loop, improves the stability of the system offering low-pass filter function. In the presence of a voltage sag, the grid current I_G is forced by the controller to have a sinusoidal waveform which is phase shifted by almost $90°$ with respect to the corresponding grid voltage.

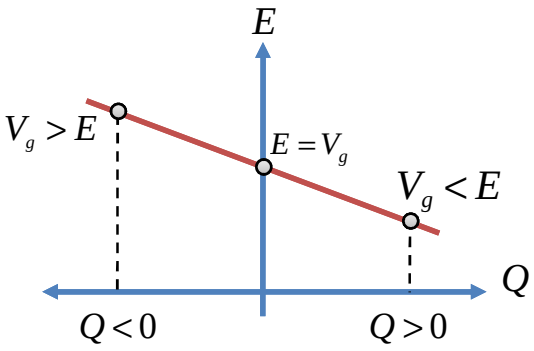

Figure 4.6: Relationship between the droop-based controller.

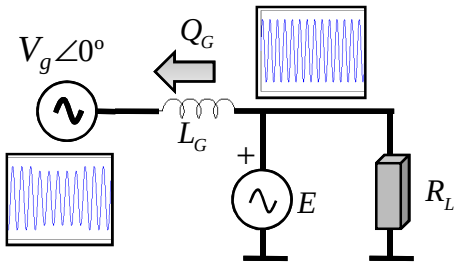

Figure 4.7: Power flow circuit in presence of a voltage dip.

4.5 Control design

The aim of this section is to develop a control structure for the proposed *PV* shunt-connected converter. The control objectives of the droop-based controller can be summed up as follows:

- ▷ Enhances the stability and the dynamic response by damping the system.
- ▷ Provides all the active power given by the *PV* source, and extracted in the previous stage by the maximum power point tracker (*MPPT*) [64].
- ▷ Supports the reactive power required by the grid when voltage sag is presented into the grid [75].

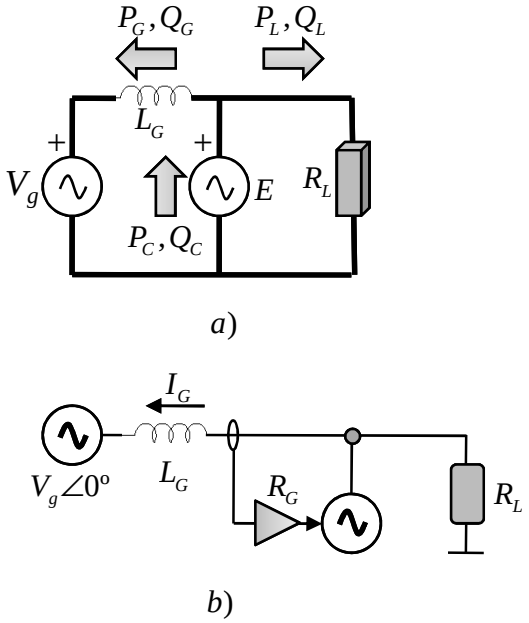

Figure 4.8: Power flow-based circuit modeling. a) Equivalent circuit b) General approach.

These three control objectives can be achieved by using the following control loops; the first one is done by implementing a virtual resistor, via the *VSI* control [34]:

$$V_{ref} < V^*_{ref} - I_G \cdot R_G. \tag{4.11}$$

However, adding damping into the system implies that the impedance seen by the *VSI* is not pure inductive, *i.e.* $R_g + jL_G$. Figure 4.5 depicts the block diagram of this proposed control strategy in which V_c and I_c denote the converter voltage and current, and I_g the grid current. By multiplying V_c by I_c and filtering the result, it is possible to obtain the active power delivered by the converter (P_c). On the other hand, multiplying V_c delayed 90^o by I_g, and then filtering the resulting value it, the reactive power flow from/to the grid (Q_g) can be obtained

$$P_C \triangleq \frac{1}{Z_g}\left[\left(EV_g - V_g^2\right)\cos\theta_g + EV_g\phi\sin\theta_g\right], \tag{4.12}$$

$$Q_C \triangleq \frac{1}{Z_g}\left[\left(EV_g - V_g^2\right)\sin\theta_g - EV_g\phi\cos\theta_g\right], \tag{4.13}$$

being $\tan\theta_g = X/R$. Based on the information of Figure 4.9, it is possible to calculate both the active P and reactive Q powers injected to the grid by the *VSI*, as can be seen in (4.1) and (4.2) For possible simplifications, is possible to transform P and Q to novel variables defined as P' and Q', which are independent from the magnitude and phase of the grid impedance:

$$P' \cong P_C \sin\theta_g - Q_G \cos\theta_g, \tag{4.14}$$

$$Q' \cong P_C \cos\theta_g + Q_G \sin\theta_g. \tag{4.15}$$

By substituting (4.12), (4.13) into (4.14), (4.15) the following expressions are yielded:

$$P' = \frac{EV_g}{Z_g}\sin\phi, \tag{4.16}$$

$$Q' = \frac{EV_g}{Z_g}\cos\phi - V_g^2. \tag{4.17}$$

Note that P' is mainly dependent on the phase ϕ, while Q' depends on the voltage difference between the *VSI* and the grid ($E - V_g$), as in pure inductive case (4.5), (4.6).

These new control variables (P' and Q') are independent from the grid impedance angle θ_g, thus we can use them into the droop method to control the active and reactive power flows. In order to inject the desired active power (P'_c , which should coincide with the power given by the *MPPT*), and to compensate the reactive power (normally $Q'_c = 0$), the following droop method control loops which uses the transformation (4.16),(4.17) are proposed

$$\phi = -G_p(s)\left[(P_C - P_C^*)\sin\theta_g - (Q_G - Q_G^*)\cos\theta_g\right], \tag{4.18}$$

$$E = E^* - G_q(s)\left[(P_C - P_C^*)\cos\theta_g + (Q_G - Q_G^*)\sin\theta_g\right]. \tag{4.19}$$

A *PI* controller is proposed to ensure that the *VSI* injects the active power delivered by the *MPPT* stage. On the other hand, a proportional controller is proposed for the reactive power compensation defined as G_p(s) and G_q(s), respectively:

$$G_p(s) = \frac{m_i + m_p s}{s}, \tag{4.20}$$

$$G_q(s) = n_p. \tag{4.21}$$

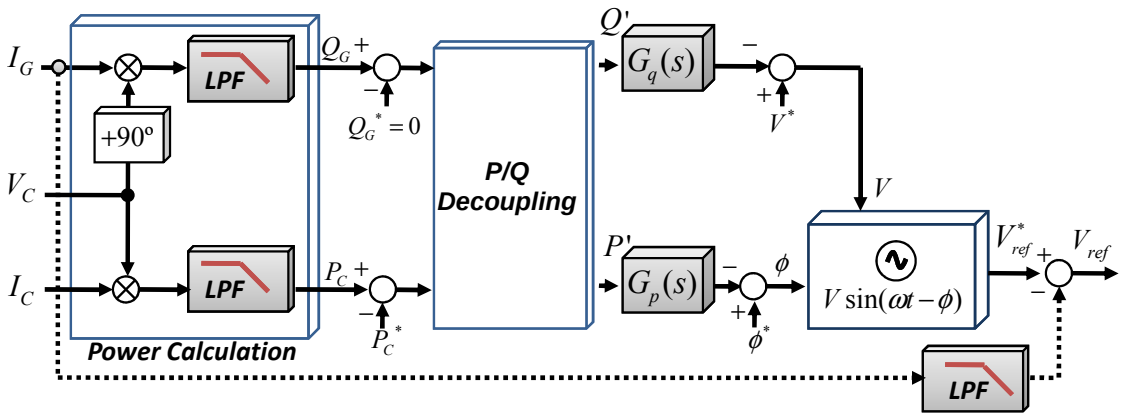

Figure 4.9: Block diagram of the droop control loops.

For reactive power compensation support, the coefficient n_p must be properly adjusted. By using (4.4), (4.6), (4.19) and (4.21) with $\theta_g = 90^o$ and $V_g = \alpha E^*$ (being α as the voltage sag percentage), is possible to obtain:

$$n_p = \frac{E^*\alpha(1-\alpha) - Q_{max}X}{Q_{min}E^*\alpha}, \tag{4.22}$$

where Q_{max} is the maximum reactive power flow that can be delivered by the *VSI*. Figure 4.9 shows details of the block diagram implementation of the droop controller, which is able to inject the desired active power P_c^* and to compensate reactive power Q_g.

4.6 System dynamics and control parameters design

In this section, the system dynamic model and the stability analysis are provided to properly design m_i and m_p coefficients of the *PI* compensator (4.20), corresponding to the active power injection control loop (4.18). A small signal analysis is provided in order to show the system stability and the transient response. The power calculation block uses a low pass second order filter in which the pass band is much smaller than the pass band of the inverter voltage control. Hence, both the power and reactive output

power measured from the power calculation block can be defined as:

$$\hat{p}_{meas}(s) = \frac{\omega_o^2}{s^2 + 2\zeta\omega_o s + \omega_o^2}\hat{p}'(s), \tag{4.23}$$

$$\hat{q}_{meas}(s) = \frac{\omega_o^2}{s^2 + 2\zeta\omega_o s + \omega_o^2}\hat{q}'(s), \tag{4.24}$$

where ω_o is the resonance frequency, and ζ the damped coefficient. By doing a small signal approximation in order to linearize the equations, it yields

$$\hat{p}_{meas}(s) = \frac{\omega_o^2}{s^2 + 2\zeta\omega_o s + \omega_o^2}\left[\frac{V_g \sin\Phi\hat{e}(s) + V_g E\cos\Phi\hat{\phi}(s)}{Z_g}\right], \tag{4.25}$$

$$\hat{q}_{meas}(s) = \frac{\omega_o^2}{s^2 + 2\zeta\omega_o s + \omega_o^2}\left[\frac{V_g \cos\Phi\hat{e}(s) - V_g E\sin\Phi\hat{\phi}(s)}{Z_g}\right] + \omega_o^2\hat{q}'(s), \tag{4.26}$$

where the lower-case variables with the symbol ˆ indicate small signal values, and uppercase variables are the steady-state values. By using (4.20), (4.21) and (4.24), (4.25) we can obtain

$$\hat{\phi}(s) = -\frac{m_i + m_p s}{s}\hat{p}_{meas}(s), \tag{4.27}$$

$$\hat{e}(s) = -n_i\hat{q}_{meas}(s). \tag{4.28}$$

From (4.27), (4.28) the following expressions can be derived

$$\hat{\phi}(s) = -\frac{m_i + m_p s}{s}\left(V_g \sin\Phi\hat{e}(s) + V_g E\cos\Phi\hat{\phi}(s)\right), \tag{4.29}$$

$$\hat{e}(s) = -n_i\left(V_g \cos\Phi\hat{e}(s) - V_g E\sin\Phi\hat{\phi}(s)\right). \tag{4.30}$$

By combining (4.25), (4.26) and (4.27), we can be obtain the following fifth order characteristic equation

$$s^5 + a_4 s^4 + a_3 s^3 + a_2 s^2 + a_1 s + a_0 = 0 \tag{4.31}$$

Being,

$$a_4 = 4\omega_o \zeta Z_g, \tag{4.32}$$

$$a_3 = V_g \omega_o^2 \cos\Phi(n_p + Em_p) + 2\omega_o^2(1 + 2\zeta^2)Z_g, \tag{4.33}$$

$$a_2 = 2V_g \omega_o^2 \zeta \cos\Phi(n_p + Em_p) + \omega_o^2 V_g E \cos\Phi m_i + 4\zeta\omega_o^3 Z_g, \tag{4.34}$$

$$a_1 = V_g \omega_o^4 \cos\Phi(n_p + Em_p) + V_g E\omega_o^3(2\zeta \cos\Phi m_i + \frac{V_g}{Z_g}\omega_o n_p m_p) + \omega_o^4 Z_g, \tag{4.35}$$

$$a_0 = V_g E \omega_o^4 m_i(\cos\Phi + \frac{V_g}{Z_g} n_p). \tag{4.36}$$

the steady-state values of the active power are $P = P^*$, and calculating Q using (4.2) in steady-state, defined as

$$Q_{ss} = \frac{1}{Z_g}\left[(EV_g \cos\Phi - V_g^2)\sin\theta_g - EV_g \sin\Phi\cos\theta_g\right], \tag{4.37}$$

the steady-state phase and amplitudes can be calculated from (4.12), and (4.13) as follows

$$\Phi = \arctan\left(\frac{P_c' \sin\theta_g - Q_{ss}\cos\theta_g - EV_g \sin\Phi\cos\theta_g}{P_C' \cos\theta_g + Q_{ss}\sin\theta_g + (V_g^2/Z_g)}\right), \tag{4.38}$$

$$E = \frac{V_g^2 \cos\theta_g + P_C^* Z_g}{V_g(\cos\theta_g \cos\Phi + \sin\theta_g \sin\Phi)}. \tag{4.39}$$

The model obtained has been used to extract the family of root locus as can be depicted in Figure 4.10(a) and Figure 4.10(b). Figure 4.10(a) shows for convenience the dominant poles (λ_1 and λ_2) root locus. It illustrates that when m_p is increased, the poles go toward the imaginary axis, becoming a faster oscillatory system. Fig 4.10(b) depicts the root locus behavior when m_i is increased. Note that λ_3, λ_4, and λ_5 are far away from λ_1 and λ_2. Thus, using m_p and m_i it is possible to locate the poles where it is more convenient. Furthermore, this dominance can illustrate that the obtained model can be adjusted as a second or even a first order system. By using this model (4.31), the stability of the system has been studied for large grid inductance L_G variations. Figure 4.10(c) shows that the fifth order system is stable if the value of L_G is more than $8mH$. Below this value, the real part of the eigenvalues λ_4 and λ_5 is positive, so the system remains unstable. On the contrary, if we increase the value of L_G, those eigenvalues are

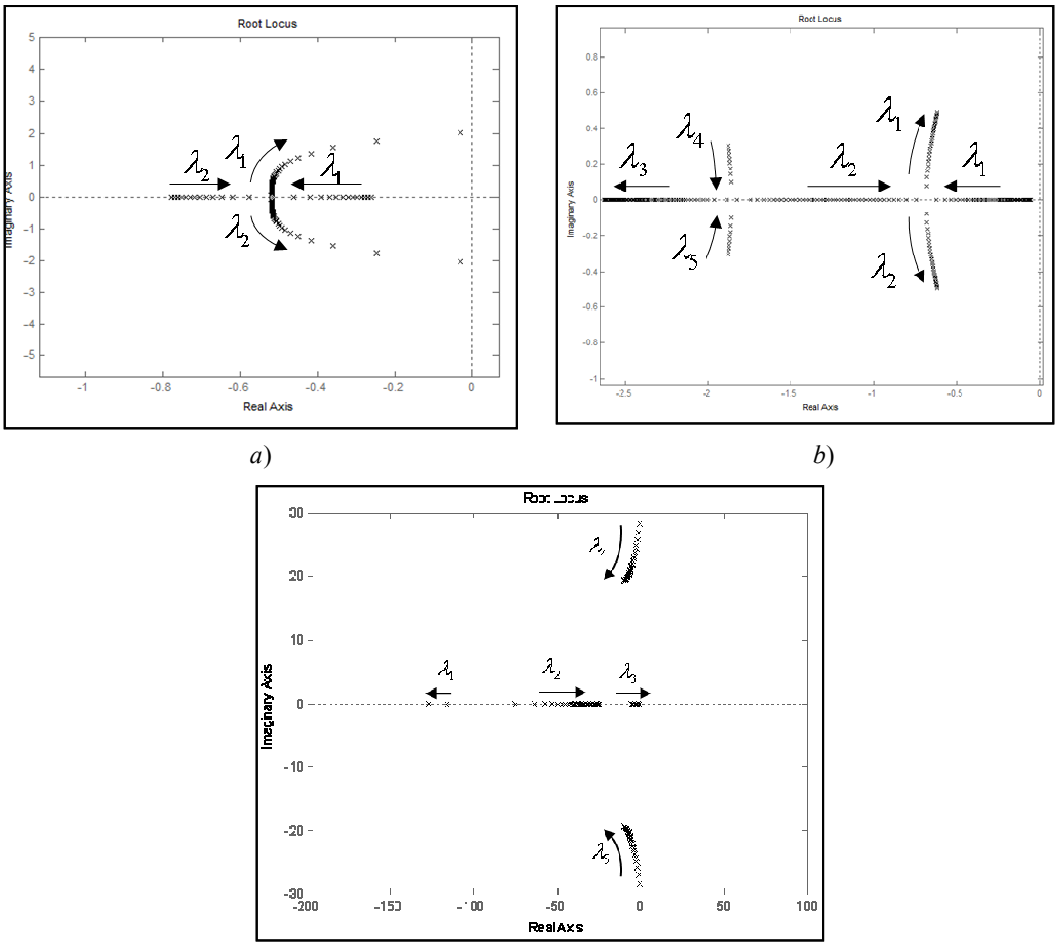

a) *b*)

c)

Figure 4.10: a) Root locus for $0.00002 < m_p < 0.001$ and $m_i = 0.0002$. b) Root locus for $0.000002 < m_i < 0.0018$ and $m_p = 0.00006$. c) Root locus diagram for grid inductance variations: $8.5mH < L_G < 5000mH$.

stable. Although λ_2 and λ_3 are attracted towards the imaginary axis, they never cross it.

Table 4.1: Power Stage and Control Parameters

Parameter	*Symbol*	*Value*	*Units*
Grid voltage	E	311	V
Grid frequency	ω	$2\pi 50$	Rad/s
Grid inductance	L_G	15	mH
Load Resistance	R	40	Ω
Sample frequency	F_s	6400	Hz
Integral droop P coefficient	m_i	0.00002	W/rd
Proportional droop P coefficient	m_p	0.006	W/rd·s
Proportional amplitude droop	n_p	0.15	VAr/V
Resonance frequency of measuring filter	ω_o	31.4	Rad/s

4.7 Simulation Results

Considering the PV system represented in Figure 4.5, different tests have been performed in order to validate the proposed control. All the physical parameters of the system are defined in Table 4.1. Figure 4.11 shows the steady-state current waveforms of the converter, grid,and load (I_c, I_g and I_L). In the case of a purely resistive load absorbing $1200W$, the block diagram shown in Figure 4.9 is modified taking into account that the active power reference P_c^* should coincide with the nominal active power and the reactive power reference $Q_c^* = 0$. The results are shown in Figure 4.12. This figure illustrates the transient response of the active and reactive powers when the active power reference was changed from $1200W$ to $600W$ at $t = 5s$ and the reactive power reference from 0 to 500 VAr at $t = 10s$. The results show the P and Q injection decoupling of the proposed control strategy. The validity of the proposed control has also been tested in the presence of a voltage sag, equals to 0.15 $p.u.$ which occurs at t=1.5s (see Figure 4.13). In this case, the converter provides the reactive power needed to compensate the sag. The current waveforms of the converter, the grid, and the load are shown in Figure 4.14. A detail of the grid voltage and grid current waveforms during the voltage sag is shown in Figure 4.15 Notice that the controller endows voltage ride-through capability to the system when voltage sags are presented in the grid.

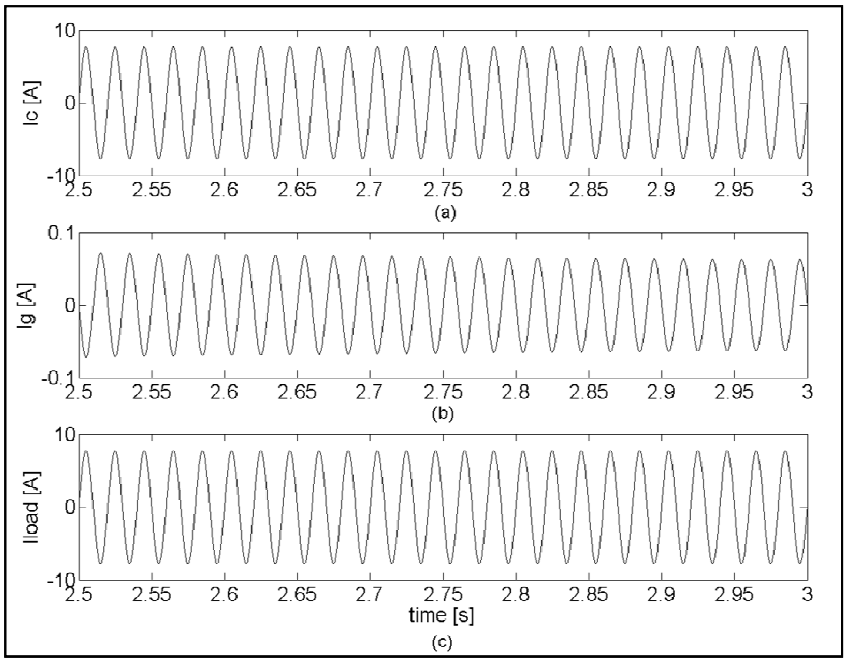

Figure 4.11: Steady-state operation during grid normal condition: (a) Inverter current I_C (b) Grid current I_G, and (c) Load current I_L.

Similar ride-through capability tests were performed when the active power provided by the inverter (500 W) is lower than the power required by the load. In this situation, the grid injects the rest of the power to the system (700 W), and the system injects to the grid the necessary reactive power in case of a voltage sag. Figure 4.16 shows the active and reactive power provided by the inverter for a voltage sag, and Figure 4.17 shows the corresponding current waveforms. From these results, we can conclude that the system also has ride-through capabilities.

Another test was performed in the case of existence of high-value voltage harmonics in the grid, as depicted in Figure 4.18. Figure 4.19 shows the voltage current waveforms. Note that the system injects harmonic current to the grid in order to maintain the quality of the load voltage waveform Figure 4.18 shows the active and reactive power transient responses for changes in the power references, as done in Figure 4.12. In this case, the system also exhibits good tracking performance.

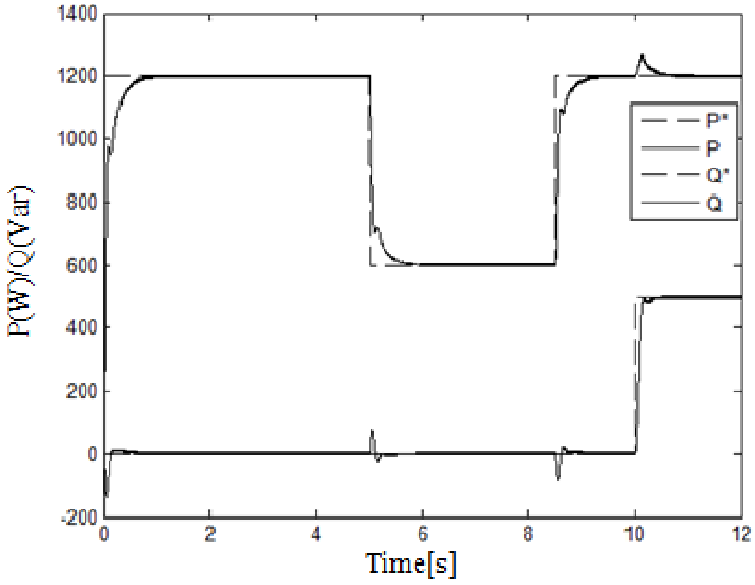

Figure 4.12: Active and reactive power transient responses and step changes provided by the *PV* inverter during normal operation.

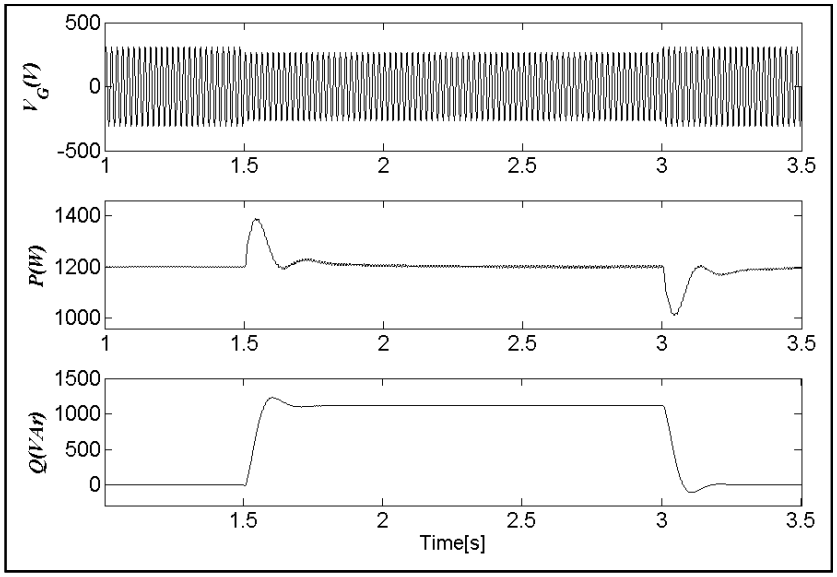

Figure 4.13: Active and reactive power provided by the PV inverter in the presence of a voltage sag of 0.15 p.u.

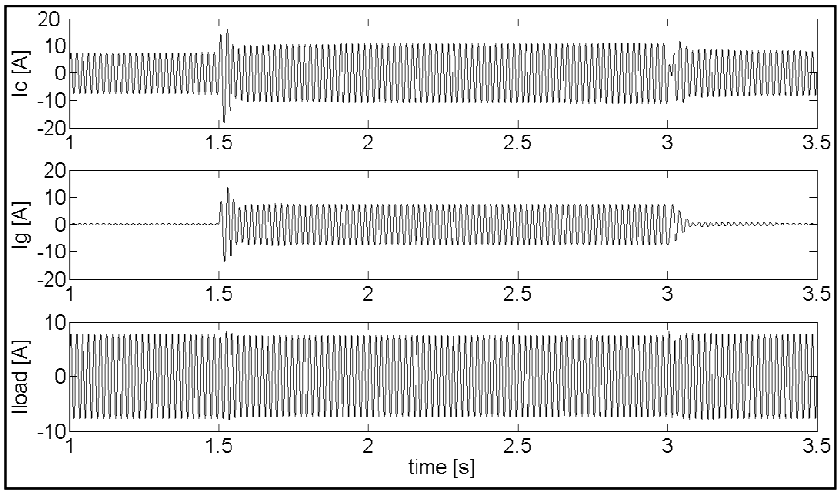

Figure 4.14: Current waveforms in case of a voltage sag of $0.15p.u.$ (inverter current I_C, grid current I_G, and load current I_L).

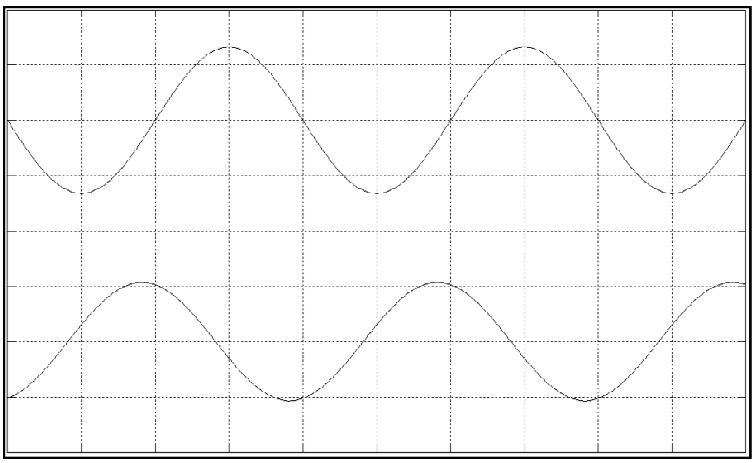

Figure 4.15: Detail of the waveforms during the sag: grid voltage (upper) [100V/div], and grid current (lower) [10A/div].

Finally, the system was tested by supplying a nonlinear load consisting of a diode-rectifier with an RC load, as is depicted in Figure 4.20. Figure 4.21 shows the inverter output voltage, and the active and reactive power provided. This case exhibits the good tracking performance, similar to the case of supplying linear loads (see Figure 4.18).

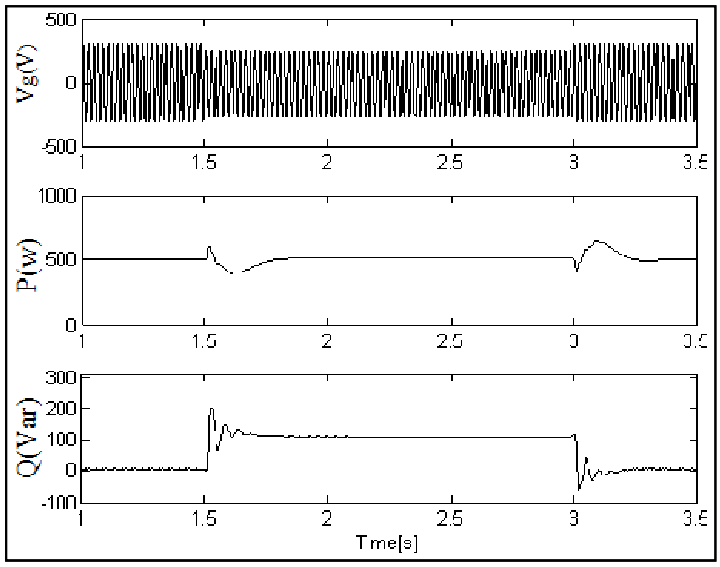

Figure 4.16: Active and reactive power provided by the *PV* inverter in presence of a voltage sag of 0.15p.u. when $P_c^* = 500W$.

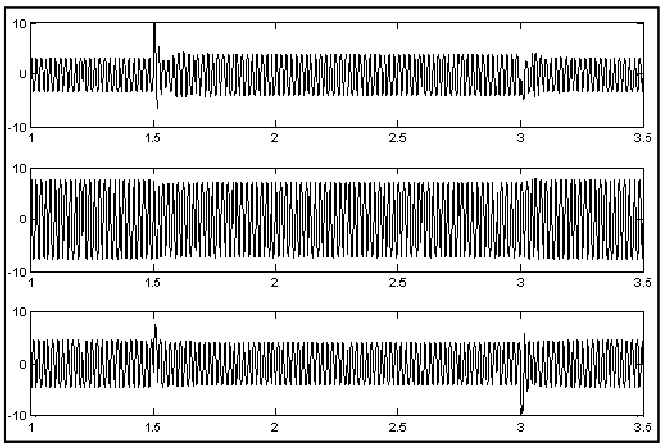

Figure 4.17: Current waveforms in case of a voltage sag of 0.15 p.u. (inverter current I_C(upper), load current I_L (middle) and grid current I_G (bottom) when $P_c^* = 500W$).

Figure 4.22 shows the current waveforms of the inverter,the nonlinear load, and the grid. The system provides shunt active power capabilities, since the grid current

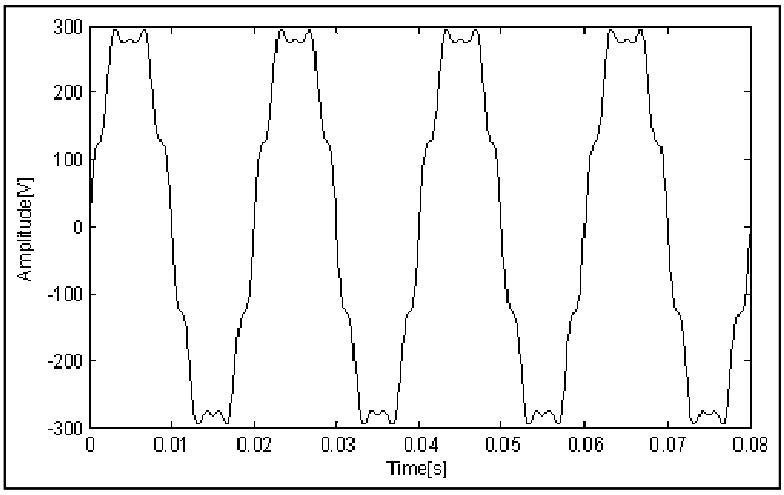

Figure 4.18: Grid voltage waveform in presence of 1st, 3rd, 5th 7th and 9th voltage harmonics.

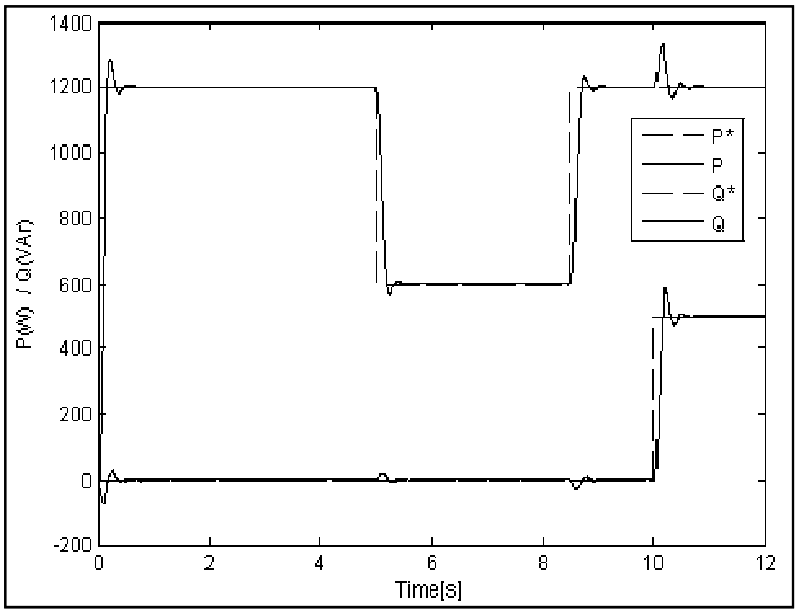

Figure 4.19: Active and reactive power transient responses and step changes provided by the *PV* inverter using the distorted grid waveform.

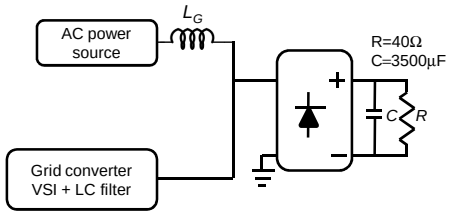

Figure 4.20: Single-phase rectifier with R-C circuit as nonlinear load.

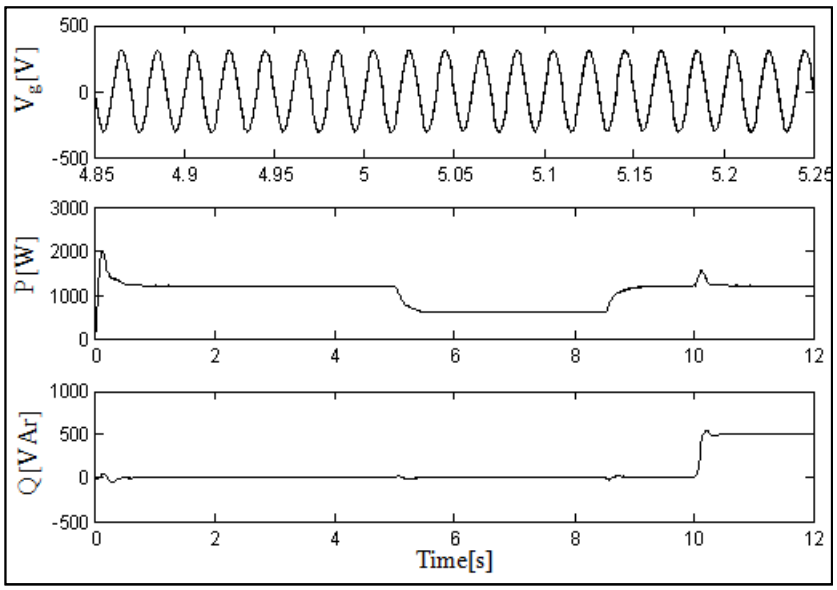

Figure 4.21: Inverter output voltage (detail), active and reactive power transient responses under a non-linear load.

waveform is harmonic free and the power factor is near one. According to the obtained results, the system shows high performances like: active and reactive power tracking, voltage sags ride-through, voltage and current harmonic compensation.

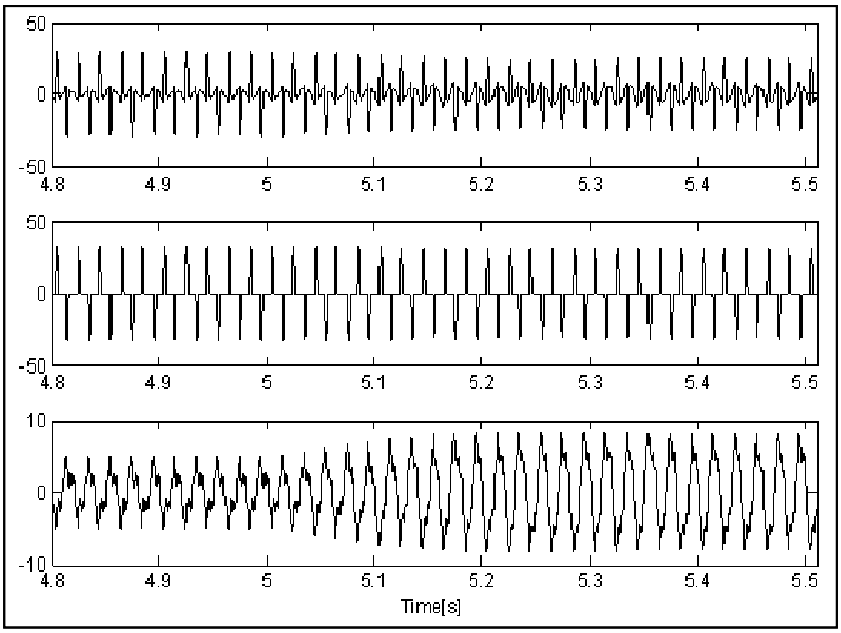

Figure 4.22: Current waveforms in case of a non-linear load and V_g with harmonics: inverter current I_C (upper), load current I_l (middle), and grid current I_G (bottom).

4.8 Experimental results

Experimental tests have been carried out in a laboratory set-up to test the performance of the *PV* system with the shunt-connected multifunctional converter. The hardware setup shown in Figure 4.23 and it consists of the following equipment: a Danfoss VLT 5006 7.6*kVA* inverter, on which only two legs are used, hence the apparent power is 2/3 of 7.6*kVA*, two series connected dc voltage sources to simulate *PV* panels string and Dspace 1104 system. A Pacific *ac* power source emulates the main grid. It is set in order to provide a voltage sag of 0.15 p.u. The *PV* multifunctional converter is connected to the grid through an *L*-*C* filter whose inductance is $1.4mH$, the capacitance is $5\mu F$ in series with a resistance of 1Ω; besides an inductance L_G of $15mH$ has been added to the grid impedance as explained in the previous Sections. The performances of the proposed controllers are in accordance with the simulation results. The experimental results obtained in the same conditions (voltage sag duration equal to 1.5s) are reported in Figure 4.24. Figure 4.25 and Figure 4.26 show a detail of the voltage waveforms,

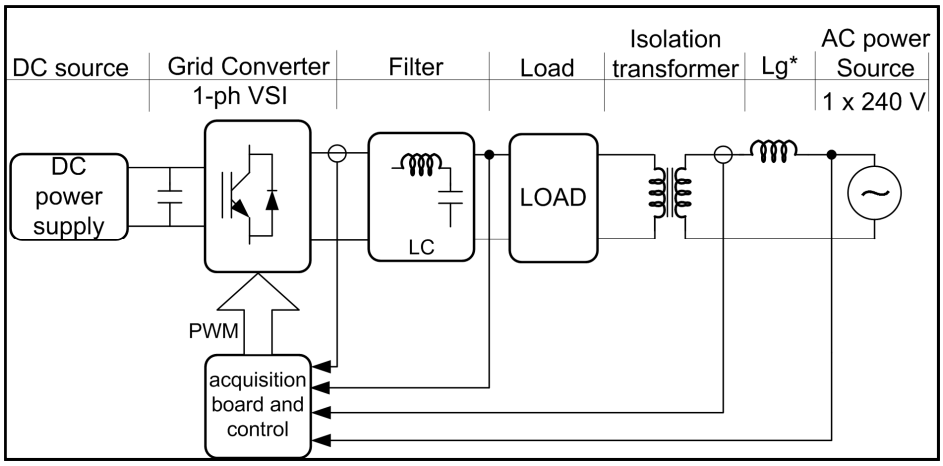

Figure 4.23: Laboratory Setup

the grid voltage, and the injected current during the sag. Notice that *PV* converter provides voltage support and maintaining the load voltage constant by injecting 7A of pure reactive current into the grid during the voltage sag. These results are in accordance with the simulation tests (see Figs. 4.13 and 4.14).

4.9 Conclusions

In this chapter, future ancillary services in *DPGS* should contribute to the reinforcement of the distribution grid and to maintain proper quality of supply. Also, a single-phase photovoltaic system with power quality conditioner functionality has been presented. The voltage-controlled *PV* converter is shunt-connected to the grid and a droop controller provides the voltage reference where a repetitive algorithm controls the voltage provided by the *PV* converter. An inductance has been added on the grid side; hence it can be considered that the *PV* system is connected to a mainly inductive grid. The control strategy of the grid frequency and the grid voltage amplitude is based on the independent adjustment of active and reactive power. The *PV* converter provides grid voltage support at fundamental frequency. In case of a voltage sag, the converter has to provide the active power required by the load and must still inject the reactive power needed to stabilize the load voltage. Hence, the system shows high performances like:

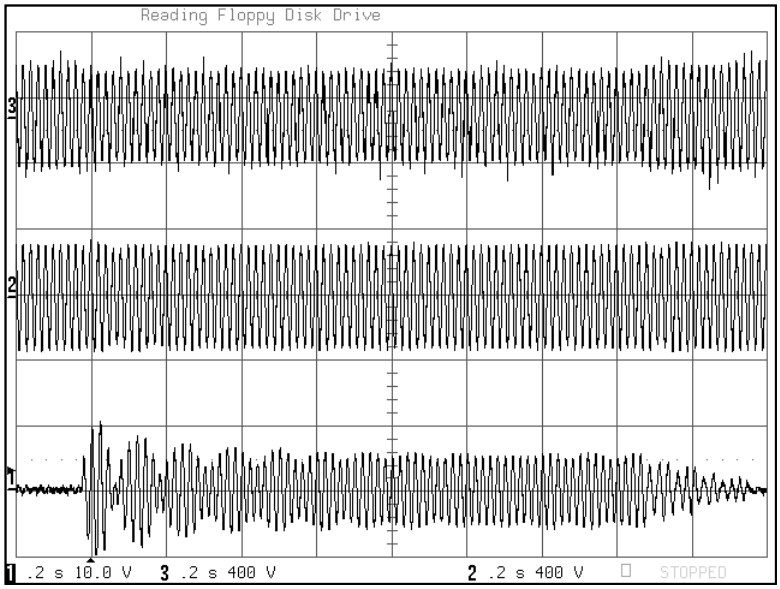

Figure 4.24: Experimental results in case of a voltage sag of 0.15 p.u. (voltage controlled inverter with droop control): 1) grid current [10V/div], 2) load voltage [400 V/div], 3) grid voltage [400V/div].

active and reactive power tracking, voltage sags ride-through, voltage and current harmonic compensation. The experimental results confirm the validity of the proposed solution in the presence of small voltage sags.

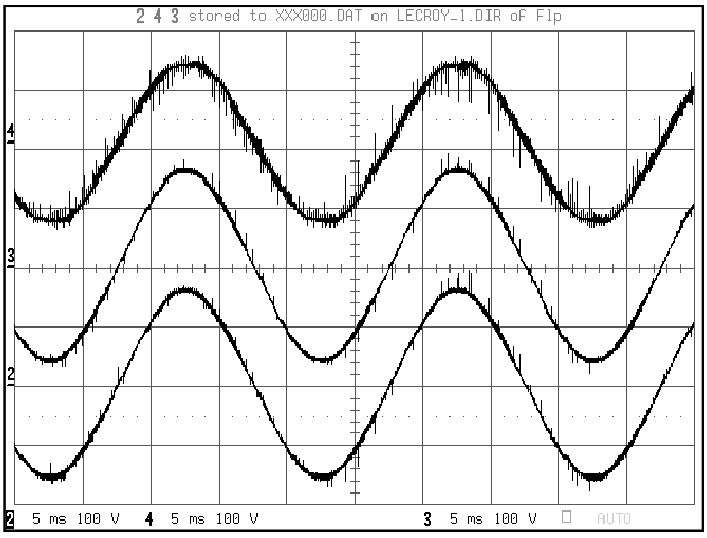

Figure 4.25: Voltage waveforms during the sag [100V/div]: grid voltage (channel 4, upper), capacitor voltage (channel 3, middle) and load voltage (channel 3, lower).

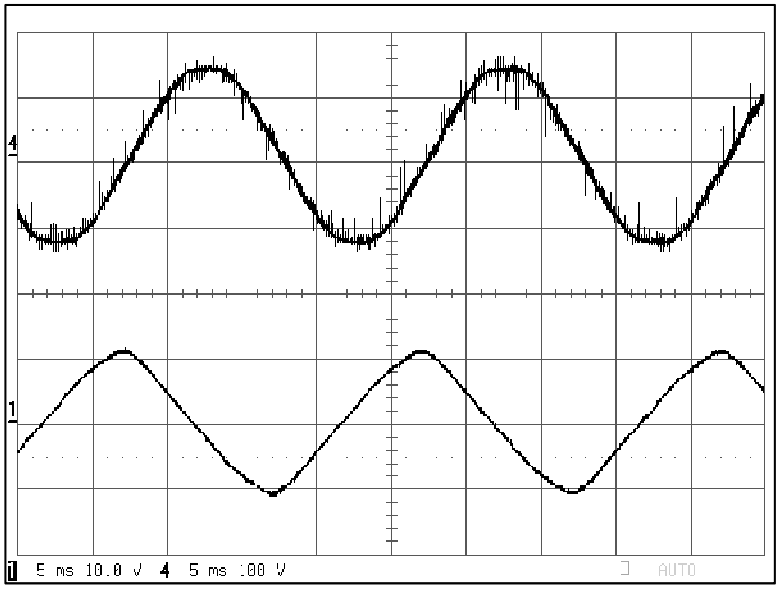

Figure 4.26: Waveforms of the grid voltage (channel 4, upper) [100V/div], and the grid current (channel 1, lower) [10A/div] during the sag.

CHAPTER 5

HIERARCHICAL CONTROL FOR FLEXIBLE MICROGRIDS

5.1 Introduction

In Microgrids field, the variable nature of some renewable energy systems, such as photovoltaic (*PV*) or wind energy, relies on natural phenomena, such as sunshine or wind. Consequently, it is difficult to predict the amount of power that can be obtained through these prime sources, and the peaks of power demand do not necessarily coincide with the generation peaks. Hence, storage energy systems are required if we want to supply the local loads in an uninterruptible power supply (*UPS*) fashion [3], [49], [18], [20]. Some small and distributed energy storage systems can be used for this purpose, such as flow batteries, fuel cells, flywheels, superconductor inductors, or compressed air devices.

The DG concept is growing in importance, pointing out that the future utility line will be formed by distributed energy resources and small grids (minigrids or Microgrids) interconnected between them [31], [32]. In fact, the responsibility of the final user is to produce and store part of the electrical power of the whole system. Hence, Microgrid can export or import energy to the utility through the point of common coupling (*PCC*). Moreover, when there is utility failure, the Microgrid can still work as

an autonomous grid. As a consequence, these two classical applications, namely, grid-connected and islanded operations, can be used in the same application. In this sense, the droop control method is proposed as a good solution to connect, in parallel, several inverters in an island mode [8, 14, 39, 60]. However, although it has been investigated and improved, this method by itself is not suitable for the coming flexible Microgrids. Further, although there are line-interactive *UPSs* in the market, still, there are no line-interactive *UPS* systems able to operate in parallel autonomously, forming a Microgrid [4], [79].

In this chapter, a control scheme for *UPSs* connected in parallel, forming a Microgrid, is proposed. The Microgrid presented is formed by parallel-connected UPS inverters. Its difference from the conventional parallel *UPS* systems [37, 58, 67] is that the flexible Microgrid can not only import and export energy to the main grid, but can also operate in grid-connected or in island modes. The presented application is a *PV* system with 6-kVA line-interactive *UPS* units [13]. The typical applications of these PV-*UPS* systems are domestic, up to 30kVA. The UPS inverters use a droop control function in order to avoid critical communication between the modules. The droop function can manage the output power of each *UPS* as a function of the battery charge level. The inverters, compared to the conventional methods, act as voltage sources even when they are connected to the grid [28], [84]. In this situation, they are able to share power with the grid, based on its nominal power. Finally, the intelligent static bypass switch connects or disconnects the Microgrid and sends proper references to the local *UPS* controllers by means of low bandwidth communications.

5.2 Microgrid structure and control

A flexible Microgrid has to be able to import/export energy from/to the grid, control the active and reactive-power flows, and manage the energy storage. Figure 5.1 shows a Microgrid, including small generators, storage devices, and local critical and noncritical loads, which can operate both, connected to the grid or autonomously in island mode. This way, the power sources (*PV* arrays, small wind turbines, or fuel cells) or storage devices (flywheels, superconductor inductors, or compressed air systems) use electronic

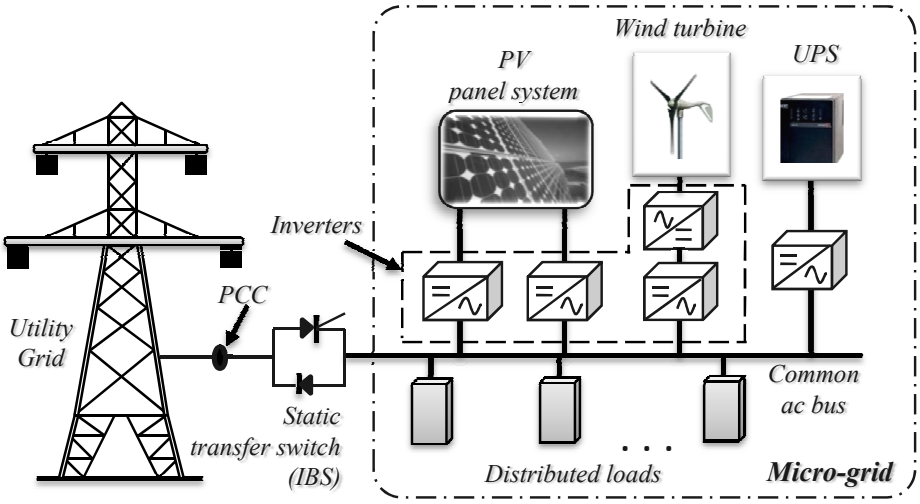

Figure 5.1: Typical structure of inverter Microgrid based on renewable energies.

interfaces between them and the Microgrid. Usually, these interfaces are ac/ac or dc/ac power electronic converters, also called inverters. Traditionally, inverters have two separate operation modes acting as a current source, if they are connected to the grid, or as a voltage source, if they work autonomously. In this last case for security reasons and to avoid islanding operation, the inverters must be disconnected from the grid when a grid fault occurs. However, if we want to impulse the use of decentralized generation of electrical power, the DG, and the implantation of the Microgrids, islanding operation should be accepted if the user is completely disconnected from the grid. In this case, the Microgrid could operate as an autonomous grid, using the following three control levels.

- ▷ *Primary control*: The inverters are programmed to act as generators by including virtual inertias through the droop method, which ensures that the active and the reactive powers are properly shared between the inverters.

- ▷ *Secondary control*: The primary control achieves power sharing by sacrificing frequency and amplitude regulation. In order to restore the Microgrid voltage to nominal values, the supervisor sends proper signals by using low bandwidth communications. This control also can be used to synchronize the Microgrid with

the main grid before they have to be interconnected, facilitating the transition from islanded to grid-connected mode.

- ▷ *Tertiary control*: The set points of the Microgrid inverters can be adjusted, in order to control the power flow, in global (the Microgrid imports/exports energy) or local terms (hierarchy of spending energy). Normally, the power-flow priority depends on economic issues. Economic data must be processed and used to make decisions in the Microgrid.

Figure 5.1 shows the schematic diagram of a Microgrid. In our example, it consists of several *PV* strings connected to a set of line-interactive *UPSs* forming a local ac Microgrid, which can be connected to the utility mains through an intelligent bypass switch (*IBS*). The *IBS* is continuously monitoring both of its sides, namely, the grid main and the Microgrid. If there is a fault in the utility main, the *IBS* will disconnect the Microgrid from the grid, creating an energetic island. When the main is restored, all *UPS* units are advised by the *IBS* to synchronize with the mains to properly manage the energy reconnection. The Microgrid has two main possible operation modes: grid-connected and islanded modes. The transitions between both modes and the connection or disconnection of UPS modules should be made seamlessly (hot-swap or plug-and-play capabilities) [25, 41, 57, 94]. In this sense, the droop control method has been proposed for islanding Microgrids [86]. Taking into account the features and limitations of the droop method, we propose a control structure for a Microgrid which could operate in both grid-connected and islanded modes. The operation of the inverters is autonomous, contrary to other Microgrid configurations [37] [67] [58] which use master-slave principles. Only low bandwidth communications are required in order to control the Microgrid power flow and synchronization with the utility grid.

5.3 Primary Control Strategy

The control of the UPS inverter is based on three control loops [29]: 1) the inner voltage and current regulation loops; 2) the intermediate virtual impedance loop; and 3) the outer active and reactive-power-sharing loops. The inner voltage and current regulation

loops can be implemented by using a conventional *PI* multiloop control or generalized integrators. The virtual output impedance loop is able to fix the output impedance of the inverter by subtracting a processed portion of the output current i_o to the voltage reference of the inverter V_{ref} [30]. The output impedance for each current harmonic has been programmed by using a discrete Fourier transformation, as follows [33]:

$$V^* = V_{ref} - s \sum_{odd}^{h-H} L_{Vh} \cdot i_{oh}, \tag{5.1}$$

where V^* is the voltage reference of the inner control loops, i_{oh} is the $h-th$ harmonic current, and L_{Vh} is the impedance associated with each component. The output impedance of each harmonic can be adjusted to share properly the load currents but without greatly increasing the voltage total harmonic distortion (*THD*). Moreover, a hot-swap operation, $i.e.$, the connection of more UPS modules without causing large current disturbances, can be achieved by using a soft-start virtual impedance. The soft start is achieved by programming a high output impedance at the inverter connection to the Microgrid. After the connection, the output impedance is then reduced slowly to a nominal value. This operation can be described by

$$L_v = L^*_{Df} + (L^*_{Do} - L^*_{Df}) \cdot e^{\frac{-t}{T_{st}}}, \tag{5.2}$$

where L^*_{Do} and L^*_{Df} are the initial and final values of the output impedance and T_{st} is the time constant of the soft-start operation. Once the output impedance is fixed, the droop method can operate properly. In the droop equations, derivative terms have been included to improve the transient response of the system [34]

$$\omega = \omega^* - m(P - P^*) - m_d \frac{d(P - P^*)}{dt}, \tag{5.3}$$

$$E = E^* - n(Q - Q^*) - n_d \frac{d(Q - Q^*)}{dt}, \tag{5.4}$$

where m_d and n_d are, respectively, the active and reactive derivative droop coefficients. Figure 5.4 shows the block diagram of the control loops of one inverter connected to the Microgrid, including the inner current and voltage loops; the virtual impedance loop (5.1) with soft start (5.2); and the power-sharing loops (5.3) and (5.4).

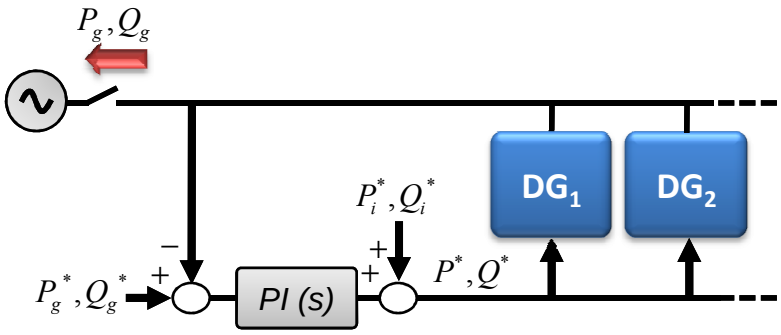

Figure 5.2: Power flow control between the grid and the Microgrid.

5.4 Secondary Control Structure

The aim of this section is to develop a flexible control that can operate in grid-connected and islanded operations and to enable the transition between both modes.

A. Grid-Connected Operation In this mode, the Microgrid is connected to the grid through an *IBS*. In this case, all *UPSs* have been programmed with the same droop function [29], [33], [82], [9], where P^* and Q^* are the desired active and reactive powers. Normally, P^*should coincide with the nominal active power of each inverter, and $Q^* = 0$.

$$\omega = \omega^* - m \cdot (P - P^*), \tag{5.5}$$

$$E = E^* - n \cdot (Q - Q^*). \tag{5.6}$$

However, we have to distinguish between two possibilities: 1) importing energy from the grid or 2) exporting energy to the grid. In the first scenario, in which the total load power is not fully supplied by the inverters, the *IBS* must adjust P. By using low bandwidth communications to absorb the nominal power from the grid in the *PCC*. This is done with small increments and decrements of P. as a function of the measured grid power, by using a slow PI controller, as follows:

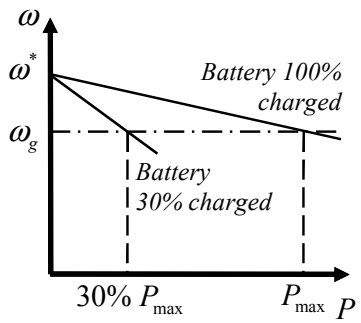

Figure 5.3: Droop characteristic as function of the battery charge level.

$$P^* = k_p(P_g^* - P_g) + k_i \int (P_g^* - P_g)dt + P_i^*, \tag{5.7}$$

where P_g and P_g^* are the measured and the reference active powers of the grid, respectively, and P_i^* is the nominal power of the inverter i. This way, the *UPSs* with a low battery level can switch to charger mode by using $P^* < 0$. Similarly, we proposed that reactive-power control law can be defined as

$$Q^* = k_p'(Q_g^* - Q_g) + k_i' \int (Q_g^* - Q_g)dt + Q_i^*, \tag{5.8}$$

where Q_g and Q_g^* are the measured and the reference reactive powers of the grid, respectively, and Q_i^* is the nominal reactive power. The second scenario occurs when the power of the prime movers ($e.g.$ *PV* panels) is much higher than those required by the loads and when the batteries are fully charged. In this case, the *IBS* may enforce to inject the rest of the power to the grid. Moreover, the *IBS* has to adjust the power references.

5.5 Islanded Operation

When the grid is not present, the *IBS* disconnects the Microgrid from the main grid, starting the autonomous operation. In such a case, the droop method is enough to

guarantee proper power sharing between the *UPSs*. However, the power sharing should take into account the batteries charging level of each module. In this case, the droop coefficient m can be adjusted to be inversely proportional to the charge level of the batteries, as shown in Figure 5.3

$$m = \frac{m_{min}}{\alpha}, \tag{5.9}$$

where m_{min} is the droop coefficient at full charge and α is the level of charge of the batteries ($\alpha = 1$ is fully charged and $\alpha = 0.01$ is empty). The coefficient α is saturated to prevent m from rising to an infinite value.

5.6 Transitions Between Grid-Connected and Islanded Operation

When the *IBS* detects some fault in the grid, it disconnects the Microgrid from the grid. In this situation, the *IBS* can readjust the power reference to the nominal values; however, this action is not mandatory. Instead, the *IBS* can measure the frequency and the amplitude of the voltage inside the Microgrid and move the set points (P^* and Q^*) in order to avoid the corresponding frequency and amplitude deviations of the droop method. In contrast, when the Microgrid is working in islanded mode and the *IBS* detects that the voltage outside of the Microgrid is stable and fault-free, the islanded mode can resynchronize the Microgrid with the frequency, amplitude, and phase of the grid in order to reconnect the Microgrid to the grid seamlessly.

5.7 Small-signal Analysis

A small-signal analysis is proposed to investigate the stability and transient response of the system. In order to ensure stability, a similar analysis as in [21] has been done, which results in a third-order system.

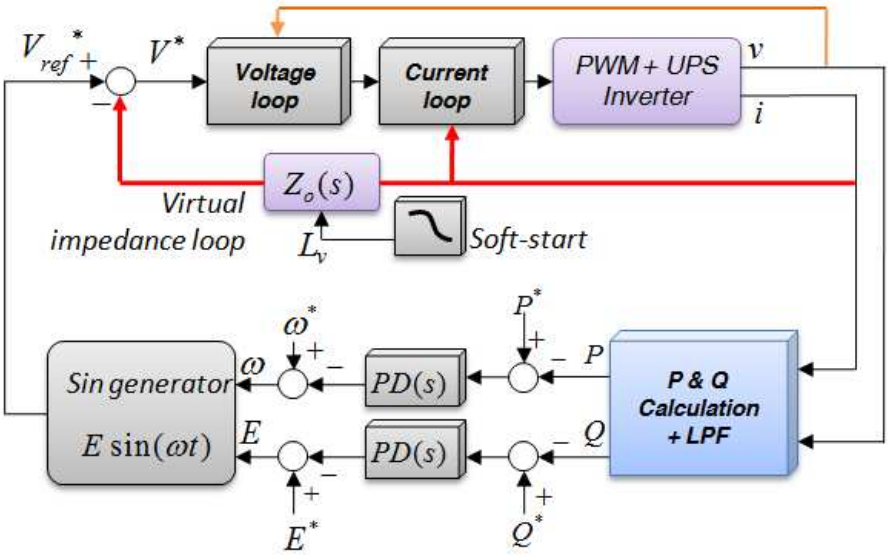

Figure 5.4: Block diagram of the inverter control loops.

5.7.1 Primary Control Analysis

The closed-loop system dynamics is derived by considering the stiff load-bus approximation [9]. The small-signal dynamics of the active and reactive powers, $i.e.$ $\hat{P}$ and $\hat{Q}$, respectively, are obtained by linearizing (5.5) and (3.8) and modeling the low-pass filters with a first-order approximation, $i.e.$

$$\begin{pmatrix} \hat{P} \\ \hat{Q} \end{pmatrix} = \frac{V\omega_c}{X(s+\omega_c)} \begin{pmatrix} \cos\Phi & -E\sin\Phi \\ \sin\Phi & E\cos\Phi \end{pmatrix} \begin{pmatrix} \hat{e} \\ \hat{\phi} \end{pmatrix} \tag{5.10}$$

where $\hat{e}$ denotes perturbed values; capital letters mean equilibrium point values; X is the output impedance at the fundamental frequency; and ω_c is the cutoff angular frequency of the low-pass filters, which are fixed over one decade below the line frequency. For simplicity, the high-frequency impedance values are not considered in this analysis since they have little effect over the system dynamics. Subsequently, by perturbing

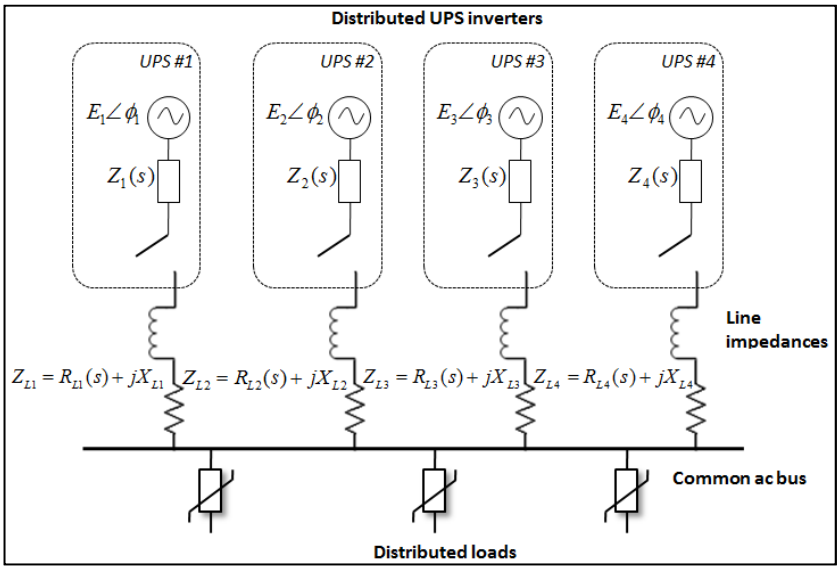

Figure 5.5: Configuration setup for simulation results of the Microgrid.

(5.3) and (5.4) and using (5.10), we obtain

$$\hat{e} = -(n + n_d s)\frac{V\omega_c}{R_d(s+\omega_c)}\left[\cos\Phi\cdot\hat{e} - E\sin\Phi\hat{\phi}\right], \tag{5.11}$$

$$\hat{\phi} = -\left(\frac{m}{s} + m_d\right)\frac{V\omega_c}{R_d(s+\omega_c)}\left[\sin\Phi\cdot\hat{e} - E\cos\Phi\hat{\phi}\right]. \tag{5.12}$$

Finally, substituting (5.11) into (5.12), we can find a third-order small-signal dynamics of the closed-loop system

$$s^3 + As^2 + Bs + C = 0 \tag{5.13}$$

where,

$$A = \frac{\omega_c}{X}\left[2R_d + nV\cos\Phi + n_d\omega_c V\cos\Phi + m_d VE\left(\cos\Phi + n_d\omega_c\frac{V}{X}\right)\right],$$

$$B = \frac{\omega_c}{X}\left[\omega_c + n\omega_c V\cos\Phi + mVE\cos\Phi + n_d\omega_c\frac{V}{X} + m_d\omega_c VE\left(\cos\Phi + n\frac{V}{X}\right)\right],$$

$$C = \frac{\omega_c}{X_d}m\omega_c VE\left(\cos\Phi + n\frac{V}{X}\right),$$

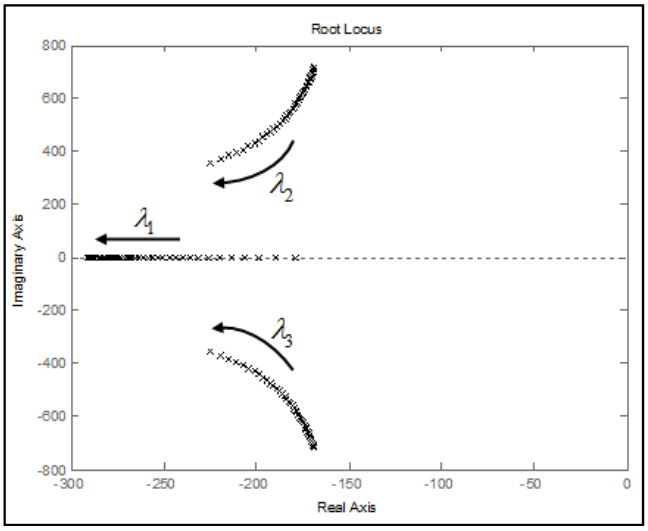

Figure 5.6: Root locus plot in function of the batteries charge level (arrows indicate decreasing value from 1 to 0.01).

with $X_d = X + n_d\omega_c V\cos\Phi$. Using (5.13), the stability of the closed-loop system can be evaluated, and the transient response can be adjusted. The eigenvalues of the system (λ_1, λ_2, and λ_3) have been studied by using the power stage and control parameters shown in Table 5.1. Figure 5.6 shows the family of root locus, showing stability for all battery charge conditions (from α=1 to α=0.01).

5.7.2 Secondary Control Analysis

Secondary control has been analyzed and modeled using a similar approach as in the last section. By using 5.7 and assuming a P/Q decoupling, the active power, given by one inverter, can be derived as

$$P_i = \frac{-mEV\omega_c(P^* - P_i^*)}{X(s+\omega_c)}, \tag{5.14}$$

Table 5.1: Control System Parameters

$Parameter$	$Symbol$	$Value$	$Units$
Nominal Frequency	ω^*	$2pi50$	rad/s
Nominal Amplitude	E	311	V
Nominal virtual output impedance	L^*_{Df}	800	μH
Initial output impedance value	L^*_{Do}	80	mH
Soft-start time constant	T_{ST}	0.1	s
P Proportional term value	k_p	1.8	W/rd·s
P Integral term value	k_i	0.1	W/rd
Q Proportional amplitude droop	k'_p	30	VAr/V
Q Integral amplitude droop	k'_i	80	sVAr/V

where P_i is the active power of the inverter i and P_i^* is the nominal active power. By combining 5.8 and 5.14 yields the following second-order transfer function:

$$\frac{P_i}{P_g^*} = \frac{m(k_i + k_p s)EV\omega_c}{N(Xs^2 + \omega_c[X + mEV(nk_p - 1)]s + NmEV\omega_c k_i)}. \tag{5.15}$$

By studying the eigenvalues of 5.15, a series of root-locus diagrams is shown in Figure 5.8(a) and 5.8(b), illustrating the stability limits which can be useful for adjusting the transient response of the system. A similar study can be done for reactive-power secondary control (12).

5.8 Simulation Results

The aim of this section is to test the proposed controller over the Microgrid in order to show its performance and limitations in different scenarios.

5.8.1 Harmonic-Current Sharing

The first step is to observe the effect of the proposed controller over the harmonic-current sharing, which is very important when the system is supplying a nonlinear load.

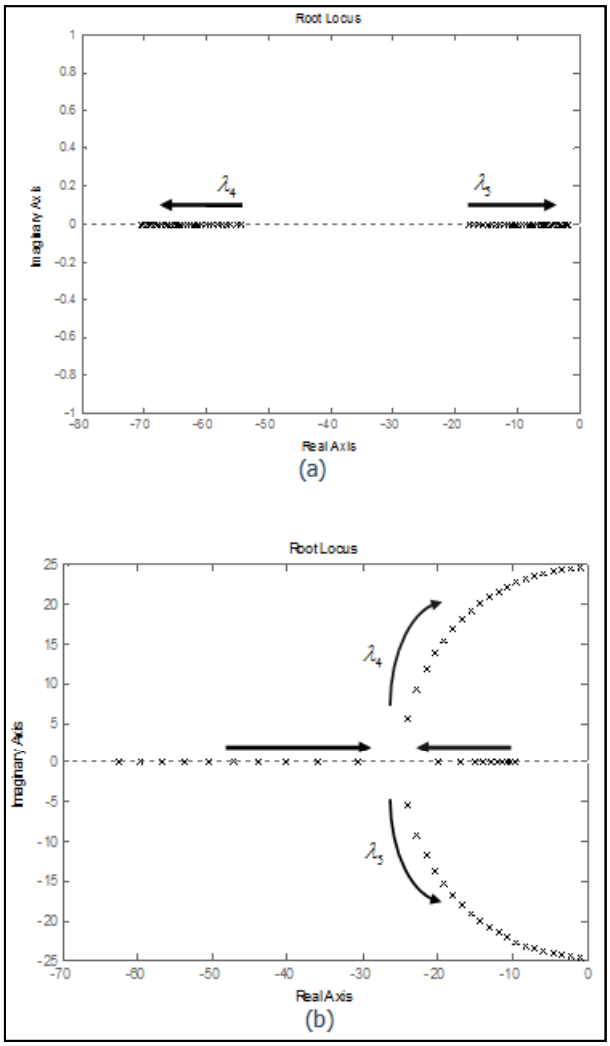

Figure 5.7: Root locus plot for a) $k_p = 0.8$ and $0.1 \leq k_i \leq 0.8$ b) $k_i = 0.5$ and $0.7 \leq k_p \leq 0.8$.

With this objective, a series of simulations have been performed for a two-*UPS* paralleled system sharing a common nonlinear load. Figure 5.9(a) shows the steady-state and the transient responses of the inverters output currents without using the harmonic sharing loop. In consequence, fundamental currents are equal; however, the third, fifth, and seventh harmonics are unbalanced. As shown in Figure 5.9(b), by using 5.1, with the harmonic-current sharing loop, fundamental and harmonic current terms are properly shared. Note that in this case, up to the seventh harmonic has been included. However, higher harmonics can be added to this control loop, if necessary.

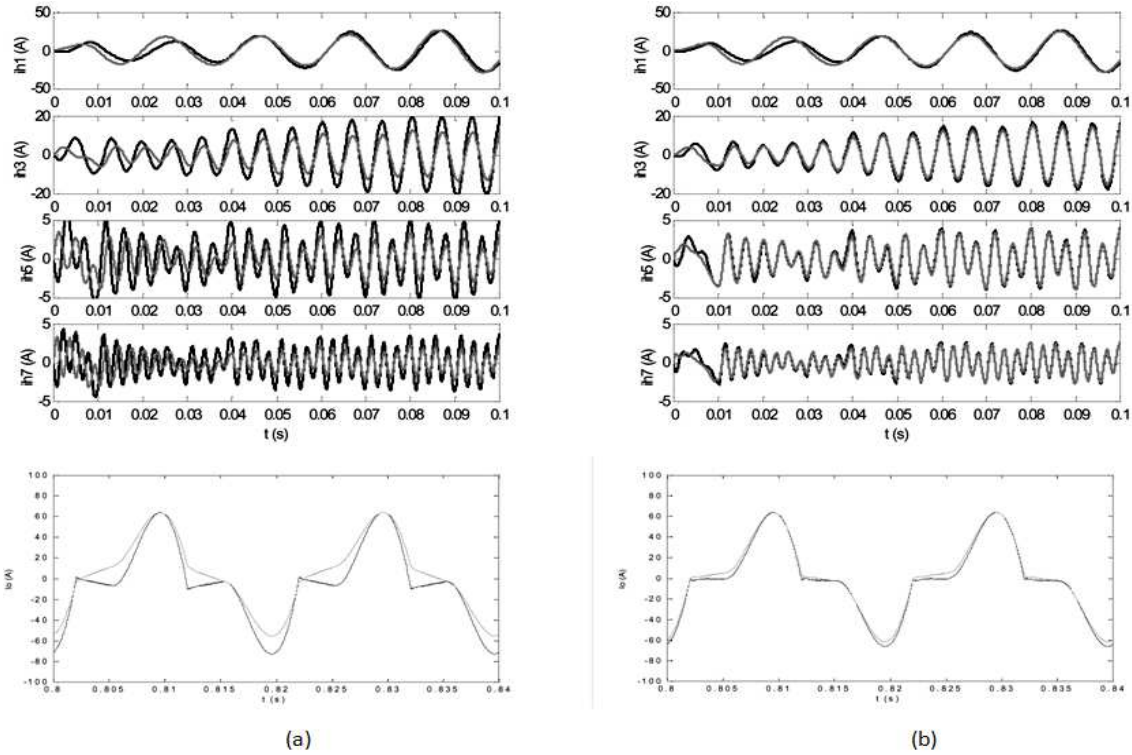

Figure 5.8: Harmonic decomposition extracted by using the (top) bank of bandpass filters and (bottom) output currents of a two-UPS system with highly unbalanced power lines, sharing a nonlinear load (a) without and (b) with the harmonic-current sharing loop.

5.8.2 Hot-Swap Operation

The second step consisted in testing the hot-swap operation of the *UPS* by using the proposed soft-start impedance. Two main scenarios must be considered, namely, the connection and the disconnection of the *UPS* in the distributed system. In the first case, when an additional *UPS* has to be connected to the common bus, the output voltage of the inverter must be synchronized with the bus by a phase-locked loop action. After that, the droop control method begins operating, together with the output impedance loop. As stated earlier, at first, the output impedance has a high value; later, however, it goes down to the nominal value in a soft-start fashion, avoiding initial current peaks.

Figure 5.9 shows the circulating current ($i_{o1} - i_{o2}$) between two *UPSs* sharing a

nonlinear load, when *UPS*$\#2$ is connected at $t = 0.8s$ and while *UPS*$\#1$ remains connected from the beginning. Figure 5.9(a) shows the transient response of the circulating current without using the soft-start impedance, thus maintaining the L constant at 800H. Notice that the circulating current is initially higher than the current supplied by *UPS*$\#1$ before the *UPS*$\#2$ connection. Figure 5.9(b) shows the transient response using the same configuration but adding the soft-start loop 5.2 with the following parameters: $T_{ST} = 0.1s$ and $L = 80H$. Note that, in this case, the circulating current has been reduced by half. Figure 5.9(c) shows the dynamic behavior of the circulating current by increasing L to 800H. Observe now that the system becomes slower while the initial current peak tends to increase.

Figure 5.10 shows a detail of the connection of *UPS*$\#2$ while *UPS*$\#1$ is connected to the load permanently. A four-*UPS* system sharing a distributed nonlinear load in order to see the effects of the inverter connection/disconnection has been simulated, and the results are shown in Figure 5.15. The impedances of the lines connected between the inverters and the load were intentionally unbalanced. $Z_{L1} = 0.12 + j0.028$, $Z_{L2} = 0.24 + j0.046$, $Z_{L3} = 0.06 + j0.014$, and $Z_{L4} = 0 + j0$ (see Figure 9). Figure 10(a) shows the progressive connection of the four *UPSs* to the common *ac* bus, with *UPS*$\#1$ at $t = 0s$, *UPS*$\#2$ at $t = 0.8s$, *UPS*$\#3$ at $t = 1.6s$, and *UPS*$\#4$ at $t = 2.4s$. As it can be seen, the *UPS* modules are seamlessly connected to the bus, increasing their output currents gradually. Figure 5.15(b) shows the disconnection of the *UPS* from the *ac* bus. Note that there are no overcurrents. Droop functions for every *UPS* accommodate properly the output currents to the amount of load without critical transients.

5.8.3 Microgrid Operation and Transitions

Figure 5.12 shows the active and reactive powers of a two-UPS Microgrid sharing power with the grid, the transition to islanded operation, and the disconnection of *UPS*$\#2$. Figure 5.13 depicts three *UPSs* connected to the Microgrid and the main grid showing the transition from grid connected and island operation ($t = 4s$). Also, observe how good the active power sharing is carried out when *UPS*$\#1$ and *UPS*$\#2$ are disconnected ($t = 6s$ and $t = 9s$ respectively). The power sharing is automatically distributed among the connected inverters corresponding to the slopes of their droops. These results are

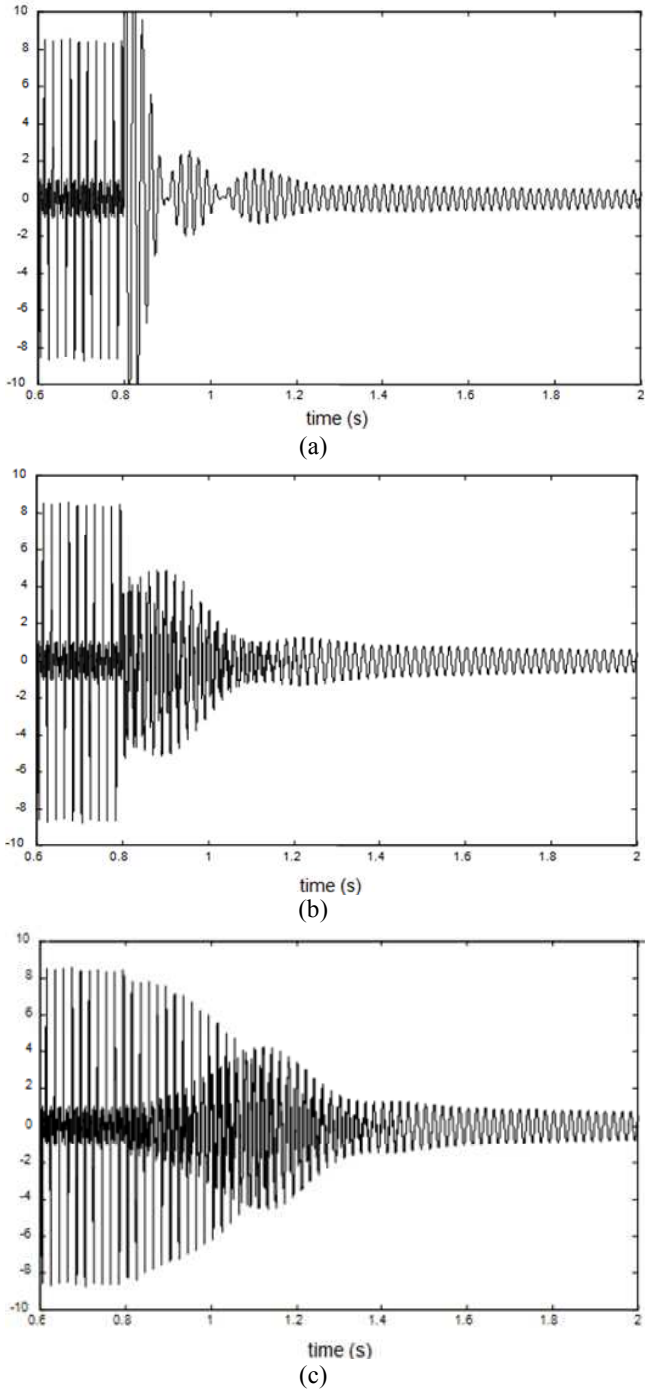

Figure 5.9: Circulating current when a second *UPS* is connected at $t = 0.8$ (a) without the soft start, (b) with the soft start L_{Do}=80 μH, and (c) L_{Do} = 800 μH (Y -axis:2A/div).

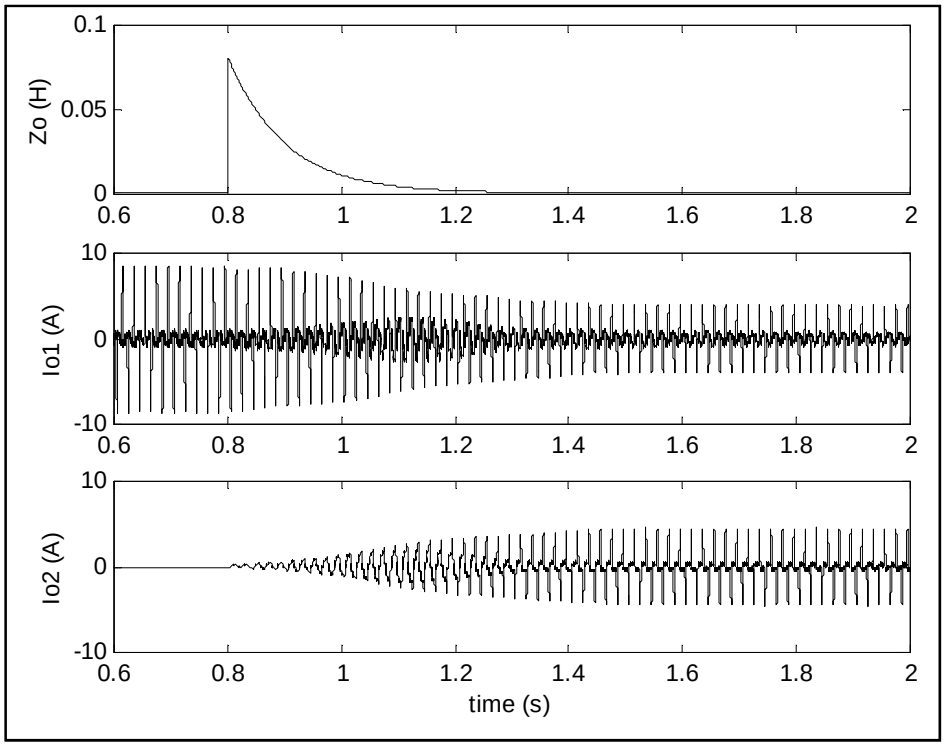

Figure 5.10: Output impedance of*UPS*$\#2$ and output currents of the UPS$\#1$ and UPS$\#2$ in soft-start operation (T_{ST}=0.1s and L_{Do} =80H).

obtained based on a hierarchical control energy management.

The system starts to be connected to the grid, with $P_g^* = 1000W$ and $Q_g^* = 0Var$. At $t = 4s$, the system is disconnected from the grid, and the two *UPS* units operate in island mode sharing the overall load. At $t = 6s$, *UPS*$\#2$ is disconnected, and *UPS*$\#1$ supplies all the power to the Microgrid. Notice the proper transient response, as well as the good power regulation of the system.

5.9 Experimental Results

Two 6-kVA single-phase *UPS* units were built and tested in order to show the validity of the proposed approach. Each inverter consisted of a single-phase insulated-gate bipolar

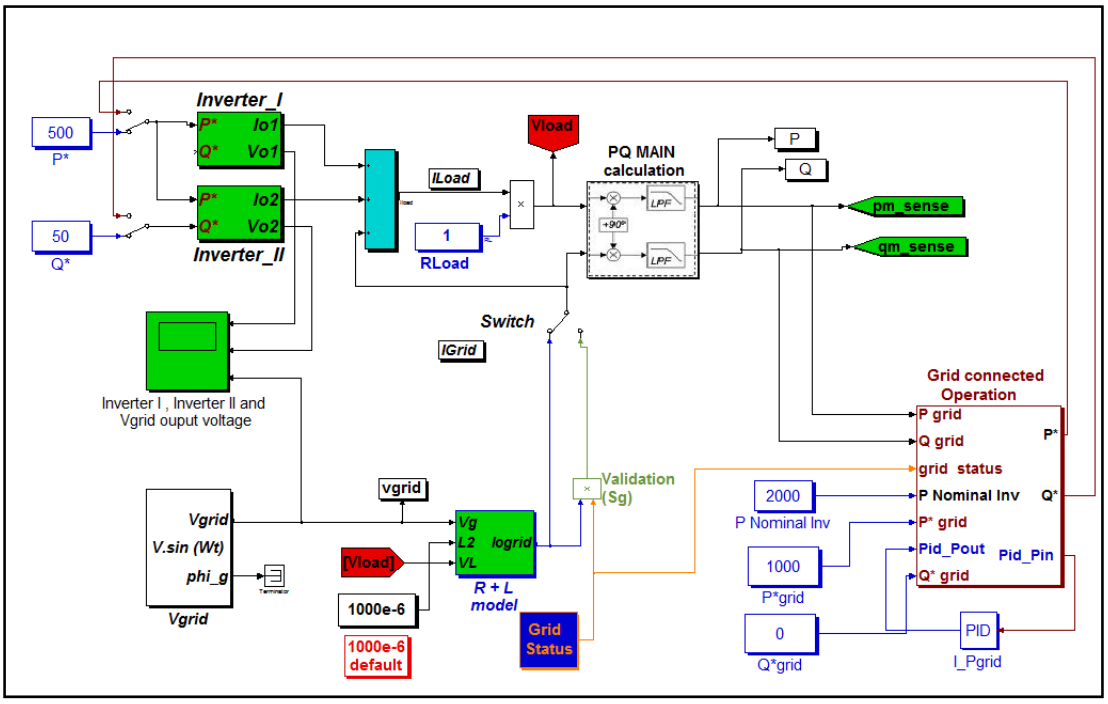

Figure 5.11: Dynamic performance of two inverters using the hierarchical control strategy.

transistor full bridge with a switching frequency of 20kHz and an LC output filter, with the following parameters: L=500H, C=100μF, V_{in}=400V, and V_o=220 V_{rms} at 50H_z. The impedance of the lines connected between the inverters and the load was intentionally unbalanced; $Z_{L1} = 0.12 + j0.028$, and $Z_{L2} = 0.24 + j0.046$. The controls for these inverters are formed by three loops, namely, an inner current loop, an outer PI controller that ensures voltage regulation, and the power-sharing controller. The first two loops were implemented by means of a TMS320LF2407A fixed-point 40-MHz digital signal processor (*DSP*) from Texas Instruments. The power sharing controller was implemented by using a TMS320C6711 floating-point 200-MHz *DSP*. The connection between the two *DSPs* was made through the host port interface of the 6711. This solution was used only in the design process. Afterward, within the developing process, we use a single fixed-point *DSP* TMS320C2811 as a controller. Thus, the cost and complexity of the control board are further reduced.

The *DSP* controller also includes a *PLL* block in order to synchronize the inverter

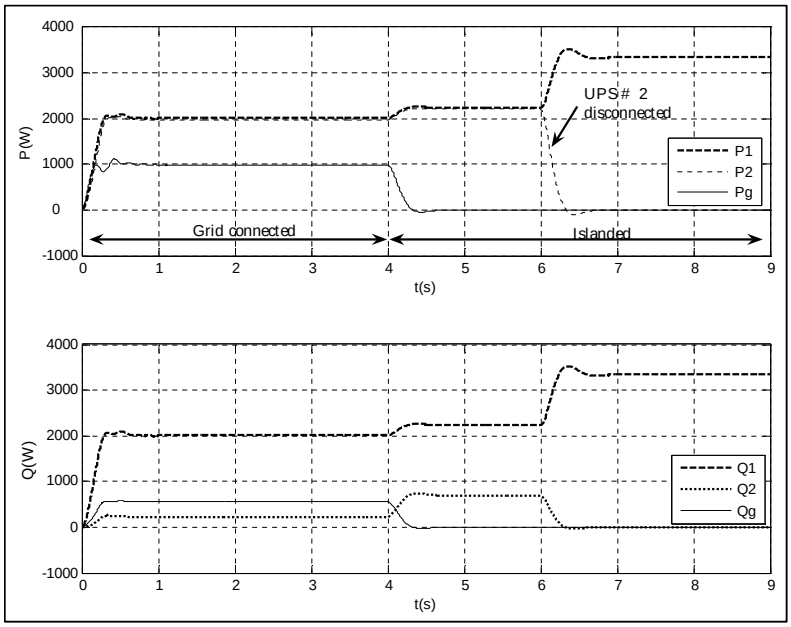

Figure 5.12: Active and reactive-power transients between grid-connected and islanded modes (Y-axis: P=1 kW/div, Q=1 kVAr/div).

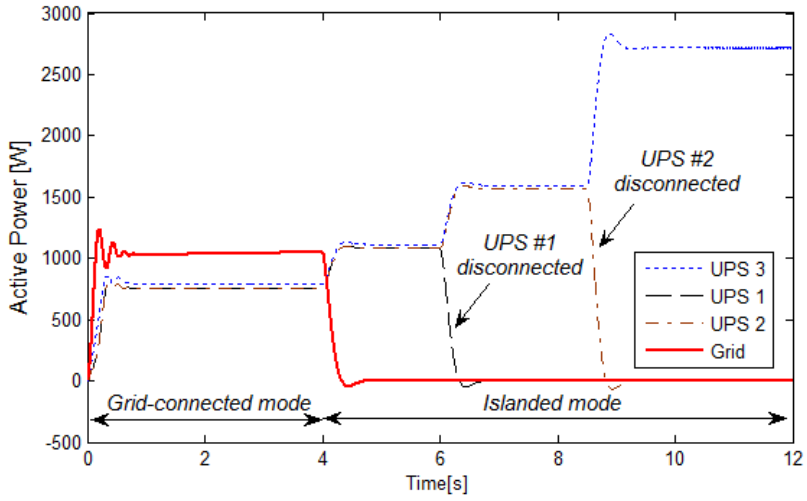

Figure 5.13: Active power dynamic during transients changes from grid-connected and islanded modes.

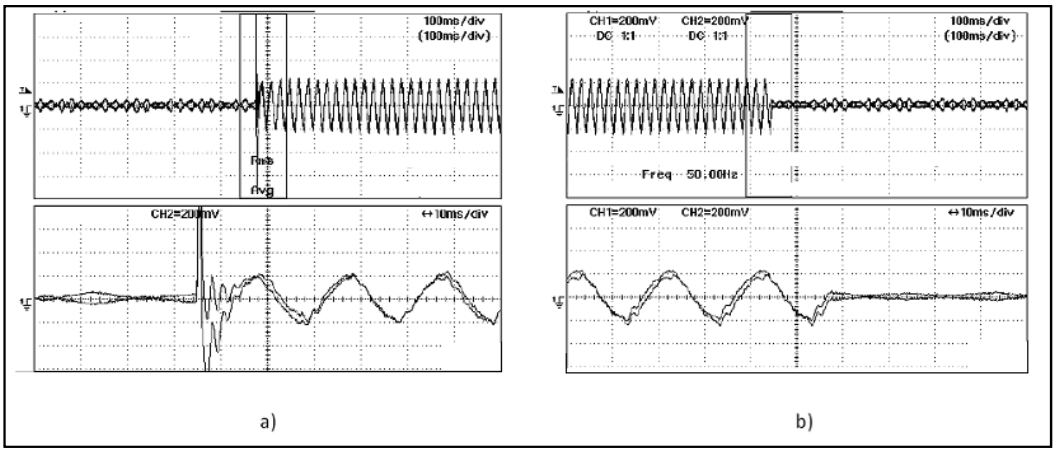

Figure 5.14: Dynamic performance of the output currents when sharing a pure 40F capacitive load. (a) Connection. (b) Disconnection (Y -axis: 4 A/div).

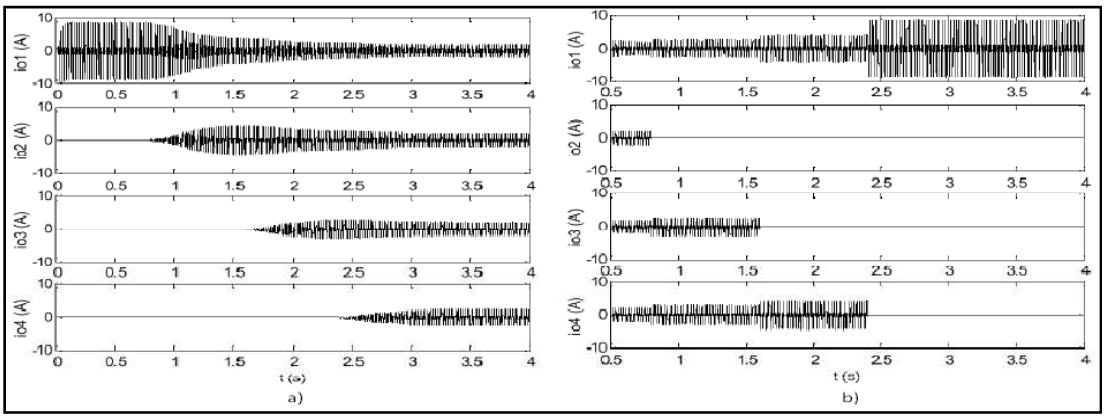

Figure 5.15: Output currents of the UPS$\#1$, UPS$\#2$, UPS$\#3$, and UPS$\#4$ in a) soft-start operation (T_{ST}=0.1s and $L_{Do} = 80mH$) and b) disconnection scenario.

with the common bus. In this situation, the static bypass switch is turned on, and the soft-start operation and the droop-based control are initiated. The first set of experiments considers a resistive load. Figure 5.17 shows the output currents of every unit and the circulating current ($i_{o1} - i_{o2}$) for sudden changes from no load to full load and

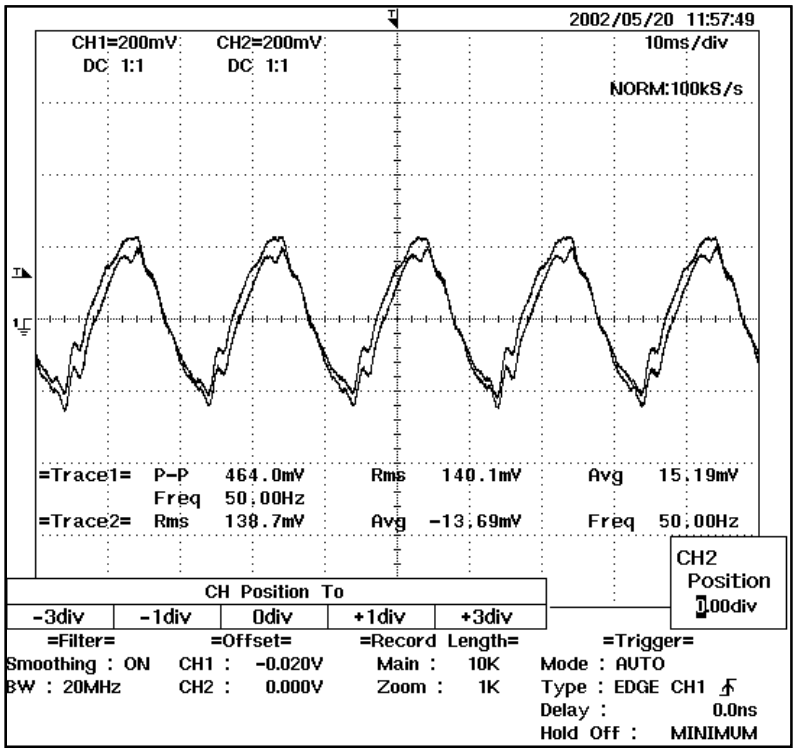

Figure 5.16: Steady state of the output currents when sharing a pure 40μF capacitive load (X-axis:10 ms/div; Y -axis: 5 A/div).

vice versa. These results show an excellent dynamic response for the proposed controller. As it can be seen, the circulating current remains very small, even for no-load conditions.

Furthermore, the supply of a purely capacitive load of 40F is evaluated. Figure 5.12 and Figure 5.14 show the steady-state and the transient responses of the output currents, respectively. The sudden connection of the capacitor to the ac bus causes a high current peak during the instantaneous charge process (see Figure 5.14(a)). The nonsinusoidal waveforms of these currents appear since the pure capacitive load compromises the performance of the inner voltage control loop. As it can be seen, the proposed control achieves a good load-sharing capability in the system. The final experiment consists in supplying a nonlinear load. Figure 5.18 shows the load voltage and current. The measured output voltage *THD* was about 2.1%.

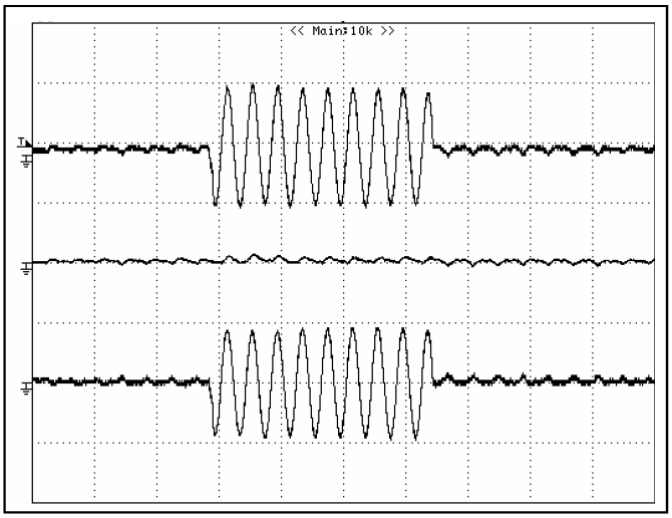

Figure 5.17: Transient response of the output currents and the circulating current (X-axis: 50 ms/div; Y -axis: 20 A/div).

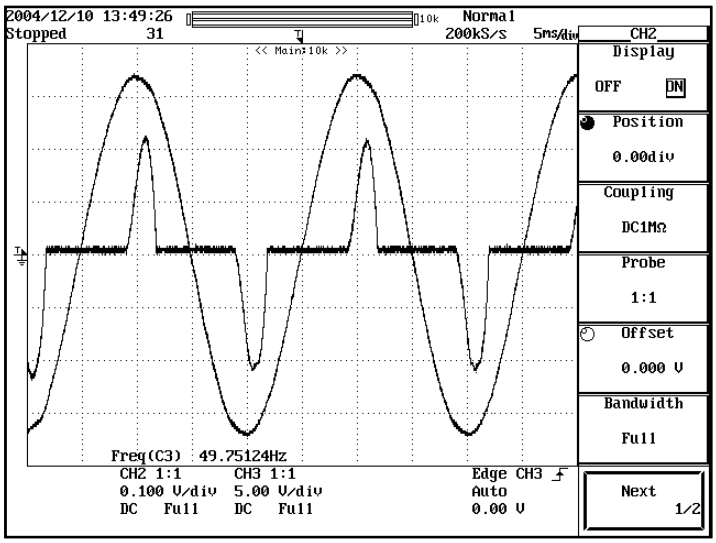

Figure 5.18: Waveforms of the parallel system sharing a nonlinear load. Output voltage and load current (X-axis: 5 ms, Y -axis: 20 A/div).

5.10 Conclusions

The control structure of this chapter was based on the droop method in order to achieve autonomous operation of each *UPS* module and how the droop control strategy can be easily adaptable to the operation of parallel inverters. Moreover, the proposed control strategy allows for achieving a tight P and Q regulation performance. A small-signal model was developed to analyze the system stability and to design the values of the control parameters. Also, experimental results have been presented in order to validate the proposed control approach, showing a good steady-state regulation and a proper transient response when sharing linear and nonlinear loads.

CHAPTER 6

CONCLUSIONS

Finally in this chapter, the conclusions derived from this dissertation thesis are presented. The main contributions of this thesis are summarized and their publication in international conference proceedings and international journal articles will be synthesized. In addition, general conclusions and the future lines of research proposed from the thesis will be discussed.

6.1 Key Contributions

Firstly, in chapter II a review of the state of the art was introduced based on on the analysis, system stability and power management control starting from a single voltage source inverter to a number of interconnected *DG* units forming flexible Microgrids showing:

- ▷ Different control strategies based on droop control characteristic.
- ▷ Inner voltage and current loops (proposed as a multiple-loop control scheme).
- ▷ Operating modes of a Microgrid applying the concept of primary, secondary and tertiary control loops conceived as a control hierarchical strategy.

In chapter III, a novel control for VSIs with the capability of flexibly operating grid-connected and islanded mode based on adaptive droop control strategy was proposed.

In addition, active and reactive power can be decoupled from the grid impedance in order to injected the desired power to the grid. An islanding detection scheme in order to achieve capability transition under unplanned scenarios was introduced. The main contributions of this chapter were:

- ▷ A dynamic system model based on adaptive droop methodology using Padé approximation.
- ▷ A novel control for injecting the desired active and reactive power independently into the grid for large range of impedance grid values was presented. This control is based on a parameters estimation provided by an identification algorithm.
- ▷ Enhancement of the classic droop control method able to decouple active and reactive power flows.
- ▷ Phase and amplitude synchronization algorithm was presented, ensuring smooth and safe reconnection between the microgrid and the utility main when the fault is cleared.

In chapter IV, a droop control method was proposed for voltage dip mitigation and reduction of the harmonic distortion of the output voltage when linear and non-linear loads are connected. A detailed analysis has shown that the novel adaptive droop control strategy has superior behavior in comparison with the existing droop control methods, ensuring efficient control of frequency and voltage even in presence of voltage sags. At the same time, the converter provides fast dynamic response and active power to local loads by injecting reactive power into the grid providing voltage support at fundamental frequency. Although the developed method is quite simple in theory, parameter tuning difficulty in practical tests must be considered. Based on the power stage configuration regarding the dependence of the maximum value of the inductance line impedance, the maximum active power flow transferred from or to the grid can be controlled.

The control technique was applied to a PV inverter connected through a decoupling inductance to the main grid. The contributions in this chapter were:

- ▷ A dynamic model design and a small signal analysis, showing system performance and stability.
- ▷ Using the basis of the droop characteristic, a new control strategy was proposed, providing all the desired active power given by the PV source.
- ▷ The validity of the proposed control showed ride-through capability to the system, even if a voltage sag is presented in the grid.

Finally in chapter V the incorporation of a hierarchical control was proposed, even if connecting several parallel line interactive UPS units, providing power injection accuracy or avoiding system sensibility to the grid parameters during power line mismatches of the supply line. Frequency and voltage amplitude regulation based on different levels of modeling, control and analysis are taken into account, as well. Also, the control of UPS inverter is important to minimize the harmonic content of the output voltage and it achieves a good load sharing capability even when supplying as local as non-linear loads. The disconnection of the UPS does not produce any overcurrent thanks to droop control strategy for every UPS that accommodate properly the output currents to the amount of load without critical transients. The main achievements of this work can be summed up as follows:

- ▷ A control scheme for parallel connected UPS systems based on a hierarchical control strategy avoiding critical communications among UPS units.
- ▷ Active and reactive power regulation control and effectiveness of the proposed method under highly unbalanced power lines, sharing non-linear loads.

6.1.1 Journal Publications

J1. J. M. Guerrero, J. C. Vasquez, J. Matas, J. L. Sosa and L. Garcia de Vicuña. *Control Strategy for Flexible Microgrid Based on Parallel Line-Interactive UPS Systems, IEEE Transactions on Industrial Electronics*, Vol. 56, pages 726-736. March 2009.

Table 6.1: Main Contributions

Chapter	*Contribution*	*Publication*	*I.Factor*
2	Revision of Microgrids and proposal control	$[B1]$	N/A
3	Voltage Sags mitigation	$[J2], [C2], [C3]$	2.216
4	Adaptive Droop for line Impedance Variations	$[J3], [C1]$	2.216
5	Multiple Inverters and Hierarchical Control	$[J1], [C4]$	2.216

J2. Juan C. Vasquez, Rosa A. Mastromauro, Josep M. Guerrero and Marco Liserre, *Voltage Support Provided by a Droop-Controlled Multifunctional Inverter*, (Forthcoming to be included in IEEE Transactions on Industrial Electronics (T-IE)).

J3. J. C. Vasquez, J. M. Guerrero, A. Luna, P. Rodriguez, R. Teodorescu, *Adaptive Droop Control Applied to Voltage Source Inverters Operating in Grid-Connected and Islanded modes*, (Forthcoming to be included in *IEEE Transactions on Industrial Electronics (T-IE)*).

6.1.2 Conference Publications

C1. J. C. Vasquez, J. M. Guerrero, E. Gregorio, P. Rodriguez, R. Teodorescu and F. Blaabjerg, *Adaptive Droop Control Applied to Distributed Generation Inverters Connected to the Grid, IEEE International Symposium on Industrial Electronics (ISIE'08)*. Pages 2420-2425. Jun. 30, 2008

C2. R. A. Mastromauro, M. Liserre, A. dell'Aquila, J. M. Guerrero and J. C. Vasquez, *Droop Control of a Multifunctional PV Inverter*. *IEEE International Symposium on Industrial Electronics (ISIE'08)*, pages 2396-2400. Jun. 30, 2008.

C3. J. Matas, P. Rodriguez, J. M. Guerrero, J. C. Vasquez, *Ride-Through Improvement of Wind-Turbines Via Feedback Linearization, In IEEE International Symposium on Industrial Electronics (ISIE'08)*, Pages 2377-2382, Jun. 30, 2008.

C4. J. M. Guerrero, J. C. Vasquez, J. Matas, J. L. Sosa and L. Garcia de Vicuña,

Parallel Operation of Uninterruptible Power Supply Systems in Microgrids, 12^{th} *European Conference on Power Electronics and Applications (EPE'07)*, sept.2007.Page(s): 1-9.

6.1.3 Book Chapters

B1. Josep M. Guerrero and Juan. C. Vasquez, *Uninterruptible Power Supplies*, The Industrial Electronics Handbook, Second edition, Irwin, J. David (ed.).

6.2 General Contributions of the Thesis

This thesis has presented an analysis, simulation and experimental results focusing on modeling, control, and analysis of DG units, according to the following steps:

- ▷ Control-oriented modeling based on active and reactive power analysis
- ▷ Control synthesis based on enhanced droop control technique.
- ▷ Small-signal stability study to give guidelines for properly adjusting the control system parameters according to the desired dynamic response

This methodology has been extended to microgrids by using hierarchical control applied to droop-controlled line interactive UPSs showing that:

- ▷ Droop-controlled inverters can be used in islanded microgrids.
- ▷ By using multilevel control systems the microgrid can operate in both grid-connected and islanded mode, in a concept called flexible microgrid.

Improvements to the conventional droop method are required for integrate inverter-based energy resources based on:

- ▷ Improvement of the transient response

- ▷ Virtual output impedance: harmonic power sharing and hot-swapping
- ▷ Adaptive droop control laws

The proposed hierarchical control required for flexible Microgrids consisted of different control levels, as following:

- ▷ Primary control is based on the droop method allowing the connection of different AC sources without any intercommunication.
- ▷ Secondary control avoids the voltage and frequency deviation produced by the primary control. Only low bandwidth communications are needed to perform this control level. A synchronization loop can be added in this level to transfer from islanding to grid connected modes.
- ▷ Tertiary control allows the import/export of active and reactive power to the grid.

Additional features were also required in order to manage a flexible Microgrid:

- ▷ Voltage ride-through capability, by controlling the injection of reactive power to solve grid voltage sags.
- ▷ Grid impedance estimation, to inject accurately active and reactive power as well as to detect islanding operation.
- ▷ Power-frequency droops used effectively contribute to ensure power sharing.

6.3 Future Work

The aforementioned conclusions in this thesis lead to several proposals for future research work being developed at present, at both a scientific and technical level of development of projects as:

- ▷ DC coupling microgrids. This line of research addresses an open field for new renewable energy power-management control strategies. New scenarios emerge for

Distributed Generation systems, electrical power quality, reliability and flexible operation in Microgrids

- ▷ Integrated energy storage systems. These systems operate within varying environments and electrical conditions, and in many different types of battery technologies. Because each technology has advantages under specific operational conditions, it is important to understand the capabilities and limitations of each storage technology. In the same way, although electrical energy storage is a well-established market, its use in PV systems is generally for stand-alone systems. The final goal is to develop and integrate energy storage systems specifically designed and optimized for grid-tied *PV* applications.

- ▷ Improving the hierarchical control strategy. Due to political and economic interest and complexity, energy management of Microgrids demand new control strategies imposed for hard power quality standards, based on intelligent/adaptive algorithms.

Nowadays, the microgrids are not in an advanced stage of clean energy development. That is why the future of the microgeneration and electricity distribution will depend on the development of smart grids as DER-based microgrids. Also, the use the renewable energy sources and advantages of the microgrids such as reliability, efficiency, quality of service, and network support makes these systems very competitive.

BIBLIOGRAPHY

[1] *IEEE 1547 Standard for Interconnecting Distributed Resources with Electric Power Systems*, 2003.

[2] *IEEE 1547.3 Guide for Monitoring, Information Exchange, and Control of Distributed Resources Interconnected with Electric Power Systems*, 2007.

[3] K. Alanne and A. Saari. Distributed energy generation and sustainable development. *Renewable and Sustainable Energy Reviews*, 10:539–558, 2006.

[4] M. Arias, A. Fernandez, D. G. Lamar, M. Rodriguez, and M. M. Hernando. Simplified voltage-sag filler for line-interactive uninterruptible power supplies. *IEEE Trans. Ind. Electron.*, 55:3005–3011, Aug 2008.

[5] M. Ashari, C. V. Nayar, and S. Islam. Steady-state performance of a grid interactive voltage source inverter. *IEEE Proc. Power Engineering Society Summer Meeting*, pages 650–655, 2001.

[6] M. Ashari, C. V. Nayar, and W. W. K. Keerthipala. A single phase parallely connected uninterruptible power supply/demand side managent system. *IEEE Trans. Energy Conversion*, 15:97–102, March 2000.

[7] L. Asiminoaei, R. Teodorescu, F. Blaabjerg, and U. Borup. Implementation and test of an online embedded grid impedance estimation technique for pv inverters. *IEEE Trans. on Ind. Electron.*, 52:1136–1144, 2005.

[8] S. Barsali, M. Ceraolo, P. Pelachi, and D. Polim. Control techniques of dispersed generators to improve the continuity of electricity supply. *in Proc. IEEE PES-Winter Meeting'02*, pages 789–794, 2002.

[9] A. R. Bergen. *Power System Analysis*. Englewood Cliffs, 1986.

[10] F. Bertling and S. Soter. A novel converter integrable impedance measuring method for islanding detection in grids with widespread use of decentral generation. *in Proc. of Power Electron Elect. Drives, Automation and Motion*, pages 503–507, 2006.

[11] F. Blaabjerg, R. Teodorescu, Z. Chen, and M. Liserre. Power converters and control of renewable energy systems. *Plenary session paper for ICPE 2004, Pusan (Korea)*, Oct 2004.

[12] F. Blaabjerg, R. Teodorescu, M. Liserre, and A. Timbus. Overview of control and grid synchronization for distributed power generation systems. *IEEE Trans. Ind. Electron.*, 53(5), Oct 2006.

[13] M. Castilla, J. Miret, J. Matas, L. Garcia de Vicuna, and J. M. Guerrero. Linear current control scheme with series resonant harmonic compensator for single-phase grid-connected photovoltaic inverters. *IEEE Trans. Ind. Electron*, 55:2724–2733, July 2008.

[14] M. C. Chandorkar and D. M. Divan. Control of parallel operating battery inverteers in stand alone ac supply sistem. *IEEE Trans. Ind. Applications*, 29:136–143, 1993.

[15] M. C. Chandorkar, D. M. Divan, Y. Hu, and B. Barnajee. Novel architectures and control for distributed ups systems. *in Proc. IEEE APEC'94*, pages 683–689, 1994.

[16] M. C Chandorkar, M. D. Divan, and R. Adapa. Control of distributed ups systems. In *IEEE Power Electronics Specialists Conference (PESC)*, pages 197–204, 1994.

[17] J. F. Chen, C. L. Chu, and O. L. Huang. The parallel operation of two ups by the coupled-inductor method. In *Proceedings of the Industrial Electronics, Control and Instrumentation*, pages 733–736, 1992.

[18] L. R. Chen, N. Y. Chu, C. S. Wang, and R. H. Liang. Design of a reflex based bidirectional converter with the energy recovery function. *IEEE Trans. Ind. Electron*, 55(8):3022–3029, Aug 2008.

[19] Y. K. Chen, Y. E. Wu, T. F. Wu, and C. P. Ku. Cwdc strategy for paralleled multi-inverter systems achieving a weighted output current distribution. In *Proceedings of the IEEE Applied Power Electronics Conference and Exposition*, pages 1018–1023, 2002.

[20] Y. C. Chuang and Y. L. Lee. High-efficiency and low-stress zvt-pwm dc-to-dc converter for battery charger. *IEEE Trans. Ind. Electron*, 55:3030–3037, Aug 2008.

[21] E. A. Coelho, P. C. Cortizo, and P. F. Garcia. Small signal stability for single phase inverter connected to stiff ac system. In *Industry Applications Conference, Thirty-Fourth IAS Annual Meeting*, volume 4, pages 2180–2187, 1999.

[22] E. A. Coelho, P. C. Cortizo, and P. F. Garcia. Small signal stability for single phase inverter connected to stiff ac system. In *IEEE Industrial Aplications Conference*, volume 38, pages 2245–2352, 2000.

[23] E. A. Coelho, P. C. Cortizo, and P. F. Garcia. Small signal stability for parallel connected inverters in stand alone ac supply systems. *IEEE Trans. Ind. Applications*, 38(2):533–541, 2002.

[24] H. Deng, R. Oruganti, and D. Srinivasan. A simple control method for high-performance ups inverters through output-impedance reduction. *IEEE Trans. Ind. Electron*, 55:888–898, Feb 2008.

[25] A. L. Dimeas and N. D. Hatziargyriou. Operation of a multiagent system for microgrid control. *IEEE Trans. Power Systems*, 20:1447–1455, 2005.

[26] O. I. Elgerd. *Electric energy systems theory. An introduction*. 2nd edition, 1982.

[27] J. M. Guerrero, N. Berbel, J. Matas L. Garcia de Vicuna, and J. Miret. Decentralized control for parallel operation of distributed generation inverters in microgrids using resistive output impedance. *In proc. IEEE ISIE '06*, pages 5149–5154, 2006.

[28] J. M. Guerrero, N. Berbel, J. Matas, J.L Sosa, and de L.G Vicuna. Control of line-interactive ups connected in parallel forming a microgrid. *IEEE International Symposium on Industrial Electronics*, pages 2667–2672, 2007.

[29] J. M. Guerrero, L. García de Vicuna, J. Matas, M. Castilla, and J. Miret. A wireless controller to enhance dynamic performance of parallel inverters in distributed generation systems. *IEEE Trans. Power. Electron*, 19(5):1551–1561, 2004.

[30] J. M. Guerrero, L. García de Vicuna, J. Matas, M. Castilla, and J. Miret. Output impedance design of parallel-connected ups inverters with wireless load-sharing control. *IEEE Trans. Ind. Electron*, 4:1126–1135, 2005.

[31] J. M. Guerrero, L. Garcia de Vicuna, and J. Uceda. Uninterruptible power supply systems provide protection. *IEEE Industrial Electronics Magazine*, 1:28–38, 2007.

[32] J. M. Guerrero, L. Hang, and J. Uceda. Control of distributed uninterruptible power supply systems. *IEEE Trans. Ind. Electron*, 55:2845–2859, Aug. 2008.

[33] J. M. Guerrero, J. Matas, L. García de Vicuna, M. Castilla, and J. Miret. Wireless-control strategy for parallel operation of distributed generation inverters. *IEEE Trans. Ind. Electron*, 53(5):1461–1470, 2006.

[34] J. M. Guerrero, J. Matas, L. Garcia de Vicuna, M. Castilla, and J. Miret. Decentralized control for parallel operation of distributed generation inverters using resistive output impedance. *IEEE Trans. Ind. Electron*, 54(2):994–1004, 2007.

[35] J. M. Guerrero, J. C. Vasquez, J. Matas, M. Castilla, and L. Garcia de Vicuna. Control strategy for flexible microgrid based on parallel line interactive ups systems. *IEEE Trans. Ind. Electron*, 56:726–736, March 2009.

[36] J. M. Guerrero, J. C. Vasquez, J. Matas, J. L. Sosa, and L. G. de Vicuna. Parallel operation of uninterruptible power supply systems in microgrids. In *12th European Conference on Power Electronics and Applications (EPE'07)*, pages 1–9, 2007.

[37] Z. He and Y. Xing. Distributed control for ups modules in parallel operation with rms voltage regulation. *IEEE Trans. Ind. Electron*, 55:2860–2869, Aug 2008.

[38] C. A. Hernandez-Aramburo, T. C. Green, and N. Mugniot. Fuel consumption minimization of a microgrid. *IEEE Trans. Ind. Applications*, 41:673–681, 2005.

[39] C. C. Hua, K. A. Liao, and J. R.Lin. Parallel operation of inverters for distributed photovoltaic power supply system. *in Proc. IEEE PESC'02 Conf*, pages 1979–1983, 2002.

[40] J. Huang and K.A. Corzine. Ac impedance measurement by line to line injected current. *in Proc. of IEEE Ind. Applicat. Conf. (IAS'06)*, pages 300–306, 2006.

[41] F. D. Kanellos, A. I. Tsouchnikas, and N. D. Hatziargyriou. Micro-grid simulation during grid-connected and islanded modes of operation. *in Proc. International Conf Power Systems Transients (IPST'05)*, 2005.

[42] F. Katiraei and M. R. Iravani. Transients of a microgrid system with multiple distributed generation resources. In *International Conference on Power Systems Transients (IPST'05)*, pages 1–6, 2005.

[43] F. Katiraei, M. R. Iravani, and P. W. Lehn. Micro-grid autonomous operation during and subsequent to island process. *IEEE Transactions on Power Delivery*, pages 1–10, 2005.

[44] K. Kawabata, N. Sashida, Y. Yamamoto, K. Ogasawara, and Y. Yamasaki. Parallel processing inverter system. *IEEE Trans. Power. Applications*, 6(3):442–450, 1991.

[45] T. Kawabata and S. Higashino. Parallel operation of voltage source inverters. *IEEE Trans. Ind. Applications*, 24 No. 2:281–287, 1998.

[46] P. Kundur. *Power System Stability and Control*. McGraw-Hill, 1994.

[47] R. H. Lasseter. Microgrids. In *IEEE PES-Winter Meeting'02*, pages 305–308, Feb 2002.

[48] R. H. Lasseter. Microgrid and distributed generation. *Journal of Energy Engineering, American Society of Civil Engineers*, pages 1–7, 2007.

[49] R. H. Lasseter, A. Akhil, C. Marnay, J. Stevens, J. Dagle, R. Guttromson, A. S. Meliopoulous, R. Yinger, and J. Eto. White paper on integration of distributed energy resources. the certs microgrid concept. In *Consortium for Electric Reliability Technology Solutions*, pages 1–27, Apr 2002.

[50] R. H. Lasseter and P. Piagi. Providing premium power through distributed resources. In *IEEE of the 33rd Hawai International Conference on System Sciences (HICSS'00)*, pages 1–9, Jan 2000.

[51] R. H. Lasseter and P. Piagi. Microgrids, a conceptual solution. In *IEEE PESC'04*, pages 4285–4290, Jun 2004.

[52] S.J. Lee, H. Kim, S.K. Sul, and F. Blaabjerg. A novel control algorithm for static series compensator by use of pqr instantaneous power theory. *IEEE Trans. Ind. Electron*, 19:814–827, May 2004.

[53] L.H. Li, T.T. Jin, and K. M. Smedley. A new analog controller for three phase voltage generation inverter. *IEEE Trans. Ind. Electron*, 55:2894–2902, 2008.

[54] W. Liu, R. Ding, and Z. Wang. Investigated optimal control of speed, excitation of load sharing of parallel operation diesel generator sets. In *IEE 2nd international conferencia on advances in power system control, operation and management*, pages 142–146, dic 1993.

[55] P. C. Loh, M. J. Newman, D. Zmood, and D. G. Holmes. Improved transient and steady state voltage regulation for single and three phase uninterruptible power supplies. In *IEEE 32nd Annual on Power Electronics Specialists Conference (PESC'01)*, volume 2, pages 498–503, 2001.

[56] P. C. Loh, M. J. Newman, D.N. Zmood, and D.G. Holmes. A comparative analisys of multiloop voltaje regulation strategies for single and three-phase ups systems. *IEEE Trans. Ind. Electron*, 18(5):1176–1185, 2003.

[57] J. A. P. Lopes, C. L. Moreira, and A. G. Madureira. Defining control strategies for microgrids islanded operation. *IEEE Trans. Power Systems*, 21(2):916–924, May 2006.

[58] K.S. Low and R. Cao. Model predictive control of parallel-connected inverter for uninterruptible power supplies. *IEEE Trans. Ind. Electron*, 55:2860–2869, Aug 2008.

[59] A. P. Martins, A. S. Carvalho, and A. S. Araújo. Design and implementation of a current controller for the parallel operation of standart upss. In *IEEE IECON*, pages 584–589, 1995.

[60] M. N. Marwali, J. W. Jung, and A. Keyhani. Control of distributed generation systems - part ii: Load sharing control. *IEEE Trans. Power Electron*, 19(6):1551–1561, 2004.

[61] R. A. Mastromauro, M. Liserre, and A. Dell Aquila. Study of the effects of inductor non-linear behavior on the performance of current controllers for single-phase pv grid converter. *IEEE Trans. Ind. Electron.*, 55, May 2008.

[62] R. A. Mastromauro, M. Liserre, and A. Dell Aquila. Frequency domain analysis of inductor saturation in current controlled grid converters. *in Proc. IEEE Industrial Electronics Society, IECON 2007*, pages 1396–1401, Nov. 2007.

[63] R. A. Mastromauro, M. Liserre, A. dell Aquila, J. M. Guerrero, and J. C. Vasquez. Droop control of a multifunctional pv inverter. In *IEEE International Symposium on Industrial Electronics (ISIE 08)*, 2008.

[64] R. A. Mastromauro, M. Liserre, T. Kerekes, and A. Dell Aquila. A single-phase voltage controlled grid connected photovoltaic system with power quality conditioner functionality. *to be published on IEEE Trans. Ind. Electron., forthcoming issue*.

[65] C. V. Nayar, M. Ashari, and W. W. K. Keerthipala. A grid-interactive photovoltaic uninterruptible power supply system using battery storage and a back up diesel generator. *IEEE Trans. Energy Conversion*, 16:348–353, Sept 2000.

[66] H. Oshima, Y. Miyazawa, and A.hirata. Parallel redundant ups with instantaneous pwm control. *in Procedings IEEE Intelec*, pages 436–442, 1991.

[67] M. Pascual, G. Garcera, E. Figueres, and F. Gonzalez-Espin. Robust model-following control of parallel ups single-phase inverters. *IEEE Trans. Ind. Electron*, 55(8):2870–2883, Aug 2008.

[68] P. Piagi and R. H. Lasseter. Autonomous control of microgrids. *IEEE on Power Engineering Society General Meeting PES*, page 8, Jun 2006.

[69] N. Pogaku, M. Prodanovic, and T. C. Green. Modeling, analysis and testing of autonomous operation of an inverter-based microgrid. *IEEE Trans. Power. Electron*, 22(2):613–625, 2007.

[70] M. Prodanovic and T.C. Green. High quality power generation through distributed control of a power park microgrid. *IEEE Trans. Ind. Electron.*, 53:1471–1482, 2006.

[71] J. P. Rhode, A.W. Kelley, and M.E. Baran. Complete characterization of utilization-voltage power system impedance using wideband measurement. *IEEE Trans. on Ind. Applicat.*, 33:1472–1479, 1997.

[72] P. Rodriguez, A. Luna, I. Candela, R. Teodorescu, and F. Blaabjerg. Grid synchronization of power converters using multiple second order generalized integrators. *in Proc. IEEE IECON 08*, pages 755–760, 2008.

[73] P. Rodriguez, A. Luna, M. Ciobotaru, R. Teodorescu, and F. Blaabjerg. Advanced grid synchronization system for power converters under unbalanced and distorted operating conditions. *in Proc. of IEEE Ind. Electron. (IECON 06)*, pages 5173–5178, 2006.

[74] M. J. Ryan and R. D. Lorenz. A high performance sine wave inverter controller with capacitor current feedback and back-emf decoupling. In *Proceedings of the IEEE Power Electronics Specialists Conference (PESC)*, pages 507–513, 1995.

[75] R. R. Sawant and M. C. Chandorkar. Methods for multi-functional converter control in three-phase four-wire systems. *IET Power Electron.*, 2:52–66, Jan 2009.

[76] S.Chakraborty, M. D. Weiss, and M. G. Simoes. Distributed intelligent energy management system for a single-phase high-frequency ac microgrid. *IEEE Trans. Ind. Electron*, 54:97–109, 2007.

[77] M. Sumner, B. Palethorpe, and D.W.P. Thomas. Impedance measurement for improved power quality-part 2: a new technique for stand-alone active shunt filter control. *IEEE Trans. on Power Delivery*, 19:1457–1463, 2004.

[78] X. Sun, Y. S. Lee, and D. Xu. Modeling, analysis and implementation of parallel multi-inverter systems with instantaneous average-current-sharing scheme. *IEEE Transactions on Power Electronics*, 18 No.3:844–856, 2003.

[79] H. Tao, J. L. Duarte, and M. A. M. Hendrix. Line interactive ups using a fuel cell as the primary source. *IEEE Trans. Ind. Electron*, 55:3012–3021, 2008.

[80] R. Teodorescu and F. Blaabjerg. Flexible control of small wind turbines with grid failure detection operating in stand-alone and grid-connected mode. *IEEE Trans. Power Electron*, 9:1323–1332, Sept. 2004.

[81] A. Tuladhar, H. Jin, T. Unger, and K. Mauch. Parallel operation of single phase inverter modules with no control interconections. In *Applied Power Electronics Conference and Exposition (APEC '99)*, volume 1, pages 94–100, 1997.

[82] A. Tuladhar, H. Jin, T. Unger, and K. Mauch. Control of parallel inverters in distributed ac power systems with consideration of line impedance effect. *IEEE transactions on industrial electronics*, 36(1):131–138, jan 2000.

[83] M. Vandenbergh, A. Engler, R. Geipel, M. Landau, and P. Strauss. Microgrid management with a high share of renewable energy sources. In *21st International Conference on European Photovoltaic Solar Energy*, 2006.

[84] J. C. Vasquez, J. M. Guerrero, E. Gregorio, P. Rodriguez, R. Teodorescu, and F. Blaabjerg. Adaptive droop control applied to distributed generation inverters connected to the grid. In *IEEE International Symposium on Industrial Electronics ISIE'08*, pages 1–6, 2008.

[85] D. M. Vilathgamuwa, P.C. Loh, and Y. Li. Protection of microgrids during utility voltage sags. *IEEE Trans. Ind. Electron*, 53:1427–1436, oct 2006.

[86] P. L. Villeneuve. Concerns generated by islanding. *IEEE Power and Energy Magazine*, pages 49–53, 49-53 2004.

[87] R.J. Wai, W.H. Wang, and C.Y. Lin. High-performance stand-alone photovoltaic generation system. *IEEE Trans. Ind. Electron*, 55:240–250, jan 2008.

[88] C.M. Wang, C.H. Su, M.C. Jiang, and Y.C. Lin. A zvs-pwm single-phase inverter using a simple zvs-pwm commutation cell. *IEEE Trans. Ind. Electron*, 55:756–766, feb 2008.

[89] A. Tabisz Wojciech, Milan M. Jovanovic, and Fred C. Lee. Present and future of distributed power systems. *Proceedings of the IEEE Applied Power Electronics Conference APEC'92*, 1992.

[90] H. Wu, D. Lin, Z. Zhang, K. Yao, and J. Zhang. A current-mode control technique with instantaneous inductor-current feedback for ups inverters. *Proceedings of the IEEE Applied Power Electronics Conference and Exposition*, pages 951–957, 1999.

[91] T. F. Wu, Y. K. Chen, and Y. H. Huang. 3c strategy for inverters in parallel operation achieving an equal current distribution. *IEEE Trans. Power Electron*, 47:273–281, 2000.

[92] X. Yuan, W. Merk, H. Stemmler, and J. Allmeling. Stationary frame generalized integrators for current control of active power filters with zero steady-state error for current harmonics of concern under unbalanced and distorted operating conditions. *IEEE Trans. on Ind. Applicat*, 38:523–532, April 2002.

[93] B. Zhang, D. W. Wang, K. L. Zhou, and Y.G. Wang. Linear phase lead compensation repetitive control of a cvcf pwm inverter. *IEEE Trans. Ind. Electron*, 55:1595–1602, April 2008.

[94] Y. Zoka, H. Sasaki, N. Yorino, K. Kawahara, and C. C. Liu. An interaction problem of distributed generators installed in a microgrid. *in Proc. IEEE DRPT'04*, pages 795–799, 2004.